THE UNIVERSITY OF ALBERTA

A SIMULATED MODEL OF TWO CENTER PIVOT SPRINKLER IRRIGATION SYSTEMS OPERATING UNDER NORMAL CLIMATIC CONDITIONS

by

BORIS CAROLUS HORVATH

A THESIS

SUBMITTED TO THE FACULTY OF GRADUATE STUDIES AND RESEARCH

IN PARTIAL FULFILMENT OF THE REQUIREMENTS FOR THE DEGREE

OF MASTER OF SCIENCE

DEPARTMENT OF AGRICULTURAL ENGINEERING

EDMONTON, ALBERTA

SPRING, 1979

ABSTRACT

A mathematical model of two Center Pivot sprinkler irrigation systems (Circle Master and Valley 1160), operating under local climatic conditions, was developed to examine the effect of wind on the uniformity of water distribution and to evaluate the systems performance under actual windy conditions.

The model consists of two parts. In the first part, the sets of equations of motion were solved for known initial conditions by means of a Continuous Simulation Modelling Program (CSMP). The simulation model described the trajectories of the particles in flight which permitted defining the geometry of the basic wetted patterns when the water particles struck the ground surface. The second part of the model simulated the relative performance of two operating C.P. systems in relation to the rows of measuring receptacles used in field measurements. This involved determining the actual wetted patterns from the basic wetted patterns, simulation of distribution patterns inside the actual wetted patterns and simulation of climatic factors and systems characteristics. The Fortran IV computer language was used to program the necessary formulation simulating the two operating C.P. systems.

Performance of the simulated model was evaluated by a direct comparison of field and theoretical simulated application depths and by comparison of the theoretical simulated coefficients of uniformity with those measured. On the whole, theoretical depths deviated approximately 14 percent from the field measurements. The spread of average deviations varied from 11 to 18 percent and from 14.3 to 30.8 percent for the "Circle Master" and the "Valley 1160", respectively. Where the the effect of wind was not included in the model the mean absolute de-

viations were increased to 17.5 percent for the former C.P. system as compared to 19.4 percent for the latter system. Close agreements were obtained between the measured weighted coefficients and those simulated in the model (a maximum deviation of approximately 6 percent).

Effect of wind on uniformity of water distribution was shown by the curves of the theoretical simulated application depths. The uniformity coefficients were affected by both the wind velocity and wind direction, however, the effect of wind direction on the uniformity was more pronounced. For a wind velocity of 20 mph and 0 degrees direction, where the line of measurement was directly opposite to the wind, the coefficients of uniformity were 87.3 percent and 91.4 percent for the "Circle Master" and the "Valley 1160" C.P. systems, respectively. For the same wind velocity of 20 mph and 80 degree direction, uniformity improved as the coefficients of uniformity were 96.02 percent and 96.54 percent for the former and latter C.P. system, respectively.

Performance of the C.P. systems was determined from field measured application depths as well as those simulated by the model. In general the field coefficients were lower than simulated coefficients, but both the field and the simulated coefficients were within the acceptable level of 80-90 percent. The spread of the weighted field coefficients varied from 87.6 percent to 93.6 percent for the "Circle Master" and from 88.4 percent to 92.6 percent for the "Valley 1160" C.P. system. The weighted simulated coefficients varied from 91.8 percent to 96.1 percent for the former C.P. system and from 93.4 percent to 96.1 percent for the latter C.P. system. The weighted coefficients, field and simulated, indicated higher uniformities than the respective non-weighted coefficients.

ACKNOWLEDGEMENT

I wish to express my sincere thanks to my advisor Professor Egon Rapp for his guidence, advice and constructive criticism in the research and the preparation of this thesis.

I would also like to express my gratitude to the following people who helped me in the completion of my thesis:

Professor Anderson for his willingness to share his knowledge in computers.

Robert Borg for sharing his expertise in the field of fluid mechanics.

My good friend S.N. Chin for his encouragement and interest in this manuscript.

Alberta Agriculture Research Trust for their financial support towards purchasing the apparatus necessary for the field experiments.

My friend Dale Baumback for his contributions in the field of drafting.

My dear wife Fern for many hours of typing and continuous encouragement during my studies.

TABLE OF CONTENTS

LIST OF FIGURES

LIST OF TABLES

CHAPTER I

INTRODUCTION

Centre pivot (C.P.) irrigation is presently an increasingly popular method of irrigating large agricultural areas. The main advantages of C.P. systems are a high degree of automation, adaptability to various soil types and topography, and a higher application uniformity capability. A relatively high initial investment is therefore justified due to the low labour requirements, the potential of increasing yields and high water application efficiencies.

By definition, a C.P. system consists of a lateral line of sprinklers continuously rotating about a pivot. Water under pressure is supplied to the lateral at the pivot. The lateral is supported by a number of self-propelled towers, each having a driving mechanism utilizing wheels or tracks. The adjustable speed of travel of C.P. systems allows the application of 1/2 to 4 inches of water per revolution. Standard C.P. systems are approximately 1/4 mile long, irrigating 135 acres of a 160-acre field.

The important features of a well-designed centre pivot system, as recognized by the American Society of Agricultural Engineers (1), are: capacity to supply an adequate amount of water to the soil at the peak water use periods, to replace moisture in the soil profile frequently enough to maintain conditions for optimum plant growth, and to refill the soil moisture reservoir uniformly.

The first two features are directly related to the soil type, the crop grown and the area to be irrigated. The usual approach to achieve relatively uniform water distribution is to increase the discharge from the first to the last sprinkler, that is, by increasing the application

rates in proportion to an increasing area irrigated by individual sprinklers. Previous research (4, 26) has indicated that the theoretical uniformity varies from the actual field uniformity. Large uniformity deviations are the result of inadequate sprinkler systems design and external factors, mainly wind. The effect of wind on the distribution from stationary sprinklers systems has been documented (14). However, the distribution from C.P. systems as affected by wind has not been examined to any great extent.

This study is an attempt to analyze experimentally and theoretically the interrelationships between wind, sprinkler patterns and uniformity of water distribution and to provide a model for predicting the application depths from centre pivot systems under windy conditions.

Objectives

The objectives of this study were:

1. To evaluate the performance characteristics of two centre pivot sprinkler irrigation systems operating under normal climatic conditions. Field measurements of application depths and a continuous record of meterological data monitored were used to examine the effects of wind on the uniformity of water distribution.
2. To obtain the desired wetted patterns of the sprinklers used, by simulating the flight path of water droplets emitted.
3. To incorporate the predicted wetted patterns into a mathematical model developed to simulate the performance of the C.P. system operating under windy conditions.
4. To validate the model by comparing the predicted and measured application rates. The effects of continuously varied wind

conditions on the uniformity of water distribution were examined using the model.

CHAPTER II

LITERATURE REVIEW

The uniformity of water distribution by sprinklers has been of interest to agricultural engineers for the past half century. Research has shown that although sprinklers distributed water uniformly in a circular area, the uniformity between the sprinklers was not satisfactory. The use of overlapping sprinkler patterns was an important breakthrough in solving the problem of poor uniformity encountered with circular sprinkler water distribution. For stationary sprinkler systems, Christiansen (6) demonstrated that nearly uniform distribution is possible with proper sprinkler patterns and proper spacings of sprinklers. The development of highly automated sprinkler systems, such as centre pivots, further increased the potential application of sprinklers in irrigation.

2.1 Measures of Uniformity

Several expressions have been developed for the purpose of comparing the sprinkler distribution patterns. Christiansen (6) introduced the coefficient of uniformity (Cu) expressed as a percentage. The uniformity coefficient (Cu) given below is dependent on the mean deviation of water distribution.

$$Cu = 100 \left(1.0 - \frac{\Sigma (x_i - \bar{x})}{N\bar{x}} \right) \qquad (1)$$

where

x_i - individual readings

$\bar{x}$ - the mean value of x_i

N - number of observations

Wilcox and Swailes (26) derived a similar coefficient of uniformity but squared the mean deviations. The distribution, as expressed by

the following equation, was considered to be adequate for values greater than 70 percent.

$$U = 100 \left(1.0 - \frac{SD}{\bar{x}} \right)$$

where

U - coefficient of uniformity

SD - standard deviation of all observations

$\bar{x}$ - the mean value of all observations

Benami and Hore (2) proposed a new coefficient of uniformity by considering the deviations from the group means rather than the general mean. The general mean was computed from all observations. The group means were determined from observations above and below the general mean. This approach gave more weight to readings with extensive deviations from the general mean.

$$A_o = 166 \frac{N_a}{N_b} \left(\frac{2T_b + D_b M_b}{2T_a + D_a M_a} \right)$$

where

A_o - uniformity coefficient

N_a - number of observations above the general mean

N_b - number of observations below the general mean

T_a - sum of the observations above the group mean in the above group

T_b - sum of the observations below the group mean in the below group

D_a - difference in the number of observations below and above the group mean in the above group

D_b - difference in the number of observations above and below the group mean in the below group

M_a - group mean of the observations larger than general mean

M_b - group mean of the observations smaller than general mean

Tezer (23), in investigating the reliability of the above three coefficients of uniformity, suggested a new coefficient (A), where (A) is the coefficient (A_o) expressed as a percentage ($A = 0.6A_o$). The coefficient (A) proved to be a better estimate of the degree of uniformity than the coefficients (Cu, U) described earlier. This was due to the sensitivity of the coefficient (A) to variation in distribution, and thus gave a greater emphasis to extreme readings below the mean.

A frequently used measure of sprinkler performance is the USDA pattern efficiency E_{PL} (7), defined as the ratio of the average of the lowest 25 percent of the application depths to the average depth of application.

$$E_{PL} = 100 \left[\frac{\sum_{i=1}^{(1/4)N} x_i}{(1/4)N\,\bar{x}} \right]$$

where

x_i - the lowest 25 percent of the readings

$\bar{x}$ - average of all readings

N - total number of readings

Skewness of the distribution either positive or negative which occurs in windy conditions would affect the above USDA pattern efficiency E_{PL} since it depends on the lower tail of the distribution.

2.2 Factors Affecting Uniformity

The main advantage of sprinkler irrigation is the capability to distribute water more uniformly onto the soil than any other method of irrigation. The factors affecting uniformity can be classified depending

on their origin as (19):

a. Sprinkler head factors; represented by the size of sprinkler nozzle, type of nozzle, angle of nozzle, rate of sprinkler rotation and operating pressure.

b. Distribution system factors; such as sprinkler and lateral spacing, height of sprinkler above field surface, stability of sprinkler riser and variation of pressure along the lateral.

c. Climatic factors; mainly wind speed and direction.

d. Management factors; varies with type of sprinkler system. With stationary systems these are the system layout and duration of system operation. With self-propelled systems the factors are the speed of the lateral and the alignment of the lateral and the sprinkler risers.

Christiansen (5) made extensive field tests to investigate the factors affecting the water distribution of sprinkler systems. He inferred that the water distribution from sprinklers could be classified into six characteristic geometrical patterns, designated as A, B, C, D, E, and F curves. The A, B, and C curves varied from triangular to conical shape and gave uniform distributions when sprinklers were no further apart than 55 to 60 percent of the diameter of a sprinkler wetted pattern. The D, E and F curves, however, resembled a rectangular cross-section and yield high uniformity coefficients with spacing up to 45 percent, dropping sharply between 45 to 75 percent and increasing again between 75 and 80 percent of the diameter covered.

Wilcox and MacDougald (25) selected eight types of distribution curves to determine their impact on the uniformity of water distribution and reported similar findings to those of Christiansen (5). The best

distribution curve was found to be one with a steady decrease in application rate from the sprinkler towards the boundary of the pattern. For squared spacings the sprinklers should not be further apart than 60 percent of the diameter of throw. A squared spacing results in better uniformity than a rectangular spacing for the same area covered when no wind is considered.

Sprinkler wetted patterns are distorted when inadequate water pressure is supplied. Bilanski and Kidder (3), conducting laboratory experiments on medium pressure sprinklers, showed that the uniformity of water distribution increased with rising pressures. With higher pressures greater breakage of the water stream occurs resulting in smaller droplets, filling the gaps normally caused by lower pressures. A further increase in uniformity was observed from sprinklers operating with oscillating arms. For a given operating pressure the distribution improved with a larger nozzle size. To minimize the decrease in uniformity due to variation in system pressure, Christiansen (6) recommended that the frictional losses along the stationary lateral should be kept within 20 percent of the average operating pressure.

The uniformity of water distribution is affected by wind because of the skewed wetted patterns. At low wind velocity (less than 3 mph) most sprinkler systems operate favourably. However, with a high wind velocity (10 to 14 mph) sprinkler wetted patterns become asymmetrical, as a result of higher concentration of water near the sprinkler and on the lee side. Christiansen (5) showed that with closer sprinkler spacings and adequate overlap between sprinklers the effect of wind on the uniformity of water distribution was less significant than that of other factors. Korven (14) in his testing various

revolving sprinklers, indicated that the effect of wind at high velocities on uniformity of water distribution was quite dramatic. From the results, it was concluded that the average coefficient of uniformity of all sprinklers tested fell from 82 to approximately 32 percent when the wind velocity incresed from 4 to about 17 mph. At fairly high wind velocities the uniformity largely depends on the design characteristics of the individual sprinklers.

2.3 Factors Affecting Sprinkler Drop Distribution

The drop size distribution of sprinkler sprays and dynamics of the individual drops are of practical importance in sprinkler irrigation. Small droplets are subject to wind drift and evaporation losses which in turn result in distorted patterns, poor uniformity and reduced sprinkler efficiency. At impact, large drops with greater kinetic energy have the potential of breaking up the soil structure and also damaging the leaves of young plants.

2.3.1 Sprinkler Jet Breakup

A jet of water emerging from a nozzle under relatively high pressures breaks into small droplets because the state of equilibrium has been disturbed.

Merrington and Richardson (15) summarized previous research concerned with different phases of disturbance of a liquid jet. In the first phase of disintegration, the jet becomes varicose due to the action of inertia and surface tension. The rate of increasing disturbance is independent of the speed of efflux. In the second phase of disturbance, the jet is further deformed and the action of the air becomes more important than surface tension. Since the air resis-

tance increases rapidly with speed, the rate of jet disturbance increases with increasing speed of efflux. The third phase of jet breakup, in which the jet is completely disrupted, is termed "atomization" by Ohnesborge, as cited by Merrington and Richardson (15).

Miesse (16) modified the criteria originated by Ohnesborge by determining the region where the three types of jet disintegration occurs. Based on dimensional analysis, Miesse indicated that the third phase of disintegration occurs in the secondary atomization region rather than in the third region. The prime forces acting in that region controlling breakup are viscous, inertia and capillary forces.

Rouse et al. (20) described the jet breakup just after emergence from the nozzle as a result of continuous action of countless numbers of turbulent eddies no longer confined by a conduit. At this stage, the density of air is too low to have any significant effect upon a jet. The action of air begins only after the jet is sufficiently disrupted. The resistance of air is proportional to the square of the velocity of the jet and the cross-sectional area. The resistance rapidly decreases as the distance of travel of the eddies carrying water from the main stream forces them to spread laterally at diminishing velocity.

2.3.2 The Drop Size Distribution

Merrington and Richardson (15) found experimentally that the mean drop diameter of water particles depends on the fluid viscosity and the jet velocity. The mean diameter was also found to be inversely proportional to the relative velocity between the jet and the surrounding air. Considering the cross-sectional profile of the jet's relative

velocity to the air, the smallest relative velocities are near the jet's periphery. This will result in smaller particles at the periphery of the jet and the largest particles near the core.

Seginer (21), examining the interrelation between the sprinkler drop size distribution, drop velocities and sprinkler distribution pattern, made the following observations:

a. With increased operating pressure, the mean drop diameter and the application rates decreased, the radius of water throw increased and the distribution pattern improved.

b. Higher rates of sprinkler rotation tended to decrease the radius of throw. The rotation of the oscillating arm did not significantly affect the distribution characteristics.

c. At a given distance, larger particles were formed from rotating sprinklers as compared with non-rotating sprinklers.

Kohl (13) demonstrated experimentally the effect of pressure and nozzle sizes on the mean drop diameter. When the nozzle size was held constant and pressure varied, the increased pressure resulted in a greater number of smaller drops. Since jet velocity is proportional to the pressure, the experiment confirmed the relation of decreasing drop size with increasing relative velocity between the jet and the air. Similarly, by decreasing nozzle size at constant pressure the mean drop size is decreased, but the effect of rising pressure on the mean diameter was more pronounced. Smaller sprinkler nozzles will produce smaller mean drop sizes than large sprinklers under normal operating conditions. Operating small sprinkler nozzles at low pressures may result in larger mean drop diameters than the mean drop diameters produced by larger sprinklers at higher pressures.

Several methods of measuring droplet size have been employed to determine the distribution. The most common method of measuring the particle sizes is the "stain method" described by Hall (10). This method is based on the assumption that a drop falling upon a uniform absorbent surface leaves a stain of a certain diameter, proportional to the diameter of the drop. Seginer (21), using the stain method, determined the drop size from this relation:

$$d = 0.444\ D^{2/3} \qquad (2)$$

where

d - diameter of the drop (mm)

D - diameter of the stain (mm)

2.3.3 Behaviour of Water Drops Emitted From a Sprinkler Nozzle

After the initial disintegration of the main stream, the individual water droplets will deform or may further break up under the high velocity depending on the size of the drop. Blanchard, cited by Umback and Lembke (24), concluded that drops below 4.6 mm are quite stable, and drops between 4.6 and 5.4 mm break up upon shock. The trajectories of the drops will largely depend on their tangential velocities. The forces exerted on the particle are the resistance of the air, gravity and under windy conditions, the wind.

Seginer (22) discussed some phenomena related to the tangential velocity of sprinkler drops. He assumed that the two forces acting on a drop are the drag force and gravity. The air drag force was described as an "ever increasing function of velocity (V) for any given body". The relation between the velocity and the drag force was expressed by means of the drag coefficient Cd.

$$Cd = \frac{2F}{\rho V^2 A} \qquad (3)$$

where

ρ - the air density (Kg - s^2/m^4)

A - the projected area of the particle (m^2)

F - the drag force (Kg)

V - the relative velocity of the particle (m/s)

The drag coefficient of a water drop was considered to be a function of the Reynolds number and Weber number because of the deformation of drops at high velocities. At high velocities, the drag coefficient (Cd) approaches a minimum value and the drag force may be considered directly proportional to the square of the velocity. The effect of gravity on the particle depends on whether the drop has an upward or downward component of velocity. The drag force F was approximated as the lower function of the velocity V.

$$F = C_n V^n \qquad (4)$$

where

C_n - coefficient depending on value of n

n - positive dimensionless constant

The effect of the constant n on various trajectories of drops was investigated. A value of n = 2 proved satisfactory, on the average, in predicting sprinkler droplet paths. The equation of motion is then:

$$\frac{d^2y}{dt^2} = C_2 \left(\frac{dy}{dt}\right)^2 \pm g \qquad (5)$$

where

g - acceleration due to gravity (m/s^2)

$\pm$ - sign indicating upward or downward movement

C_2 - drag coefficient

$\frac{dy}{dt}$ - relative velocity of a particle (m/s)

$\frac{d^2y}{dt^2}$ - acceleration of a particle (m/s^2)

Okamura (17) derived an equation of motion for water particles emitted from a sprinkler nozzle in still air conditions and under windy conditions. The drops were assumed to retain a spherical shape for the average flying time. Under no wind conditions, the equations of motion was based on the air drag force and the evaporation losses. The air drag force consists of two components; namely, the viscous and inertia resistance expressed respectively as:

$$f_1 = 6 \pi \eta V a \qquad (6)$$

$$f_2 = \frac{1}{2} C_d S \rho V^2 \qquad (7)$$

where

η - dynamic viscosity ($Kg - s/m^2$)

V - velocity of the particle (m/s)

a - radius of sphere (m)

Cd - air drag coefficient

S - projected area of the sphere (m^2)

ρ - density of the fluid ($kg - s^2/m^4$)

When the Reynolds number is greater than 1, the viscous resistance

is negligible and the inertia resistance may be considered the drag force. The drag coefficient Cd was approximated from the following equations:

$$\left.\begin{array}{ll} R_e \leqslant 100 & C_d = 33.3/R_e - 0.0033\ R_e + 12 \\ 100 < R_e < 1000 & C_d = 72.2/R_e - 0.0000556\ R_e + 0.48 \\ R_e \geqslant 1000 & C_d = 0{,}45 \end{array}\right\} \quad (7,a,b,c)$$

The equation of motion of the spherical drops in still air in the direction x and y are:

$$\ddot{x} = C_d \frac{\rho_a}{\rho_w} \frac{3}{4D} q\dot{x} \qquad (8)$$

$$\ddot{y} = C_d \frac{\rho_a}{\rho_w} \frac{3}{4D} q\dot{y} \qquad (9)$$

where

$\ddot{x}$ - acceleration in the x direction (m/s^2)

$\ddot{y}$ - acceleration in the y direction (m/s^2)

ρ_a - density of the air ($Kg\text{-}s^2/m^4$)

ρ_w - density of the fluid ($Kg\text{-}s^2/m^4$)

D - diameter of the sphere (m)

q - velocity of the particle (m/s)

The effect of evaporation causes a decrease in droplet size while the drop travels in the air. Okamura (17) showed that the change in diameter due to evaporation can be calculated from equations by incorporating the heat balance term in the equations of motion. Nevertheless, when particles greater than 0.5 mm are considered the effect of evapora-

tion may be neglected.

The difficulties inherent in the study of the motion of particles when influenced by wind may be considered in two aspects; the lack of research on motion of water drops in still air and the problem of obtaining reliable data due to the turbulent flow nature of wind near the surface and the chaotic variation of wind in most climatic conditions.

In deriving the equations of motion of sprinkler droplets under wind conditions, the following assumptions were made (18):

a. Within some period of time, the wind velocity is assumed to be constant. The instantaneous values of the wind velocity are the sum of the mean and fluctuating values.

b. The wind profile is assumed to be a uniform, vertical distribution at a large distance from the surface. Near the ground the profile is described logarithmically, thus the slope depends on the surface roughness. Coriolis forces have a negligible effect at this relatively small scale.

Using the above assumptions, the equations of motion of flying droplets were derived for the case when the wind direction is parallel to the x axis of the x, y and z coordinates and the magnitude of the mean wind speed is w.

$$\ddot{x} = -C_d \frac{\rho_a}{\rho_w} \frac{3}{4D} q(\dot{x} - w) \qquad (10)$$

$$\ddot{y} = -C_d \frac{\rho_a}{\rho_w} \frac{3}{4D} q\dot{y} \qquad (11)$$

$$\ddot{z} = -C_d \frac{\rho_a}{\rho_w} \frac{3}{4D} q\dot{z} - g \qquad (12)$$

where

$\ddot{x}$ - acceleration in x direction (m/s^2)

$\dot{z}$ - velocity in z direction (m/s)

w - wind velocity (m/s)

g - acceleration due to gravity (m/s^2)

The trajectories of flying water droplets with various diameters emitted from a sprinkler nozzle are obtained by solving the differential equations (10), (11) and (12) for the known initial conditions, using the computer. From the calculated trajectories, drop size distribution at any level and at any height were evaluated. The phenomenon of wind drift was clarified by considering the average wind velocity and the varied discharge direction in respect to the wind direction in the equations of motion. Because of the presence of a vertical component of wind velocity, fine water droplets are carried away by wind drift, thus accounting for losses in sprinkler spray.

2.4 Theoretical Distribution of Water by Moving Sprinklers

In modelling the cross-sectional distribution of sprinklers, two types of distribution curves, resembling a triangle or half an ellipse, are commonly used. Both these geometrical curves were found to give good uniformity within specific spacings (4). The maximum rate with the triangular distribution is double the maximum application rate with the elliptical pattern.

2.4.1 Single Moving Sprinkler

Bittinger and Longenbaugh (4) analysed elliptical and triangular patterns of a single moving sprinkler to determine the degree of skewness when the sprinkler is moved in a straight line and in a circular path. From

the geometry, (see figures (1) and (1a), precipitation at any point (P) for triangular and elliptical pattern respectively, were defined as:

$$P_p = h \left(\frac{r-s}{r} \right) \qquad (13)$$

$$P_p = \frac{h}{r} (r^2 - s^2)^{1/2} \qquad (14)$$

where

h - maximum precipitation rate at middle of the pattern (in/hr)

r - radius of sprinkler pattern (ft)

s - distance from sprinkler to point P (ft)

The total depth of application from one sprinkler was evaluated by integrating the rate over the total time. The total depths from one sprinkler moving in a straight line at constant velocity assuming the triangular and elliptical patterns are respectively:

$$D_{tr} = \frac{hr}{\omega R} \left((1-m^2)^{1/2} - m^2 \ln \frac{(1-m^2)^{1/2} + 1}{m} \right) \qquad (15)$$

$$D_{el} = \frac{hr \pi (1-m^2)}{2\omega R} \qquad (16)$$

where

D_{tr} - total application depth with a triangular distribution (in)

D_{el} - total application depth with an elliptical distribution (in)

S - distance from the pivot to a point p (ft)

α - angle of rotation about the pivot (radians)

ω - angular velocity of the sprinkler (radians/hr)

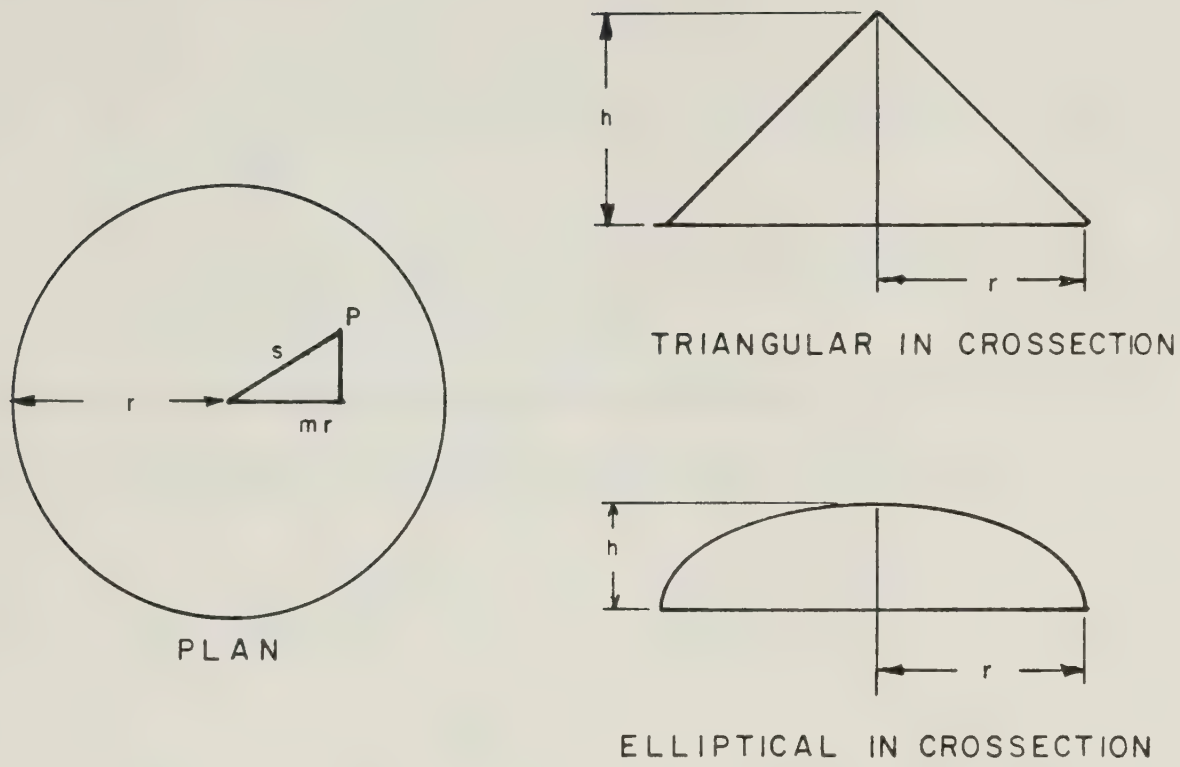

Figure 1. Application rate patterns of a stationary sprinkler.

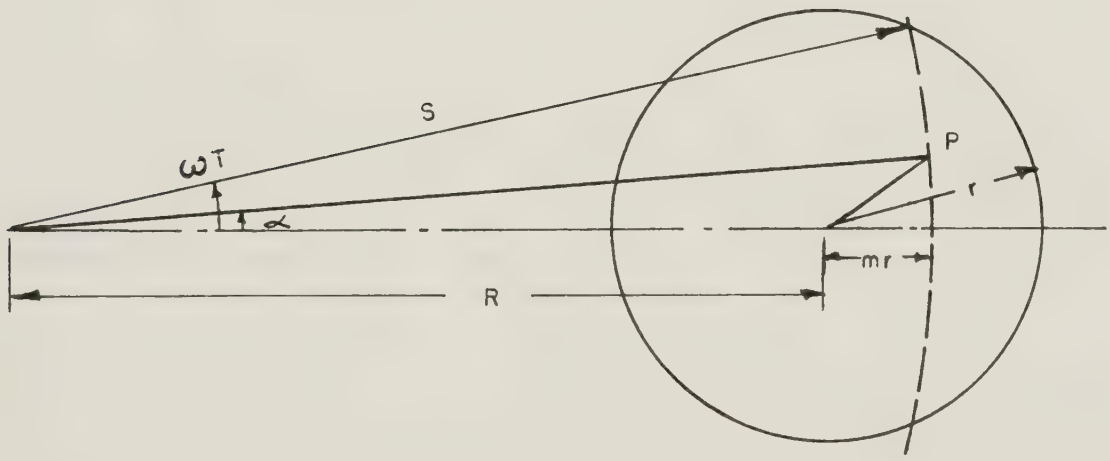

Figure 1a. Geometric Representation of a sprinkler moving in a circular path at constant velocity.

n - ratio $\left(\frac{R}{r}\right)$

m - ratio $\left(\frac{s-r}{r}\right)$

R - distance from the pivot to the sprinkler (ft)

ϕ - angle of integration; $\phi = \frac{1}{2}(\pi - \alpha)$ radians

T - time required for one half of the sprinkler pattern to pass point P (hr)

h - rate of precipitation at centre of sprinkler pattern (in/hr)

r - radius of sprinkler patter (ft)

The total depths from one sprinkler moving in a circular path assuming a triangular and elliptical pattern are respectively:

$$D_{tr} = 2hT - \frac{2h}{r\omega} \int_0^{\omega T} \left(S^2 + R^2 - 2\,RS \cos \alpha \right)^{1/2} d\alpha \qquad (17)$$

$$D_{el} = \frac{4h}{\omega} (1 - m^2)^{\frac{1}{2}} \int_0^{\frac{\omega T}{2}} \left(1 - \frac{4n\,(n+m)}{1 - m^2} \sin^2 \phi \right)^{1/2} d\phi \qquad (18)$$

Bittinger and Longenbaugh (4) observed the distribution for both patterns moving in a straight line by plotting (D_{tr}/r) and (D_{el}/r) against (m) from equations (15) and (16). For the case of a sprinkler moving in a circular path equation (17) was solved as an elliptical integral of the second kind $E(k,\phi)$. Equation (18) was not readily evaluated except by numerical means. They also noted that for (n) greater than 5 the circular path could be approximated with a straight line path.

The maximum precipation rate from a stationary sprinkler for both distribution patterns is near the centre. When the sprinkler is moved in a straight line or a circular path, this rate is further intensified. The pattern is skewed toward the centre of curvature when moved in an arc. The degree of skewness varies inversely with the distance between the

sprinkler and the pivot. With effective overlap between adjacent sprinkler and the pivot. With effective overlap between adjacent sprinklers both the triangular and elliptical distribution curve will result in high uniformities. The optimum spacings for the two types of distribution curves respectively are 1.0 and 1.4 times the pattern radius (4).

2.4.2 Rotating Lateral

The application rate on a point (P) at a distance (S) from the centre pivot includes discharge from more than one sprinkler and can be determined by summing the individual rates from overlapping adjacent patterns. The equations for application rate for the triangular and elliptical patterns, respectively are:

$$A_{tr} = \sum_i h_i - \frac{h_i}{r_i} (S^2 + R_i^2 - 2R_i S \cos \alpha)^{\frac{1}{2}} \qquad (19)$$

$$A_{el} = \sum_i \frac{h_i}{r_i} (r_i^2 - S^2 - R_i^2 + 2R_i S \cos \alpha)^{\frac{1}{2}} \qquad (20)$$

where

i - subscript referring to i^{th} sprinkler on the lateral

A_t - application rate with a triangular distribution (in./hr)

A_e - application rate with an elliptical distribution (in./hr)

h,r,S, R, , - as previously defined

The equations (19) and (20) solved by Heermann and Hein (11) for small increments of (α) from zero to (ωT) gave one half of the symmetric rate-time relationship for a complete pass of the pattern over point (P).

For the C.P. system analyzed, the equations solved to determine the total depth at a distance (S) from the pivot for the triangular and el-

lliptical patterns, respectively, were:

$$D_{tr} = 2\sum_{i=1}^{N} h_i T_i - \frac{h_i}{r_i \omega} \int_0^{\omega T_i} \left(S^2 + R_i^2 - 2R_i S \cos \alpha \right)^{\frac{1}{2}} d\alpha \quad (21)$$

and

$$D_{el} = \frac{4}{\omega} \sum_{i=1}^{N} h_i (1-m_i)^{\frac{1}{2}} \int_0^{\frac{\omega T_i}{2}} \left(1 - \frac{4n_i (n_i + m_i)}{1-m_i^2} \sin^2 \phi \right)^{\frac{1}{2}} d\phi \quad (22)$$

The distribution patterns for a C.P. system are obtained by numerically solving equations (21) and (22). The large number of repetitive solutions suggests the use of a computer. For application depths beyond 650 ft (i.e., the skewness for the circular path is less than 0.01 in. from inner to outer radius for one sprinkler) straight line approximations for triangular and elliptical patterns could be used (11).

For comparison of theoretical and field distribution Heermann and Hein (11) found a close fit between computed and measured application depths for triangular and elliptical distribution were almost identical. The small differences of the two distributions were associated with the close spacings of sprinklers in the systems studied.

CHAPTER III

MODEL DEVELOPMENT

The model simulating the centre pivot irrigation system consists of two separate parts. The first part involves the dynamics of water droplets emerging from the rotating sprinklers. The water droplet paths define the basic wetted patterns of a sprinkler for a range of angles and discrete values of particle sizes, initial particle velocities and wind velocities. The second part of the model, which simulates the relative performance of the C.P. system, performs two distinct functions, namely:

a. The interpolation of the geometric variables that define the finite number of calculated wetted patterns. Predicted wetted patterns could then be determined for a range of initial conditions encountered.

b. The determination of the system performance described by the application rates, depths and coefficients of uniformity.

3.1 Dynamics of Water Droplet in Flight

Experimental research on the distribution of water droplets inside the wetted patterns has shown that the largest droplets assume the largest flight trajectories (21). Blanchard, cited by Umback and Lembke (24), indicated that, after the initial break-up of the main stream, the water droplets will further deform or disintegrate depending on the tangential flight velocities and the droplet sizes. In modelling the the flight of water droplets from a sprinkler the following assumptions were made:

a. The viscous component of the drag force acting on the water droplet is negligible since the Reynolds number under most flight conditions is greater than 1. The drag coefficient Cd is therefore a function of Reynolds number.

b. The water droplet retains a spherical shape throughout the flight time.

c. The effect of evaporation on droplet size is negligible.

d. For the flight time considered, the wind velocity is constant with a uniform vertical profile. The wind resistance acts only in the horizontal direction.

Taking the above assumptions into consideration, the equations of motion of flying water droplets were derived. The forces acting on a water particle at a particular instant in flight are the drag force (F_d), the gravitational force (mg), and the inertia force ($m\ddot{x}$) as shown in figure 2. Applying D'Alembert's principle, the sum of forces on the particle in the inertial reference frame (R) equals zero.

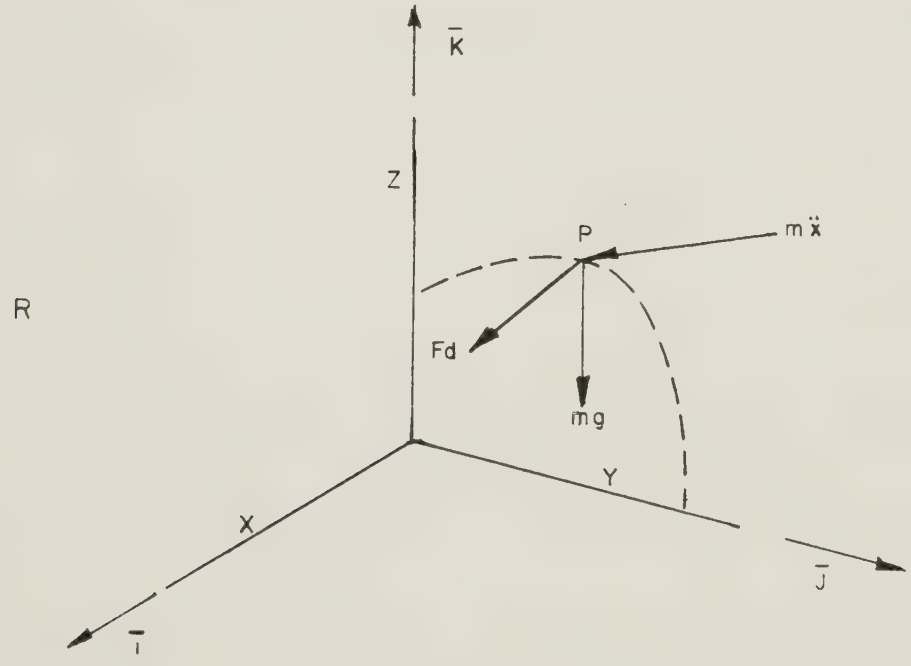

Figure 2. Forces acting on a water droplet in free flight.

The drag force acts in a direction opposite to that of the relative velocity between the particle and the air and is given by the equation:

$$F_d = -kV^2 \qquad (1)$$

and

$$k = 1/2\ C_d\ \rho\ A \qquad (2)$$

where

C_d - the drag coefficient (dimensionless)

ρ - the density of air (slugs/ft^3)

A - projected area of the spherical droplet (ft^2)

Consider a water particle at an instant (t) in flight whose position relative to the ground was described by a coordinate system R(x,y,z) as shown in figure 1. Assume $\dot{x}$, $\dot{y}$ and $\dot{z}$ to be the positive particle velocity components in the positive x, y and z directions. The velocities of the water particle (p) and wind (w) were given as:

$$\bar{V}_p = \dot{x}_p i + \dot{y}_p j + \dot{z}_p k \qquad (3)$$

$$\bar{V}_w = \dot{x}_w i + \dot{y}_w j \qquad (4)$$

The relative velocity between the water particle and the wind is:

$$\bar{V}_R = (\dot{x}_p - \dot{x}_w)\ i + (\dot{y}_p - \dot{y}_w)\ j + \dot{z} k \qquad (5)$$

$$\bar{V}_R = \left((\dot{x}_p - \dot{x}_w)^2 + (\dot{y}_p - \dot{y}_w)^2 + \dot{z}_p^{\,2} \right)^{1/2} \qquad (6)$$

with α, β and γ defined as the angles the relative velocity vector V_R makes with the x, y and z coordinates respectively; the drag force can be resolved in x, y and z directions to obtain:

$$\bar{F}_d = f_x \bar{i} + f_y \bar{j} + f_z \bar{k}$$

$$f_x = -kV_R^2 \cos \alpha$$

$$f_y = -kV_R^2 \cos \beta$$

$$f_z = -kV_R^2 \cos \gamma$$

where the directional cosines are:

$$\cos \alpha = (\dot{x}_p - \dot{x}_w / V_R)$$

$$\cos \beta = (\dot{y}_p - \dot{y}_w / V_R)$$

$$\cos \gamma = (\dot{z} / V_R)$$

Substituting for α, β and γ the components of the drag force are:

$$f_x = -kV_R(\dot{x}_p - \dot{x}_w) \qquad (7)$$

$$f_y = -kV_R(\dot{y}_p - \dot{y}_w) \qquad (8)$$

$$f_z = -kV_R(\dot{z}_p) \qquad (9)$$

Summing the forces acting on the particle we obtain the following reactions:

$$F_x = 0 = -m\ddot{x}_p - kV_R(\dot{x}_p - \dot{x}_w)$$

$$F_y = 0 = -m\ddot{y}_p - kV_R(\dot{y}_p - \dot{y}_w)$$

$$F_z = 0 = -m\ddot{z}_p - kV_R\dot{z}_p - mg$$

The accelerations of the particle in the x, y, z direction are:

$$\ddot{x}_p = -\frac{k}{m} V_R (\dot{x}_p - \dot{x}_w) \qquad (10)$$

$$\ddot{y}_p = -\frac{k}{m} V_R (\dot{y}_p - \dot{y}_w) \qquad (11)$$

$$\ddot{z}_p = -\frac{k}{m} V_R \dot{z}_p - g \qquad (12)$$

The differential equations (10, 11, 12) were solved for known initial conditions by means of a continuous simulation modelling program (CSMP). The model performs continuous integration of the particle acceleration and velocity during the specified flight time (t). The simulation model not only describes the trajectory of the particle in flight but also permits the geometry of the wetted pattern to be defined when the water particle strikes the ground surface.

The ratio (k/m) must be known to solve the differential equations. The mass of the particle (m) for a predetermined particle diameter

(d) is obtained by using the earlier assumption that the droplet is spherical in shape. Therefore,

$$A = \frac{\pi d^2}{4} \tag{13}$$

and

$$m = \frac{(\gamma_w)(V_o)(G_s)}{g} \tag{14}$$

where,

A - projected area of the spherical droplet (ft^2)

d - diameter of droplet (ft)

g - acceleration due to gravity (ft/sec^2)

V_o - volume occupied by spherical droplet (ft^3) = $\frac{1}{6}\pi d^3$

γ_w - density of water (62.4 lb/ft^3)

G_s - specific gravity of water (dimensionless)

The mass density of the air (ρ) is obtained from the relation:

$$\rho = (\frac{1}{vg}) \quad (slugs/ft^3) \tag{15}$$

where,

v - specific volume of air at 65°F

The drag coefficients (C_d) were estimated from the diagram as a function of Reynolds number R_e:

$$R_e = (\frac{Vd}{\nu}) \tag{16}$$

where,

ν - kinematic viscosity of air for atmospheric pressure (1 atm) at air temperature of 65°F (ft^2/s) (8).

Various values of the ratio ($-\frac{k}{m}$) are determined for selected range of discrete values of particle diameters (d) and the associated initial velocities by using the above relationships.

Initial analysis indicated that the simulated patterns could

be categorized into two types:

a. when no wind condition existed, the wetted patterns approximated a circular shape that was described by the equation of a circle ($x^2 + y^2 = r^2$).

b. with the inclusion of wind as a vector in the initial conditions, the resulting skewed wetted patterns were best approximated by joining two halves of two ellipses with a common minor axis ($x^2/a^2 + y^2/b^2 = 1$ and $x^2/e^2 + y^2/b^2 = 1$).

These geometric variables (a, b, c, e, and x) were simulated in the model to represent all possible wetted patterns that resulted from the initial conditions considered in this study.

3.2 Determination of Predicted Wetted Patterns by Interpolation.

The basic wetted patterns that were simulated in the first part of the model were defined by the variables a, b, c, e and x; where a, b and e are the semi-axes of the elliptical shaped pattern, c the location of maximum application rate relative to the sprinkler and x is the radius of the circular pattern when no wind condition prevail. (See fig. 3). For specific values of the system variables such as sprinkler nozzle angles (γ), sprinkler height (z) and wind velocity V_w, these geometric variables (a,b, c, e and x) were interpolated from those simulated with the measured particle size (P_s) and initial particle velocity (V_{pi}) as the specified arguments. A two dimensional interpolation technique (the natural bicubic spline approximation) was used, in this section of the model, to interpolate the given set of unequal spaced data (9). A subroutine, ICS2VU, from the IMSL statistical package (12), was used to do the interpol-

ation. The subroutine was necessarily incorporated in the model to eliminate the lengthy computer time required in simulating the predicted wetted patterns for all combinations of initial conditions.

Preliminary investigation of simulated variables a,b, c, e and x suggest a linear relationship for a change in wind velocity. Therefore, the predicted wetted patterns for measured wind velocity within the simulated range were approximated by linear interpolation. The predicted wetted patterns outside the simulated range of wind velocities were extrapolated assuming that the linear function holds.

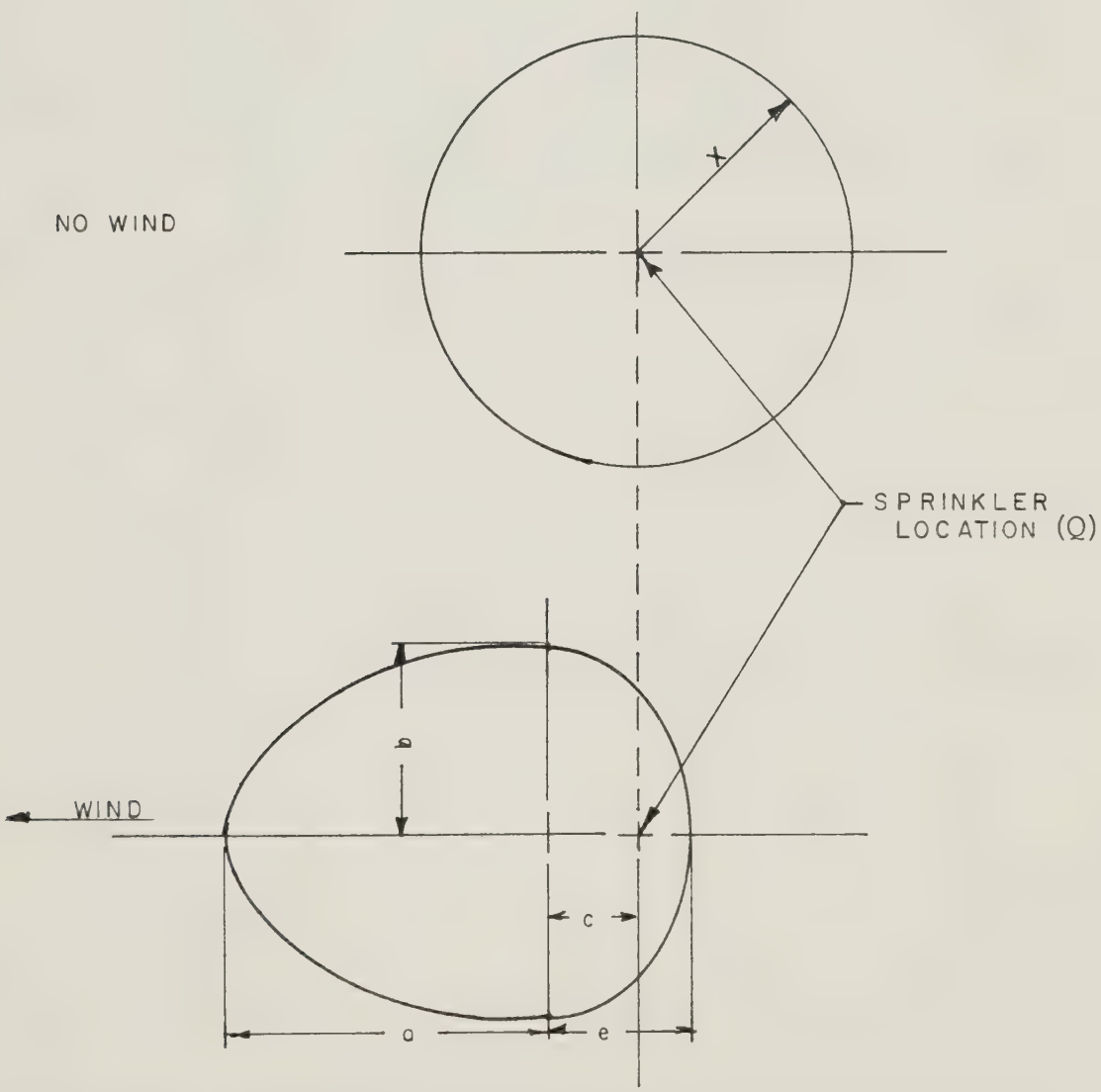

Figure 3. Geometric variables and configurations describing the sprinkler patterns.

3.3 Performance Parameters of C.P. Systems

This section of the model evaluates performance parameters of a C.P. system. The relative performance is assessed in terms of application depth (D_s), application rates(A_s) and the uniformity coefficient (C_u). In order to determine these performance parameters, the dimensions (a,b,c,e and x) of the predicted wetted patterns and the system characteristics were used in the program proper. The system characteristics were the maximum application rates for the triangular distribution (H_t) and the elliptical distribution (H_e), the sprinkler volume discharge (V) and the angular velocity of the centre pivot (ω_t).

In modelling the distribution of individual sprinklers along the lateral, triangular and semi-elliptical distribution profiles were assumed from earlier research (4). The two distribution profiles differ in that the maximum application rate of the elliptical case is approximately half that of the triangular profile. The location of maximum application rates for circular wetted patterns is located immediately below the sprinkler, but in the case of skewed wetted patterns, however, this is offset a distance (C) from the sprinkler (Q) along the major axis. The assumed distribution profiles for both circular (no wind condition) and skewed wetted patterns are shown in figure 4. The maximum application rates for circular wetted patterns (no wind condition) are given by the following:

$$H_t = \frac{289V}{\pi x^2} \qquad (17)$$

$$H_e = \frac{45.94V}{x^2} \qquad (18)$$

where:

H_t - maximum application rate of circular wetted pattern with

triangular distribution (in./hr)

H_e - maximum application rate of circular wetted pattern with elliptical distribution (in./hr)

V - discharge volume of sprinkler (gpm)

x - radius of circular wetted patterns (ft)

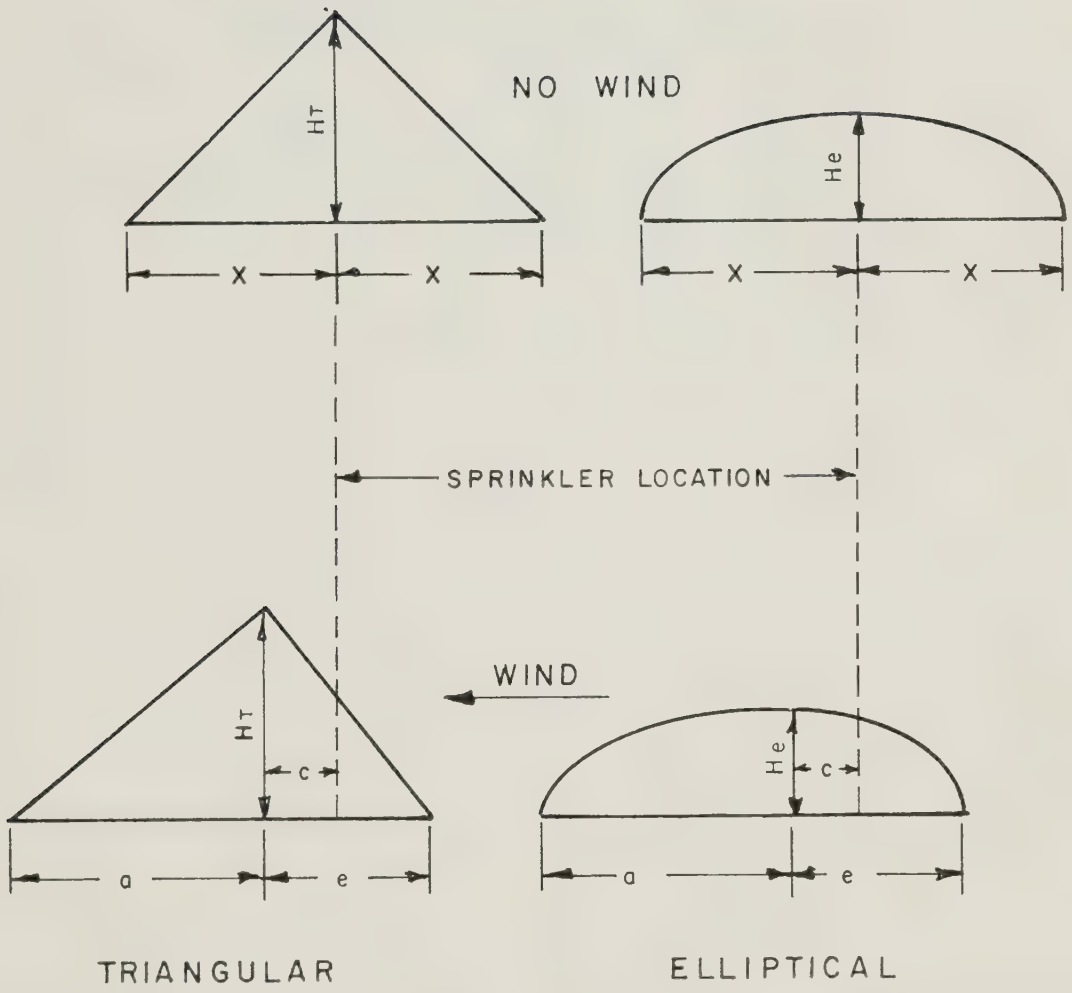

Figure 4. Triangular and Elliptical distribution profiles under wind and no wind conditions.

For wetted patterns distorted by the effect of the wind, the maximum application rates are:

$$H_{tw} = \frac{578V}{\pi (ab + be)} \qquad (19)$$

$$H_{ew} = \frac{1}{2} H_{tw} \qquad (20)$$

where:

H_{tw} - maximum application rate of distorted wetted patterns with triangular distribution (in./hr)

H_{ew} - maximum application of distorted wetted pattern with elliptical distribution (in./hr)

a,b,e - dimensions of skewed wetted patterns (ft)

In determining the application rates (A_p) for any given point within the wetted pattern, the location of point P and the point of maximum application rate (H_p) need to be described with reference to the centre pivot (0). The analysis considers the two following cases, depending on whether or not the distorting effect of the wind is included.

Case I: Circular wetted patterns (no wind condition).

Consider an instant (t) when the lateral (OM) makes an angle (θ) with the (x) coordinate, and a sprinkler located at point (Q) along the lateral imposes a circular wetted pattern of radius(x), as shown in figure 5 . Let P be any point within the wetted pattern (T), and the distance ($\overline{QP}$) in relation to the point (O) is:

$$\overline{QP} = \left(R^2 + S^2 - 2RS \cos (\theta - \beta) \right)^{\frac{1}{2}} \qquad (21)$$

where:

$\overline{QP}$ - distance of point P to the sprinkler location Q (ft)

R - distance of sprinkler Q to the pivot O (ft.)

S - distance of point P to the pivot O (ft)

θ - angle between the lateral OM and the x coordinates (radians)

P - point represents a measuring recepticle along a row of cans

β - angle between $\overline{OP}$ and the x coordinate (radians)

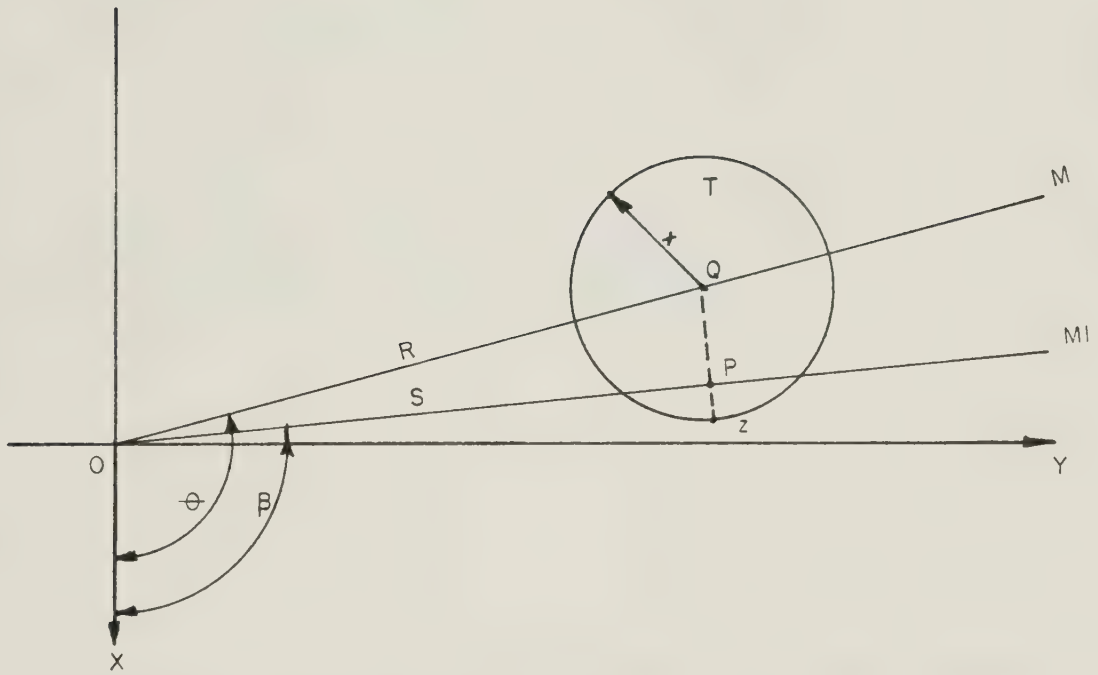

Figure 5. Circular wetted pattern of a moving sprinkler under no wind condition.

The application rate of the sprinkler (Q) at the point (P) for both triangular and elliptical distribution are:

$$A_{tr} = H_t - \left(\frac{H_t}{x} \quad QP \right) \qquad (22)$$

and

$$A_{el} = \frac{H_e}{x} \left(x^2 - \overline{QP}^2 \right)^{1/2} \qquad (23)$$

In simulating the rotating lateral the effect of overlap by adjacent sprinkler patterns is incorporated as:

$$A_{tr} = \sum_{i=1}^{n} \left[H_{t(i)} - \frac{H_{t(i)}}{x_{(i)}} \overline{QP}_{(i)} \right] \qquad (24)$$

$$A_{el} = \sum_{i=1}^{n} \left[\frac{H_{e\ (i)}}{x_{\ (i)}} \left(x^2_{\ (i)} - \overline{QP}^2_{\ (i)} \right)^{\frac{1}{2}} \right] \qquad (25)$$

where:

i = subscript referring to the i^{th} sprinkler on the lateral.

n = number of sprinklers with overlapping wetted patterns.

The application rate at the point (P) varies continuously as the moving wetted pattern passes over it in a given period of time. For a small time interval (Δ t) the application rate is assumed constant, the application depth at point (P) is hence a sum of the partial instantaneous application depths:

$$D_{tr} = \left[\sum_{i=1}^{n} H_{t(i)} - \frac{H_{t(i)}}{x_{(i)}} \overline{QP}_{(i)} \right] \sum_{j=1}^{T} \Delta t_{(j)} \qquad (26)$$

and

$$D_{el} = \left[\sum_{i=1}^{n} \frac{H_{e(i)}}{x_{(i)}} \left(x^2_{(i)} - \overline{QP}^2_{(i)} \right)^{1/2} \right] \sum_{j=1}^{T} \Delta t_{(j)} \qquad (27)$$

where

j - subscript referring to j^{th} time interval t.

T - total time when point P is located within the wetted pattern (hrs)

Case II: Skewed Wetted Patterns

In this case the skewed wetted pattern assumes an elliptical shape with wind acting in a direction parallel to the principal axis of the ellipse making an angle (θ) with the lateral (OM) (see fig. 6). The point of maximum application rate (A) is displaced a distance (c) from the sprinkler location (Q) on the lateral. To compute the application rate of any point (P) located within the skewed wetted pattern, the dimension $\overline{AP}$ and $\overline{AZ}$ in relation to the pivot O are required.

$$\overline{AP} = \left(U^2 + V^2 \right)^{1/2} \qquad (28)$$

where:

$\overline{AP}$ - distance between the point P and the point of maximum application rate A. (ft.)

U - S cos $(\beta - \gamma)$ - R cos $(\gamma + \theta)$. (ft)

V - S (Sin β cos γ - cos β sin γ) - R sin $(\theta + \gamma)$ (ft)

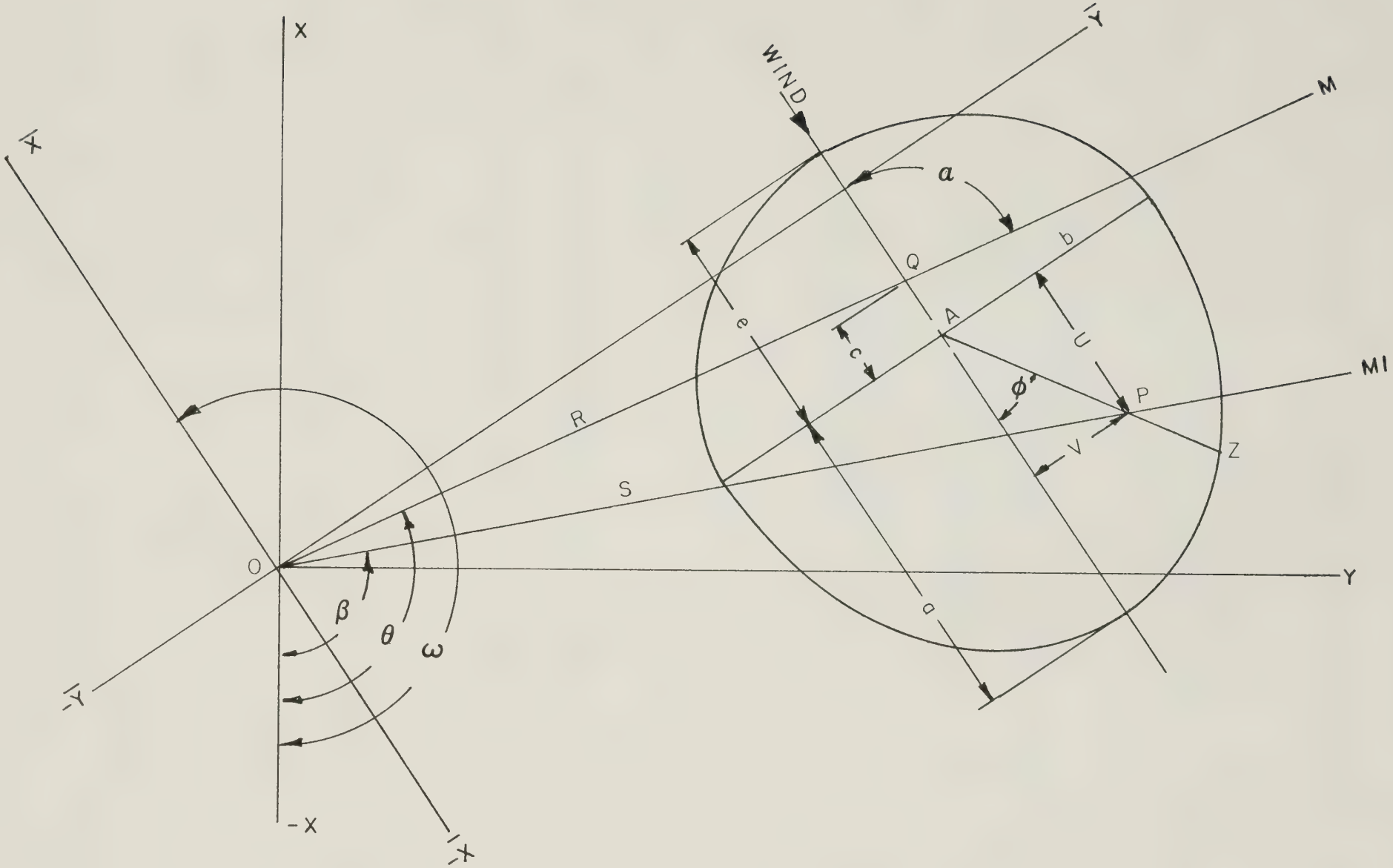

Figure 6. Elliptical wetted pattern of a moving sprinkler under windy conditions.

R - distance between the sprinkler at Q and the pivot O. (ft)

S - distance between the point P and the pivot O. (ft)

c - distance between point A and the sprinkler Q. (ft)

θ - angle the lateral makes with the x coordinate of the pivot O. (ft)

γ - ($\alpha + \theta$). (radians)

α - angle between the lateral and the direction of wind. (radians)

β - angle between OP and the x coordinate of the pivot O. (radians)

and,

$$\overline{AZ} = \left(\frac{a^2 b^2}{a^2 \cos^2\phi + b^2 \sin^2\phi} \right)^{1/2} \qquad (29)$$

where:

$$\phi = \tan^{-1}\left(\frac{U}{V}\right),$$

a,b - the semi-axes of the ellipsoidal wetted pattern.

The major axis (a) is equal to e in Equation (29) when the point of interest (P) lies above the minor axis (b).

The application rates at the point (P) of the sprinkler at (Q) and from the adjacent contributing sprinklers are:

$$A_{TR} = \sum_{i=1}^{n} \left[H_{T(i)} - \frac{H_{T(i)}}{\overline{AZ}_{(i)}} \overline{AP}_{(i)} \right] \qquad (30)$$

$$A_{EL} = \sum_{i=1}^{n} \left[\frac{H_{E(i)}}{\overline{AZ}_{(i)}} \left(\overline{AZ}^2_{(i)} - \overline{AP}^2_{(i)} \right)^{1/2} \right] \qquad (31)$$

where:

A_{TR}, A_{EL} - the application rates at a point (P) from the pivot (O) for the triangular and elliptical distribution profiles, respectively. (in./hr).

i - subscript referring to i^{th} sprinkler on the lateral.

n - number of sprinklers with overlapping skewed wetted patterns at point (P).

The total application depths at the point (P) for the cummulative time interval (Δt) are:

$$D_{TR} = \left[\sum_{i=1}^{n} H_{T(i)} - \frac{H_{T(i)}}{\overline{AZ}_{(i)}} \overline{AP}_{(i)} \right] \sum_{j=1}^{n} \Delta t_{(j)} \qquad (32)$$

$$D_{EL} = \left[\sum_{i=1}^{n} \frac{H_{E(i)}}{\overline{AZ}_{(i)}} \left(\overline{AZ}^2_{(i)} - \overline{AP}^2_{(i)} \right)^{1/2} \right] \sum_{j=1}^{n} \Delta t_{(j)} \qquad (33)$$

where:

D_{TR}, D_{EL} - the respective application depths at point (P) for triangular and elliptical distribution profiles within a time span (T). (in.)

T - total time when the point (P) is located within the wetted patterns

The uniformity of distribution for the C.P. system was evaluated by means of the following coefficients of uniformity:

$$Cu_{(1)} = 100 \left[1 - \left(\frac{\sum S_{(i)} \left| D_{(i)} - \frac{\sum \left(D_{(i)} - S_{(i)} \right)}{\sum S_{(i)}} \right|}{\sum D_{(i)} \; S_{(i)}} \right) \right] \quad (34)$$

$$Cu_{(2)} = 100 \left[1 - \left(\frac{\sum \left| D_{(i)} - \frac{\sum D_{(i)}}{N} \right|}{\sum D_{(i)}} \right) \right] \quad (35)$$

where:

$Cu_{(1)}$, $Cu_{(2)}$ - the respective weighted and non-weighted Christiansen coefficients of uniformity (percent).

$D_{(i)}$ - the application depth at point (i). (in.)

$S_{(i)}$ - the distance from the pivot O to the point (i). (ft)

i - subscript referring to the i^{th} point along the line of measuring cans.

N - the number of observations.

These two coefficients of uniformity were incorporated in the model to assess their sensitivity in relation to the effects of variable windy conditions affecting the C.P. system.

The application depths at each predetermined point along a given radial line were computed for both triangular and elliptical distributions. The system analysed, in this study, took into account the overlap effect of adjacent sprinklers along the lateral. The total depths at a distance (S) from the pivot were determined by solving the equations (30), (31) and (32),

(33) for one pass of the lateral at half degree increments ($\Delta\alpha = \frac{1}{2}°$). The overall application depth distributions for both distribution profiles are determined by using a numerical method in solving the equations. Considerable computer time is needed since a large number of repetitive solutions are required.

The Fortran IV Computer Language was used to program the modelling formulation simulating the dynamic operation of two manufactured centre pivot irrigation systems (Circle Master, Valley 1160) used in Southern Alberta.

Chapter IV

CENTRE PIVOT SYSTEM SIMULATION MODEL PROCEDURE

Sprinklers of the C.P. systems were modeled in the program using a CSMP technique to determine their respective wetted patterns. The model took into consideration the effect of wind. Predicted wetted patterns were then modeled in the main program to assess the performance of the functional C.P. system.

4.1 Model Input Requirements

The sprinkler simulation model was executed on the IBM 1800 digital computer using the CSMP package. The program proper, however, was written in Fortran IV for use with the University of Alberta, Michigan Terminal System (MTS). Program execution was performed on the Amdal 470 computer. Once the model was programmed, the rapid speed of computation permitted the study of variations attributed to particularly sensitive input parameters.

The information required in the sprinkler simulation model deals with the geometric and physical characteristics of the sprinklers and the influencing environmental parameters. These parameters are listed as follows along with their corresponding variable names:

1. Angle of sprinkler range nozzle (ALFA)
2. Height of sprinkler above ground surface (ZH)
3. Projected area of spherical water particle (AP)
4. Mass of water particle (MAS)
5. Initial particle velocity (IV)
6. Drag coefficient (DCF)

7. Density of air (DA)
8. Acceleration due to gravity (AG)
9. Wind velocity and direction (WV) and (WD)
10. Total integration time and the desired integration interval (DT) and (TI) respectively.

For the range of initial conditions considered in this study, the corresponding geometric variables (a, b, c, e and x) obtained as output from the above simulation program are stored as arrays in disc files for specific input ranges of particle size (xx) and particle initial velocity (yy). These geometric variables (a, b, c, e and x) were assigned variables TA, TB, TC, TE and TX in the storage files.

The input information required in the main simulation program deals with not only the measurable environmental and particle trajectory parameters but also the system characteristics. The measured field parameters are:

1. Particle diameters (PS)
2. Wind velocities (VW)
3. Initial particle velocities (VIN).

The program at this stage performs the necessary two stage interpolation to determine the predicted wetted patterns of the individual sprinklers.

The system characteristics are next entered as:

1. Location of sprinklers on the lateral (R)
2. Number of sprinklers on the lateral (M)
3. Sprinkler volume discharged (VV)
4. Angular velocity of lateral (T)
5. Direction of wind velocity relative to the lateral (AL)
6. Location of measuring receptacles along a line relative to pivot (Y)

7. Number of measuring receptacles along the line (MO)
8. The angle between the lateral at any position and the x axis of a co-ordinate system established at the pivot O (THE)
9. Integer specifying the number of increments of ($\Delta\theta$) for constant wind velocity and direction (INC)
10. Angle between the line of receptacle (OP) and the x axis (BETA)

The computer model then completes the computation to determine the outputs for C.P. system performance analysis. Several options are available in the model to determine the sensitivity of the input variables in an attempt to obtain optimum performance of the C.P. system.

4.2 Model Operational Logic

The sets of simultaneous differential equations, that describe the flight dynamics of a water particle emitted from a sprinkler, were solved by means of the CSMP model using the block diagram approach. The schematic diagram showing the functional blocks for this model is shown in Appendix (I). The program uses basically two Fortran statements, namely the configuration statements which define the inter-connection and function operation of the blocks and the parameter statements that associate numerical values with the block elements to particularize their functions.

The C.P. system simulation model performs the following functions at various stages of the program:

(a) Firstly, the program compiles the input data (i.e. the output information of the CSMP program, measured field parameters and system characteristics) from the source files using several read statements.

(b) Interpolation is then used to determine the predicted wetted patterns for each individual sprinkler along the lateral. The predicted wetted patterns are defined for a range of measured field parameters and characteristics of the C.P. system considered. When wind effects were taken into account, both two-dimensional and linear interpolations were performed; however, for no wind situations only two-dimensional interpolation was required.

(c) The model then proceeds to perform a search to determine whether the point (P_1) is enclosed within the boundaries of wetted patterns, and the partial application rates for both triangular and elliptical distribution (TR, EL) are calculated; then separately summed to compute the total application rates. The application depths for both distributions are computed as the product of the total application rates and the differential time (Δt) required for the lateral to sweep across an angle of half a degree. However, if the point (P_1) is not enclosed by any wetted patterns the program continues to select the next adjacent (P_2) along the line ($\overline{OM1}$), as shown in figures 5 and 6 . A similar test and computation is imposed on point P_2, nevertheless, when five consecutive points (P_1, P_2, ... P_5) are found to be outside the boundaries of the wetted patterns, the search and test is extended to the points along the next lines ($\overline{OM}_2$) and ($\overline{OM}_3$). This analysis was performed for 180 half a degree increments of the lateral position to ensure that the initial and final influence of the moving wetted patterns on the points along line ($\overline{OM}_1$), ($\overline{OM}_2$) and ($\overline{OM}_3$) were fully considered. The

total application depth for each point (P_1) is computed as the sum of each depth calculated at every increment of the lateral position considered.

(d) Finally, the coefficients of uniformity for the C.P. system are computed.

The flow chart of the program simulating the C.P. system is shown in Appendix (II). After completing the computation of performance parameters for all desired input variations the program may be started over at the beginning to model a different set of system characteristics or terminated.

CHAPTER V

COLLECTION AND ANALYSIS OF FIELD DATA

Two different centre pivot sprinkler irrigation systems were selected in order that their relative performance could be evaluated. Both C.P. systems were located on sites that were free of wind barriers so that the micro-climate represented the typical climatic conditions of Southern Alberta. Perennial forage crops with rapid growth rates such as alfalfa and grass were grown on these sites. The frequent harvest of these crops permitted repeat measurement of application depths without the interference of the crops.

5.1 C.P. System Characteristics

The two C.P. sprinkler systems under investigation were 'Valley 1160' manufactured by Valmont Industries Inc.,Valley, Nebraska, U.S.A., and 'Circle Master' manufactured by Pierce Corp., Eugene, Oregon, U.S.A..

The two systems were selected because of their conceptual differences in design such as height of lateral, rotational speed of travel, sprinkler spacing, number of sprinklers and the type of sprinklers used. The general specifications of the systems are given in table 1. The detailed performance data for the sprinklers used in both systems is given in Appendix (3). The majority of these system parameters for either systems were fixed as specified by their manufacturers. Evaluation of variation in system performance attributed to change in system parameters were not possible since field measurements were taken on sites at the disposal of the owners. The rotational speed of system travel, however, is the only parameter adjustable to some degree. Two rotation speeds for each system were used to increase or decrease the application rates of the sprinklers.

TABLE 1. GENERAL APPLICATION OF TWO C.P. IRRIGATION SYSTEMS

Type of System	Lateral Length	Drive Mechanism	No. of Towers	No. of sprinklers on lateral	Sprinkler Spacings	System Capacity	Rate of Travel
	Ft				Ft	(U.S.) G.P.M.	H/R
Circle Master	1287	Electric Motor	10	93 + 2*	variable	1100	33.4 or 42
Valley 1160	1291	Water Cylinder	13	40 + 2*	32	1000	64 or 67

* Large volume "end gun" nozzles

5.2 Experimental Layout for Field Test

The application depths for the C.P. systems are traditionally measured using a grid system of receiving receptacles. Conventional cans (4 in. in diameter and 6 in. in height), held in place by a 9 in. long rod were used to capture the water droplets. In each row the cans were spaced 20 feet apart, the first can, however, was spaced 10 feet from the centre pivot. The accuracy of the measured application depths was enhanced by placing two other rows of cans set at an angle of 3 degrees apart. In an earlier analysis (section 3-3) the rows of measuring cans represented lines ($\overline{OM}_1$), ($\overline{OM}_2$), and ($\overline{OM}_3$), while the individual cans were designated as points P_1, P_2 ... P_n. Additional rows of measuring cans were placed in a similar fashion at intervals of 90 or 120 degrees between the grids of cans as shown in figures 7a and 7b respectively.

From meterological records the prevailing wind directions in Southern Alberta are west and south west. The grids of measuring cans on both sites were placed in directions as shown in figures 7a and 7b in order that the varied effect of the wind direction relative to the lateral could be readily investigated.

Meteorological data was recorded at the station installed on the site sufficiently distanced away from the effect of the sprinklers. A thermo-hygrograph and a wind recorder were located in a standard meterological booth 4 feet above the ground. Temperature and relative humidity were measured by the thermo-hygrograph and recorded on a chart calibrated for a period of 7 days. Wind velocity and direction were sensed 9 feet above the ground by a weather vane and separately recorded on charts of an event recorder. The instruments functioned continuously during the experimental period.

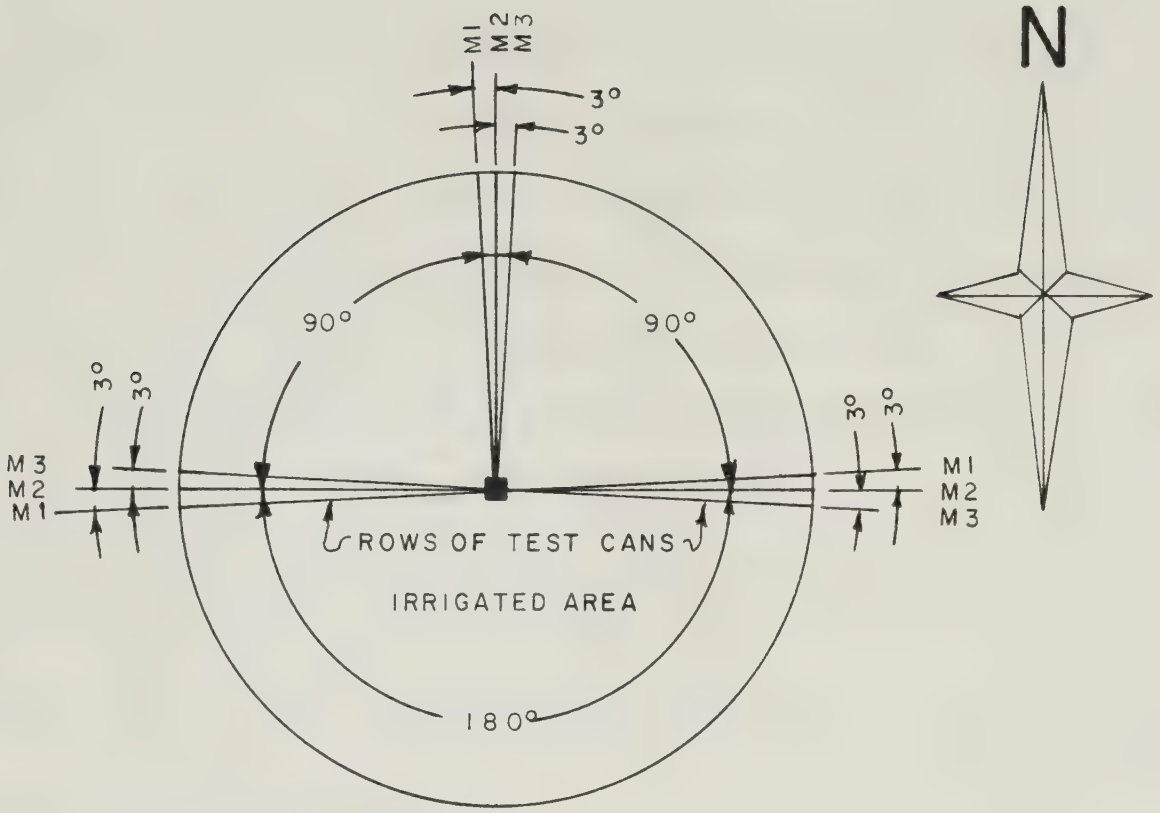

Figure 7a. Schematic of experimental field layout at site 1. (Cranford, Alberta.)

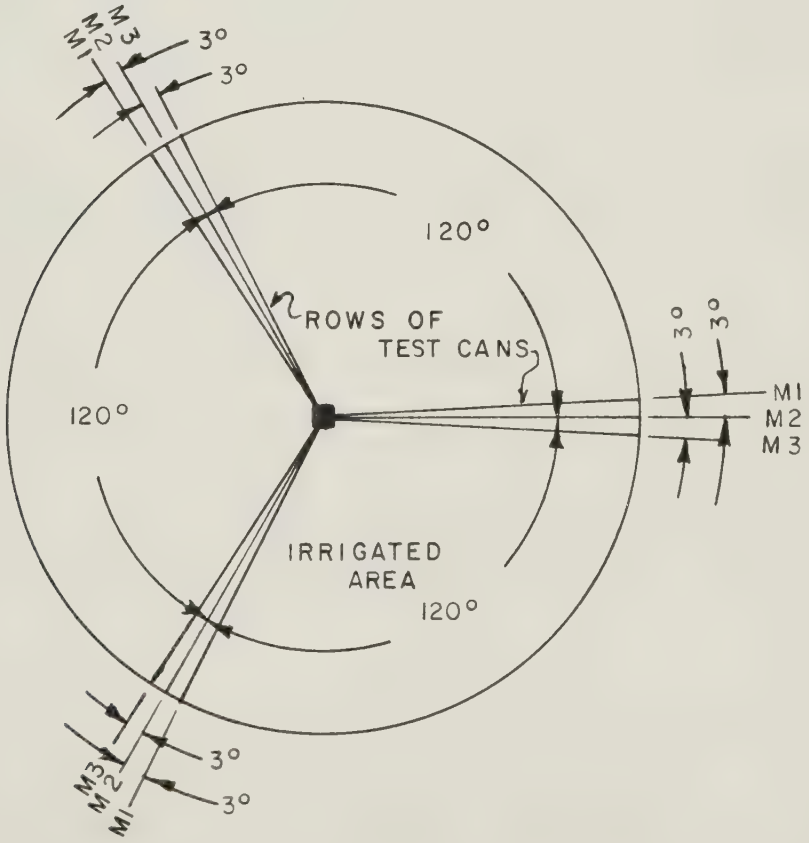

Figure 7b. Schematic of experimental field layout at site 2. (Granum, Alberta.)

The amount of precipitation and evaporation during the experimental period were measured using a set of control receptacles. These receptacles were identical to the measuring cans used in application depths measurements and were located away from the effect of the sprinklers. In addition to this equipment, two tipping bucket rain gauge recorders were used in the experiment. The rain gauges were calibrated to respond to a change of 1/100 of an inch of precipitation depth. Continuous recording for 24 hours was recorded on the charts. The tipping bucket rain gauge recorders were used to spot check the rainfall precipitation and to synchronize the measurement of application depths to the meteorological data recorded.

5.3 Application Depth Measurements

The measurements of application rates for both C.P. systems were made for two rotational speeds of travel during periods of varied weather conditions. After the lateral made a complete pass over the grid of cans, the volume of water collected in each can was measured using a graduated cylinder and converted to a depth in inches. When application depths measurements were delayed, the necessary corrections were made for either evaporation losses or gains due to precipitation. The loss or gain was estimated from the change in volume in the control measuring cans. For the hydraulic driven C.P. system (Valley 1160), some of the measuring cans were affected by the water discharge from the piston. Measurements in this case were discarded and an average reading was taken by considering the measurements of the adjacent cans.

5.4 Sprinkler Droplet Size Determination

The size of the droplets with the longest trajectories was determined for the purpose of simulating the sprinkler's wetted patterns. Droplet

sizes were measured for each individual sprinkler of both C.P. systems with the exception of the large volume 'end gun' sprinklers. In the case of sprinklers with double nozzles, droplets emitted by the range nozzle only were considered. The size of droplets were determined experimentally using the stain method (10).

Filter papers (Whatman No. 1) sprayed with a suspension of methylene blue in carbon tetrachloride gave permanent stains when a water droplet fell on the surface. The diameter of stain was assumed proportional to the assumed spherical flight diameter of the particle. Calibration of equation (2) (section 2.3.1) for the filter paper, conducted in the laboratory with known diameters of water droplets, indicated (see figure 8) that the equation can be used in approximating the droplet size measured in the field.

For field measurements of the emitted droplets a box containing the stain-sensitive filter paper was used. The box had a sliding surface that operated like a camera shutter. The sprinklers were held stationary when the filter paper was exposed to the farthest falling droplets. Repeated sampling was necessary for each sprinkler to ensure that the falling droplets did not give large overlapped stains. From these resulting stains the average diameter of the droplets for each sprinkler was estimated.

5.5 Field Data Analysis

The variations in wind velocities and wind directions were recorded continuously throughout the experiment. Since it was not possible to determine the application rates measured at each individual can in the row during a complete pass of the lateral, the effects of wind on each sprinkler cannot be fully evaluated. Therefore, a mean wind velocity and direction was used to relate the wind effects to the uniformity distribution of the sprinklers.

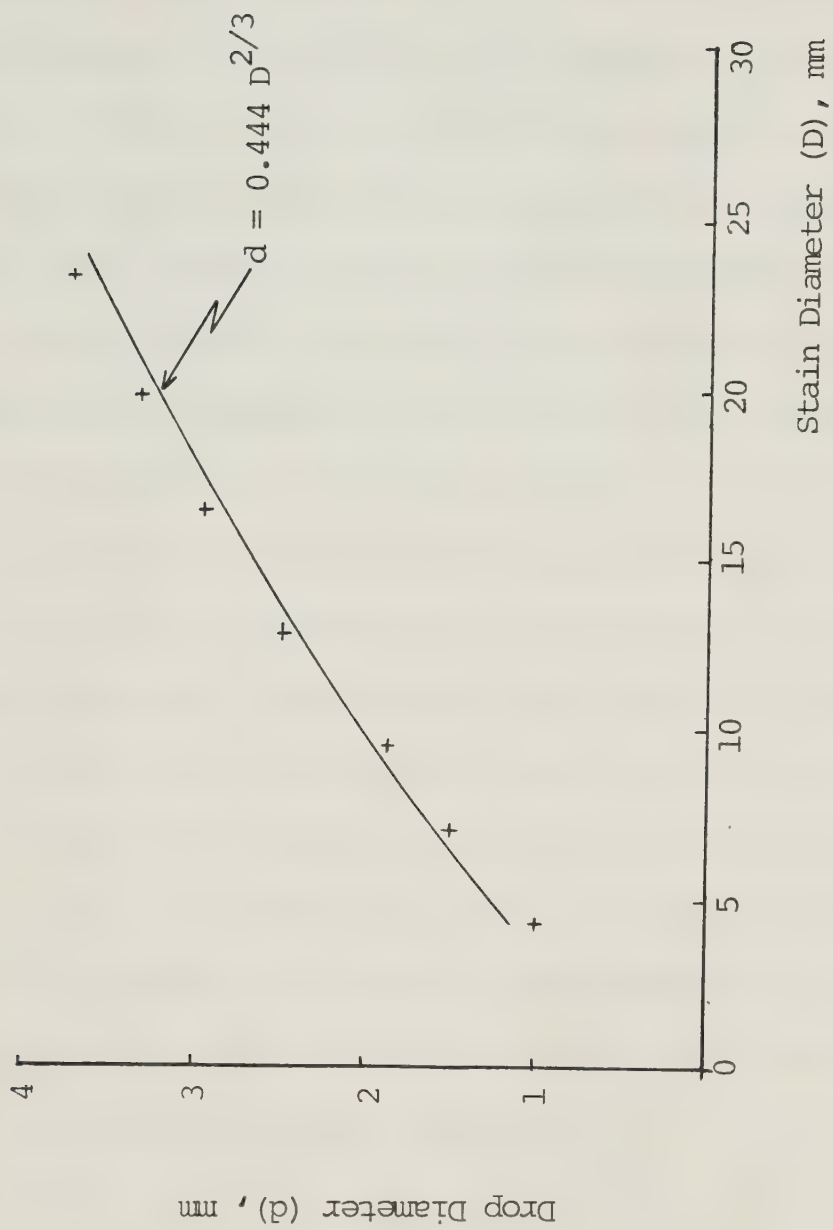

Figure 8. Calibration curve for determining the sprinkler droplet size.

This mean velocity and direction was derived as an average of the values recorded for every 15 minute time interval throughout the duration of a single lateral pass.

Wind velocities and directions were required as input variables in the C.P. performance model as discussed in Chapter IV, (section 4.1). Because of the lengthy time taken for the lateral to make a complete pass across the grid of measuring cans (approximately 14 hours, 1/4 revolution), simulation of each change of the continuously fluctuating wind conditions was not feasible. For this reason, an approximate time interval of 15 minutes was specified during which a representative average wind velocity and direction was computed for each interval throughout the experimental period. The time interval was adjusted to ensure an integer number of half-degree increments of the lateral rotation. This was necessary to facilitate the iterative computation in the main program.

A range of particle sizes and initial velocities of the droplets emitted by the sprinklers was required as input variables in the simulation of predicted wetted patterns. Sufficiently large samples of stains were obtained from field tests for all sprinklers to permit the determination of a range of particle sizes. The average sizes measured in the field were, therefore, assumed to always fall within this range. The range of initial velocities was determined from the manufacturer's specifications of the individual sprinklers as shown in Appendix (IIIA) and (IIIB). The initial velocities were noted for a given discharge and nozzle size.

CHAPTER VI

RESULTS AND DISCUSSION

Simulation of the relative performance of the C.P. system was made possible by first determining the wetted patterns that were developed in the first part of the model (see section 3.1, Chapter 3). The flight of water droplets was simulated for known initial conditions for each sprinkler along the lateral.

6.1 Input Variables for Model Simulating the Flight of Water Droplets

The initial particle velocities (IV) were calculated using the manufacturer's specifications (see Appendix III) as a guide. The droplet flight characteristics were determined from field measurements and applied in the theory that described the forces developed in the moving fluids. Preliminary estimation indicated that approximately 500 computing hours were required on the IBM II80 Computor to simulate the requisite trajectories. To reduce the large number of computations yet maintaining sufficient accuracy, the simulations were performed for all combinations of a particular range of input variables. This range of input variables enveloped all the situations that were encountered in the field. The interval of the discrete values of those variables were selected to maintain the accurracy. The droplet sizes, for example, were input as 2,3,4, and 5 mm in diameter as shown in table (2), for initial droplet velocities of 90 ft/sec and wind velocity of 10 mph. The range of droplet initial velocities (75,80,85,90,95,100,105 ft/sec) and wind velocity (0,10,20 mph)were used in the simulation model for given physical characteristics of each sprinkler. The resulting parameters defined the basic wetted patterns that were used to derive the actual wetted patterns

TABLE 2. TYPICAL INPUT VARIABLES FOR THE SPRINKLER WETTED PATTERN SIMULATION MODEL.

Drop Diameter (D)		Drop Mass (M)	Projected Area (A)	Initial Drop Velocity (I.P.V.)	Reynolds Number (Re)	Drag Coefficient (Cd)	Air Density (ρ)	Wind Velocity (WV)
$ft(x10^{-3})$	mm	$lbs/ft^3(x10^{-7})$	$ft^2(x10^{-5})$	ft/s			$(slugs/ft^3(x10^{-3})$	ft/s
6.56	2	2.86	3.38	90	3690	0.394	2.39	10
9.84	3	9.67	7.61	90	5536	0.384	2.39	10
13.12	4	22.93	13.52	90	7382	0.390	2.39	10
16.40	5	44.79	21.13	90	9227	0.395	2.39	10

by method of interpolation.

6.2 Wetted Patterns

From the output of the simulation model the boundaries of the wetted patterns are geometrically described either by the equations of a circle of radius (x) (no wind condition) or that of two ellipses with a common minor axis. The validity of using these equations used to curve fit the actual simulated wetted patterns are shown in table 3 . The points along the boundary of the wetted pattern are represented in rectangular coordinates, with the same x coordinate for the purpose of statistical comparison. The goodness of fit of these points derived from the simulated model and those obtained from the equations of the ellipse are represented by the correlation coefficient that is in the order of 0.989. Under no wind condition, the correlation coefficients of circular wetted patterns are best fitted as they are equal to 1. The possibility of using a more sophisticated curve fitting technique to obtain the best fit conic equation for distorted wetted pattern is beyond the scope of this study. Similar representation of circular wetted patterns were used by other researchers (11).

The distributions of application rates within the boundaries of a wetted pattern were assumed to approximate a triangular and semi-elliptical profile as suggested by Bittenger and Longenbaugh (4). Under windy conditions the point of maximum concentration is distorted for a distance (c) from the location sprinkler. For a wind velocity of 20 mph, the distortions for a range of particle sizes 2,3,4, and 5 mm are shown in figure 9. The relative displacement of the distortion of the centre of maximum concentration for a given wind velocity is small (in the vicinity of 2 ft), relative to the throw. The previous

TABLE 3. COMPARISON OF THE SIMULATED AND COMPUTED BOUNDARY POINTS OF SPRINKLER WETTED PATTERNS.

Particle size mm, (ft x 10^{-3})											
2 (6.5)	Simulated coordinate (x_s)	ft	-41.0	-38	-34.5	-28	-21.5	-14	-8	8	16	22
	Simulated coordinate (y_c)	ft	12	16.5	20	24	27.5	30	31.2	32	29.5	23
	Computed coordinate (y_c)	ft	12.7	17.7	21.2	25.8	29.0	31.4	32.5		27.1	20.4
	Correlation coefficient (r)						0.984					
3 (9.8)	Simulated coordinate (x_s)	ft	-51.5	-47	-42.1	-34	-27	-20	-10	20	28	33.5
	Simulated coordinate (y_s)	ft	16	28.5	27.5	33	37	40	43	38.2	30	20.5
	Computed coordinate (y_s)	ft	15.5	22.9	28.4	34.6	38.4	41.1	43.4		29.8	20.8
	Correlation coefficient (r)						0.993					

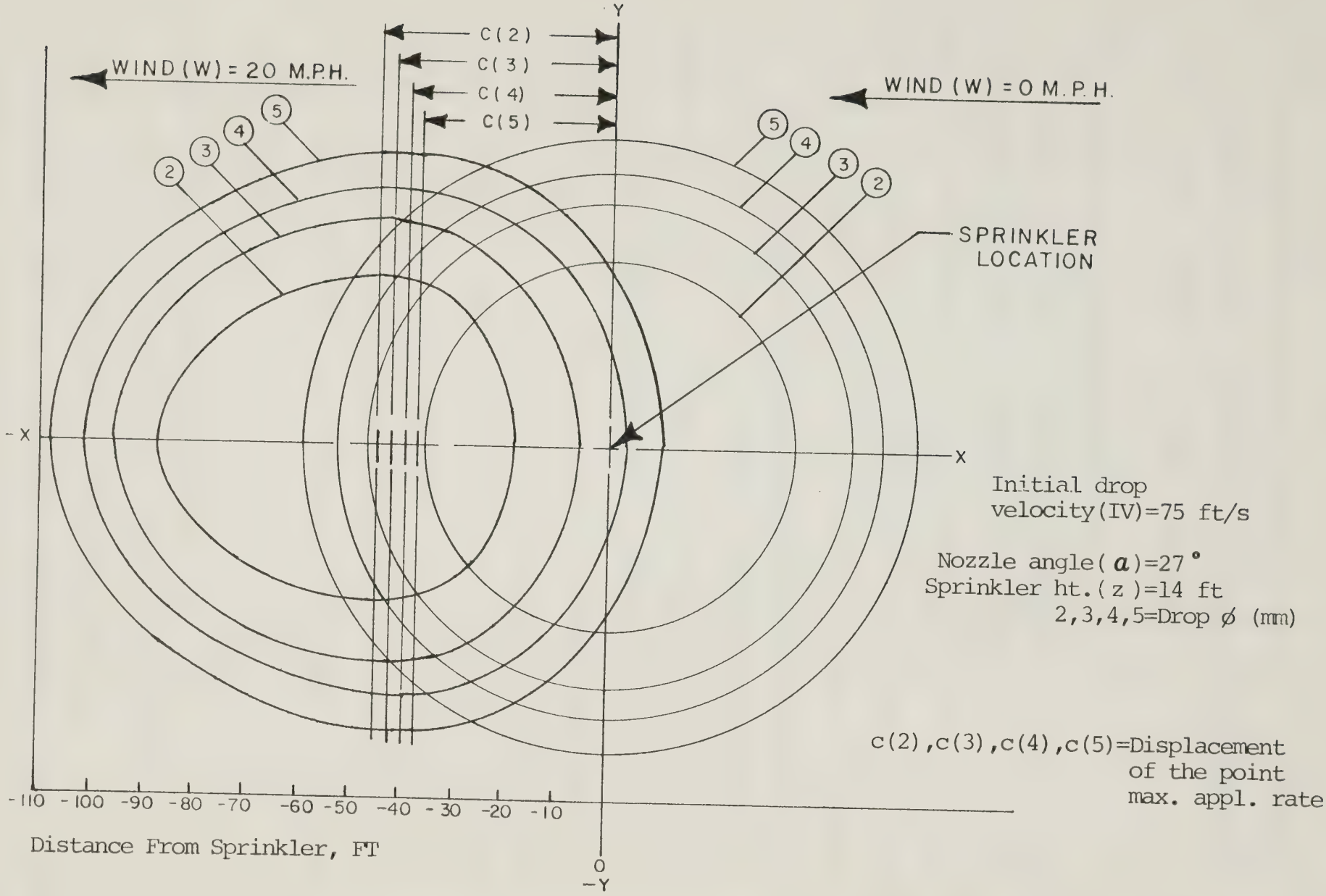

Figure 9. Distribution of droplets inside sprinkler wetted patterns under windy and no wind conditions.

distribution profiles can thus be assumed to hold in the distorted case with the point of maximum concentration located at the displacement (c) of the largest particle (5mm) under consideration.

6.3 Validity of Interpolation Technique

Interpolation from the basic wetted patterns were necessarily incorporated in the model for reasons discussed in section 6.1. The method of interpolation for unequal space data is noted in section 3.2, Chapter 3. Plots of the input variables (d), (IV) and (VW) against the output parameters (g), (b), (c), (e) and (x), as shown in figures (10), (11), (12), (13), (14) and (15), indicated a linear dependence relationship exists. However, the unequal slopes of the plotted lines suggested the use of a two dimensional interpolation technique (the natural bicubic spline approximation). The accuracy of the two dimension interpolation technique was substantiated when correlation coefficients of 0.98 were obtained when interpolated values were compared to those simulated (see table 4). More than two dimension interpolation techniques may be used to increase the accuracy of the desired output parameters for the purpose of reducing the computer simulation time. Accessibility to these programs was not possible during the course of this study.

6.4 Centre Pivot Performance Analysis

In evaluating the performance of the simulation model eleven comparisons of simulated and field data were available for the two C.P. systems tested. The effect of the wind was incorporated in the model as a vector for a fifteen minute sequential interval. The triangular and elliptical distribution profiles were used to represent the actual case.

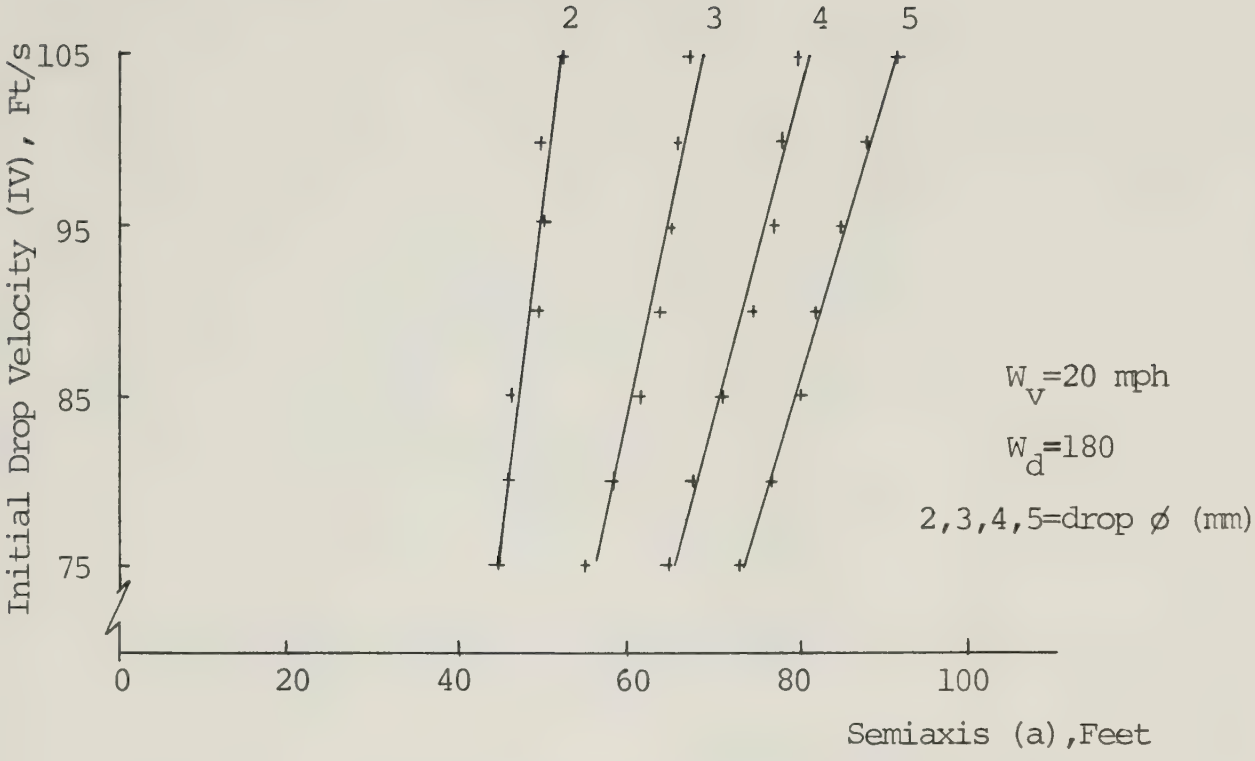

Figure 10. Relationship between the semiaxis (a) and the input variables.

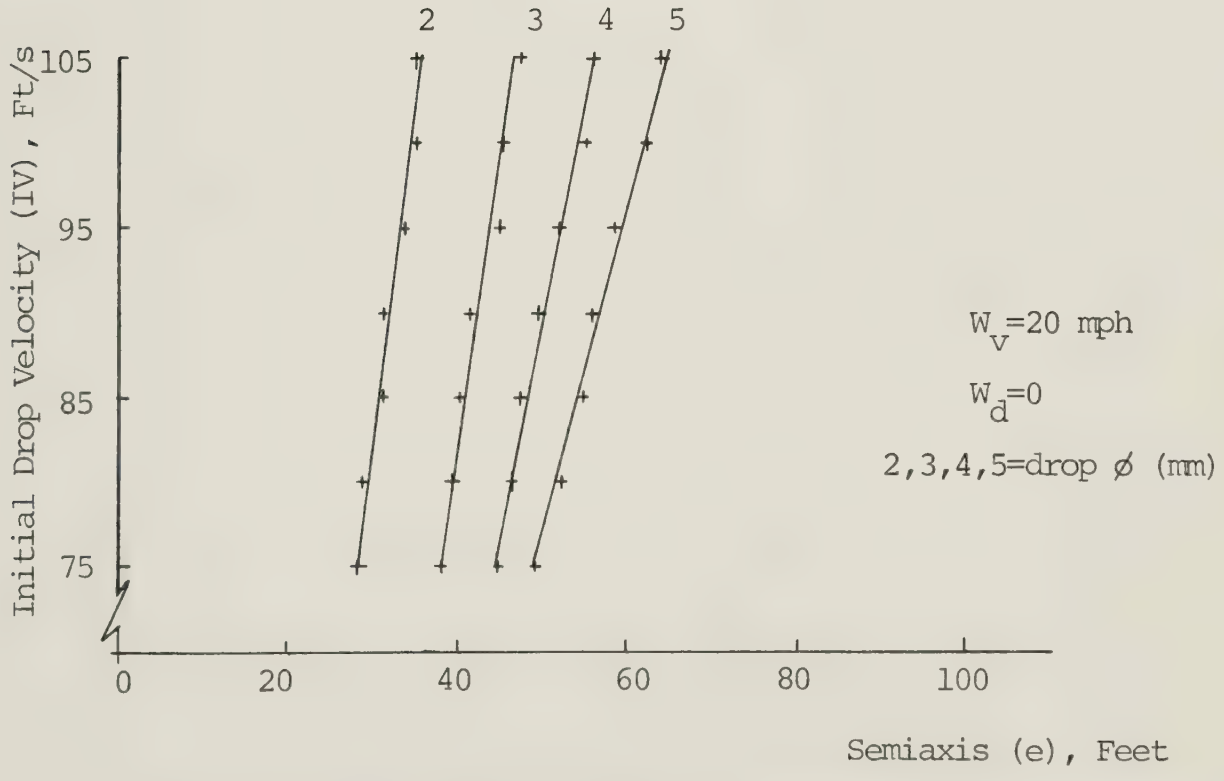

Figure 11. Relationship between the semiaxis (e) and the input variables.

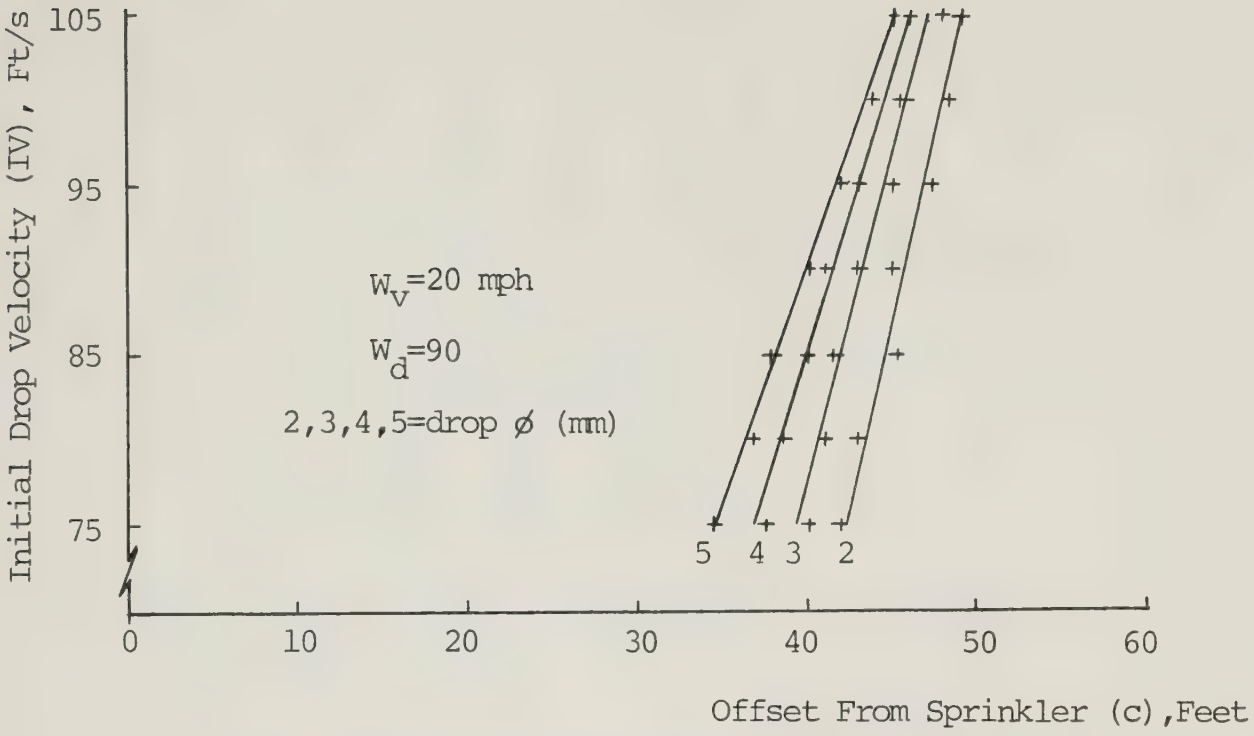

Figure 12. Relationship between the offset from sprinkler (c) and the input variables.

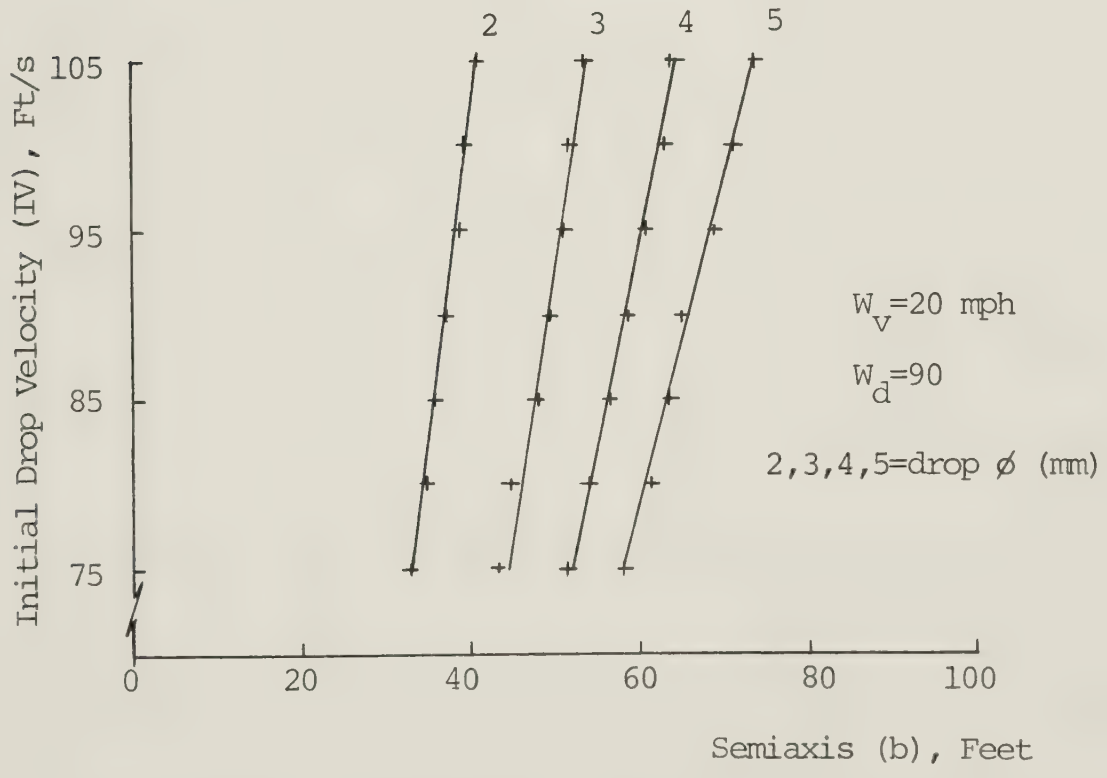

Figure 13. Relationship between the semiaxis (b) and the input variables.

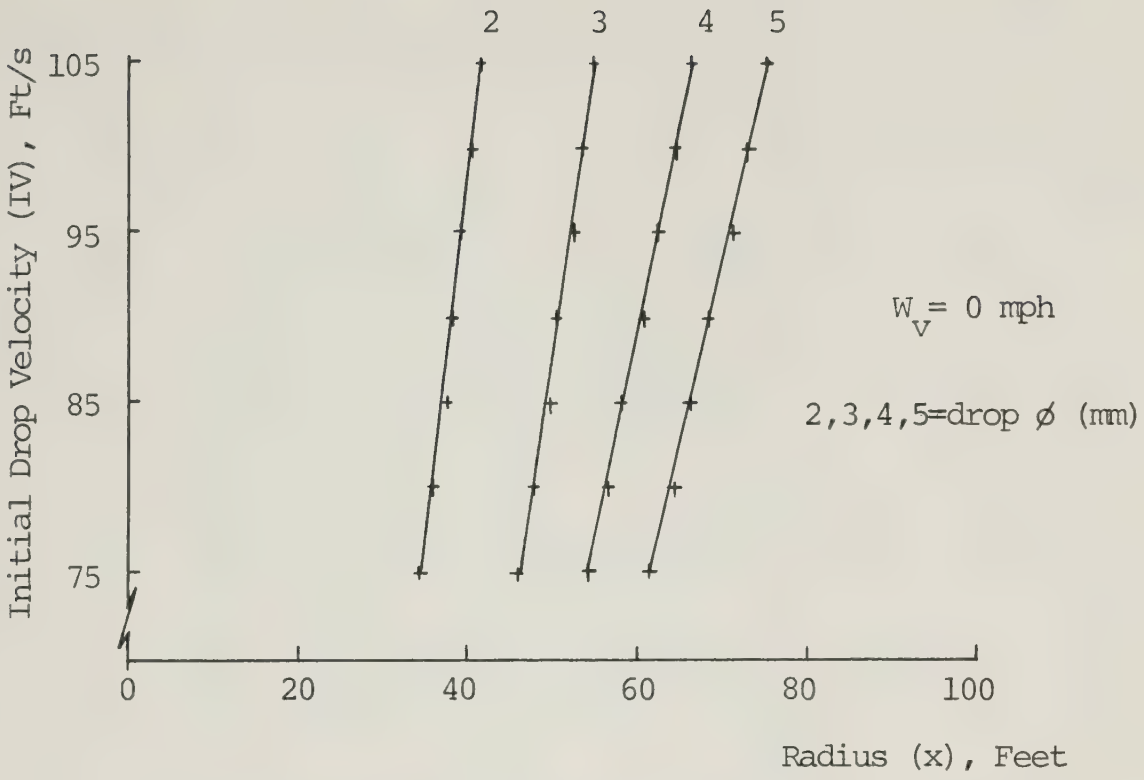

Figure 14. Relationship between the radius (x) and the input variables.

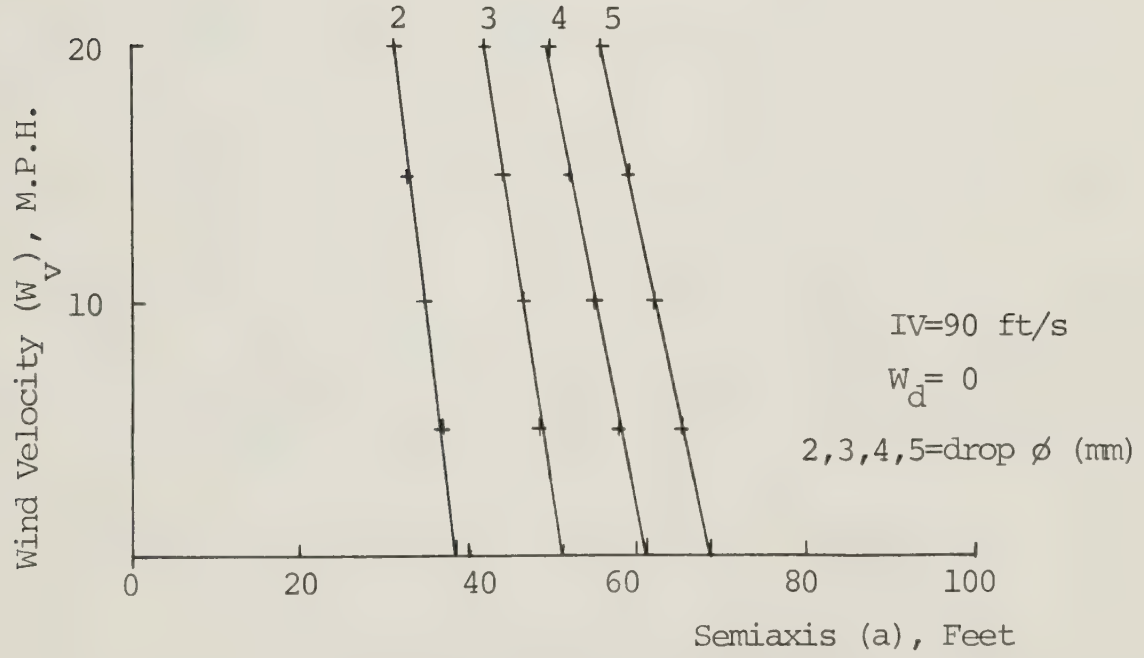

Figure 15. Relationship between the semiaxis (a) and the input variables.

TABLE 4. COMPARISON OF THE SIMULATED AND INTERPOLATED PARAMETERS DEFINING SPRINKLER WETTED PATTERNS.

Particle size mm, (ft x 10^{-3})									
	2.8 (9.2)	Initial Droplet Velocity (IV)	(ft/s)	75	80	85	90	95	100	105
		Minor Axis Interpolated b(s)	(ft)	40.8	41.5	42	43.0	43.7	44.1	45
		Minor Axis Computed b(c)	(ft)	41.5	42	42.8	43.5	44.2	45.0	45.8
		Correlation Coefficient (r)		0.994						
	2.8 (9.2)	Initial Droplet Velocity (IV)	(ft)	75	80	85	90	95	100	105
		Major Axis Interpolated a(s)	(ft)	51.2	51.8	52.5	54.0	54.8	55.2	56.2
		Major Axis Computed a(c)	(ft)	52.5	52.5	54.0	55.0	55.8	56.5	57.0
		Correlation Coefficient (r)		0.988						

Evaluation of the model involved the comparison of the application depths and the coefficient of uniformity.

6.4.1 Comparison of Field and Simulated Application Depths

The adequacy of the model for predicting the depth of application was determined by comparing with experimental measurements from the two operational C.P. systems. Field application depths were measured in receptacles spaced 20 ft apart and extending radially outward from the center-point (see figure 7a and 7b, section 5.2). The individual sprinkler wetted pattern, the angular velocity of the lateral and the wind characteristics were measured and input in the model to allow a direct comparison of field and theoretical simulated depths. Attempts to use a statistical test for comparison to a standard or control set of field measured application depths were not possible because of the chaotic nature of the influencing environmental factors. The disparity between the measured and simulated depths were situated in terms of the absolute deviation (AAD1) and percentage absolute deviation AAD2, computed by the following relations:

$$AAD1 = \frac{\sum |O_{(i)} - T_{(i)}|}{N} \qquad (36)$$

$$AAD2 = \frac{\sum \frac{|O_{(i)} - T_{(i)}|}{O_{(i)}}}{N} \qquad (37)$$

where,

O_i - individual measured application depths (ins)

T_i - individual simulated application depths (ins)

N - number of sets of measurements used in comparison (integer)

The theoretical application depths were determined for both triangular and elliptical distribution patterns and plotted against the field measurements that were determined for 20-ft radial intervals. Only small differences were observed between computed application depths for triangular and elliptical sprinkler patterns (see figures ($IV_{(1)}$ to ($IV_{(11)}$ in Appendix IV). The close spacings of the adjacent sprinklers along the lateral probably concealed the effect of the two assumed distribution profiles. A similar observation was made by Heerman and Hein (11). The triangular distribution profiles were selected for further comparative analysis because they gave a slightly better estimate of the actual field application depths. In general, the average absolute deviations of the theoretical application depths for triangular distribution profiles were less more frequently than those of the elliptical profiles (see table (5), (6), (7) and (8).

Further evaluation of the model includes the comparison of measured application depths and those theoretically derived using the triangular distribution profile for wind and no wind conditions. Plots of the field and simulated depths for all the tests carried out on the two C.P. systems are shown in figures (16) to (26). From figures (16) to (20) the following observations may be summarized as follows:

(i) There is generally good agreement between field and theoretical application depths along the lateral. This is shown by the approximately similar trend in the plots.

(ii) A closer agreement is obtained when the wind magnitude and direction is considered in the simulation model. In this case the model attempts to approximate the effect of the wind in sequential time intervals of fifteen minutes. In some

TABLE 5. EVALUATION OF THE MODEL SIMULATING THE PERFORMANCE OF THE "CIRCLE MASTER" C.P. SYSTEM.

Test No.	Row No.	Field Data			Simulated Data (with wind)									
					Triangular Distribution					Elliptical Distribution				
		Cu. (Wt.)	Cu. (N.Wt.)	Ave. Depth (Wt.)	Cu. (Wt.)	Cu. (N.Wt.)	Ave. Depth (Wt.)	$\Sigma\frac{\lvert O-T\rvert}{N}$	$\Sigma\frac{\lvert O-T\rvert}{O}{N}$	Cu. (Wt.)	Cu. (N.Wt.)	Ave. Depth (Wt.)	$\Sigma\frac{\lvert O-T\rvert}{N}$	$\Sigma\frac{\lvert O-T\rvert}{O}{N}$
		%	%	ins.	%	%	ins.	ins.	%	%	%	ins.	ins.	%
7	1	90.8	85.4	0.62	96.0	92.5	.57	.08	16.88	95.3	91.6	.58	.08	15.90
	2	89.3	83.0	0.64	94.3	89.6	.64	.08	16.19	93.8	89.1	.64	.07	14.56
	3	90.0	79.7	0.67	93.4	85.9	.68	.05	15.26	93.2	86.2	.66	.06	14.60
	Ave.	93.2	85.3	0.65	96.1	90.9	.63	.06	14.02	95.7	90.5	.63	.06	12.95
8	1	88.9	85.6	0.67	94.5	91.5	.63	.07	11.76	94.4	92.3	.62	.07	12.37
	2	90.6	87.1	0.66	96.0	92.9	.60	.07	11.58	95.6	92.7	.59	.07	11.25
	3	90.6	86.3	0.71	96.1	93.5	.60	.10	15.19	95.6	93.0	.60	.11	15.66
	Ave.	92.1	88.0	0.68	96.4	93.1	.61	.07	11.45	96.1	93.1	.61	.07	11.89
9	1	90.8	84.5	0.64	95.4	93.9	.61	.09	17.00	95.2	93.6	.60	.09	17.92
	2	92.7	87.3	0.68	96.1	94.5	.61	.09	16.04	95.6	93.9	.61	.09	16.07
	3	90.7	86.2	0.66	96.1	94.3	.58	.09	15.82	95.6	94.0	.58	.10	16.15
	Ave.	93.0	87.4	0.66	96.1	94.4	.6	109	15.13	94.6	94.0	.60	.09	15.64

TABLE 6. EVALUATION OF THE MODEL SIMULATING THE PERFORMANCE OF THE "CIRCLE MASTER" C.P. SYSTEM.

Test No.	Row No.	Field Data			Simulated Data (with wind)									
					Triangular Distribution					Elliptical Distribution				
		Cu. (Wt.)	Cu. (N.Wt.)	Ave. Depth (Wt.)	Cu. (Wt.)	Cu. (N.Wt.)	Ave. Depth (Wt.)	$\Sigma\left\lvert\frac{O-T}{N}\right\rvert$	$\Sigma\left\lvert\frac{\frac{O-T}{O}}{N}\right\rvert$	Cu. (Wt.)	Cu. (N.Wt.)	Ave. Depth (Wt.)	$\Sigma\left\lvert\frac{O-T}{N}\right\rvert$	$\Sigma\left\lvert\frac{\frac{O-T}{O}}{N}\right\rvert$
		%	%	ins.	%	%	ins.	ins.	%	%	%	ins.	ins.	%
10	1	90.4	87.2	0.77	94.7	94.5	.68	.12	17.06	94.0	93.6	.69	.12	17.47
	2	92.0	90.2	0.71	93.1	91.6	.79	.11	17.03	92.4	91.8	.78	.10	15.98
	3	90.7	89.1	0.68	95.5	95.4	.69	.08	13.89	94.8	94.8	.70	.09	15.02
	Ave.	92.7	90.5	0.72	95.1	94.9	.72	.07	11.02	94.5	94.3	.72	.07	11.85
11	1	91.7	86.3	0.84	94.1	93.3	.91	.13	14.10	93.5	92.6	.78	.12	12.40
	2	91.7	87.4	0.87	91.8	90.4	.82	.11	11.36	92.0	91.2	.83	.12	11.47
	3	92.0	88.4	0.87	94.7	91.4	.78	.14	13.51	94.0	90.7	.78	.14	13.92
	Ave.	92.2	88.1	0.86	93.9	92.4	.84	.09	9.13	93.5	92.3	.73	.10	9.78
12	1	90.3	85.5	0.72	95.4	95.2	.75	.11	12.69	94.9	94.5	.75	.10	12.84
	2	90.9	87.9	0.78	95.6	94.6	.70	.13	15.03	94.9	94.2	.71	.13	14.11
	3	87.6	87.1	0.85	95.2	95.1	.75	.17	18.0	94.7	94.7	.74	.18	18.20
	Ave.	90.5	88.6	0.78	95.7	95.4	.74	.12	13.29	95.2	94.9	.74	.12	13.11

TABLE 7. EVALUATION OF THE MODEL SIMULATING THE PERFORMANCE OF THE "CIRCLE MASTER" C.P. SYSTEM.

Test No.	Row No.	Field Data			Simulated Data (with wind)									
					Triangular Distribution					Elliptical Distribution				
		Cu. (Wt.)	Cu. (N.Wt.)	Ave. Depth (Wt.)	Cu. (Wt.)	Cu. (N.Wt.)	Ave. Depth (Wt.)	$\Sigma\left\|\frac{O-T}{N}\right\|$	$\Sigma\left\|\frac{O-T}{O}\right\|$	Cu. (Wt.)	Cu. (N.Wt.)	Ave. Depth (Wt.)	$\Sigma\left\|\frac{O-T}{N}\right\|$	$\Sigma\left\|\frac{O-T}{O}\right\|$
		%	%	ins.	%	%	ins.	ins.	%	%	%	ins.	ins.	%
13	1	93.7	88.2	.79	93.9	93.2	.88	.13	15.07	93.7	92.8	.85	.11	12.57
	2	93.1	86.9	.77	92.6	89.9	.7	.12	12.81	92.6	90.7	.72	.11	11.34
	3	93.5	89.5	.86	95.1	94.7	.8	.12	12.01	94.2	93.3	.78	.12	12.99
	Ave.	94.4	88.6	.81	95.7	95.1	.79	.09	9.21	95.2	94.0	.78	.09	9.56
14	1	93.6	89.8	1.02	92.5	90.9	.88	.15	14.30	92.4	91.1	.88	.16	14.45
	2	92.3	88.1	.91	94.5	93.3	1.04	.16	16.48	93.9	92.2	.99	.14	13.87
	3	93.2	88.8	.88	93.3	89.5	.78	.13	13.93	92.0	88.4	.81	.14	14.63
	Ave.	93.9	89.8	.94	94.4	93.1	.90	.09	8.94	93.7	92.2	.88	.10	10.0

TABLE 8. EVALUATION OF THE MODEL SIMULATING THE PERFORMANCE OF THE "VALLEY 1160" C.P. SYSTEM.

Test No.	Row No.	Field Data			Simulated Data (with wind)									
					Triangular Distribution					Elliptical Distribution				
		Cu. (Wt.)	Cu. (N.Wt.)	Ave. Depth (Wt.)	Cu. (Wt.)	Cu. (N.Wt.)	Ave. Depth (Wt.)	$\Sigma\frac{\lvert O-T\rvert}{N}$	$\Sigma\frac{\frac{\lvert O-T\rvert}{O}}{N}$	Cu. (Wt.)	Cu. (N.Wt.)	Ave. Depth (Wt.)	$\Sigma\frac{\lvert O-T\rvert}{N}$	$\Sigma\frac{\frac{\lvert O-T\rvert}{O}}{N}$
		%	%	ins.	%	%	ins.	ins.	%	%	%	ins.	ins.	%
2	1	92.6	88.0	.97	94.4	93.8	1.03	.13	15.67	94.1	93.6	1.02	.13	17.23
	2	89.8	86.6	.97	93.4	92.6	.89	.14	16.02	92.8	92.3	.94	.14	16.75
	3	89.7	86.8	.97	93.7	90.7	1.14	.17	20.51	92.3	90.6	1.10	.15	18.46
	Ave.	92.1	88.6	.97	95.1	94.0	1.03	.11	12.99	94.4	93.6	1.0	.11	14.17
3	1	88.4	81.3	1.21	96.1	91.5	1.04	.20	19.34	95.9	91.5	1.04	.20	20.22
	2	90.3	75.1	1.11	96.1	92.1	1.05	.13	14.30	95.9	95.7	1.06	.13	14.92
	3	91.8	87.5	1.02	95.6	91.3	1.15	.15	17.11	95.5	91.6	1.13	.13	16.21
	Ave.	92.6	86.9	1.11	96.2	91.8	1.08	.11	12.66	96.1	91.8	1.08	.11	13.39
6	1	89.8	86.4	.84	96.1	94.8	1.01	.16	23.56	95.2	95.3	1.00	.17	24.97
	2	90.1	86.2	.99	95.6	94.2	1.09	.14	18.38	95.1	94.1	1.06	.12	18.33
	3	89.2	87.0	.84	95.1	93.6	1.08	.22	29.70	94.3	92.9	1.07	.22	30.8
	Ave.	91.2	87.9	.89	96.2	94.9	1.06	.16	22.06	95.8	94.4	1.04	.15	22.60

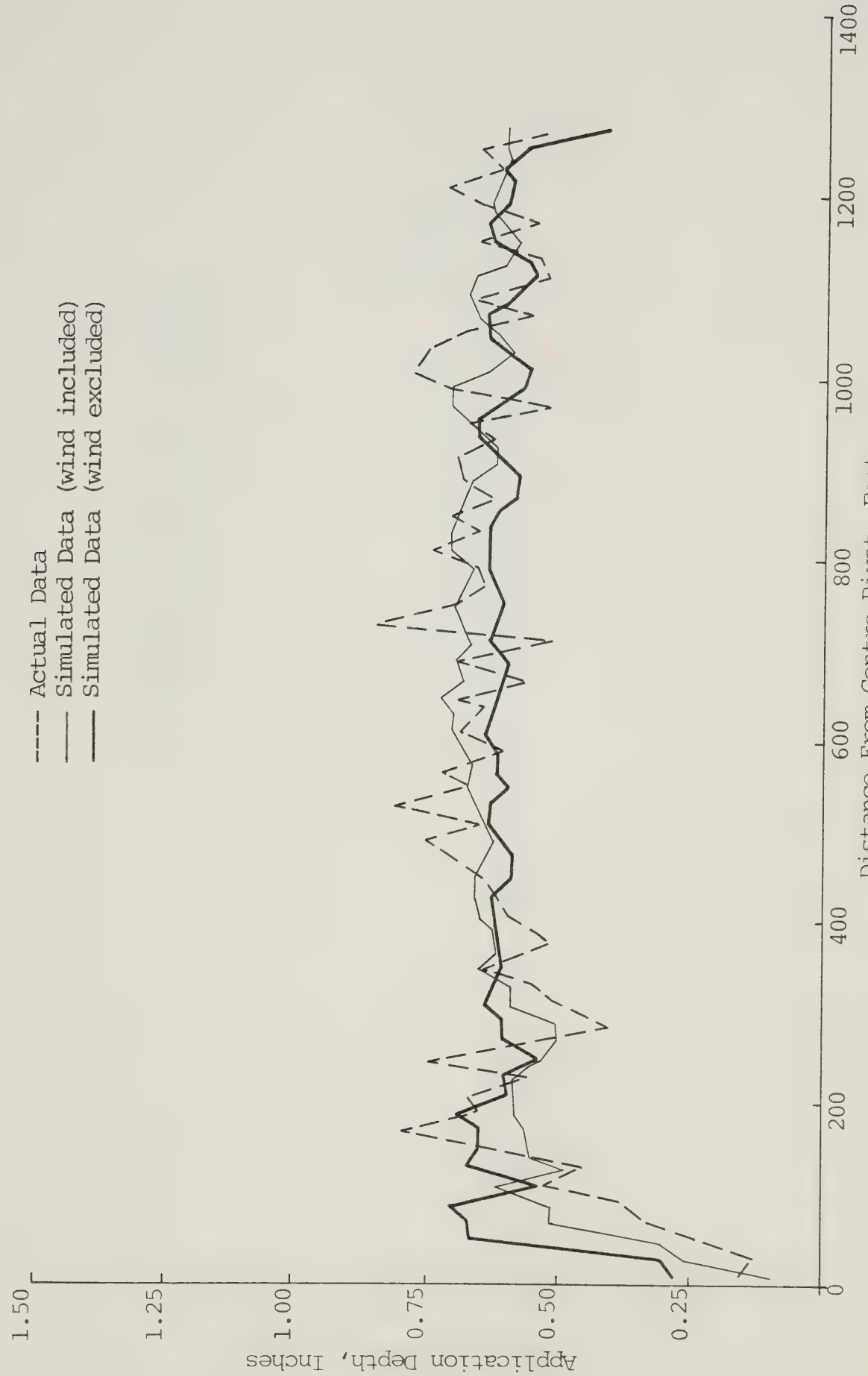

Figure 16. Comparison of field and simulated application depths. "Circle Master" C.P. System test 7 row 2.

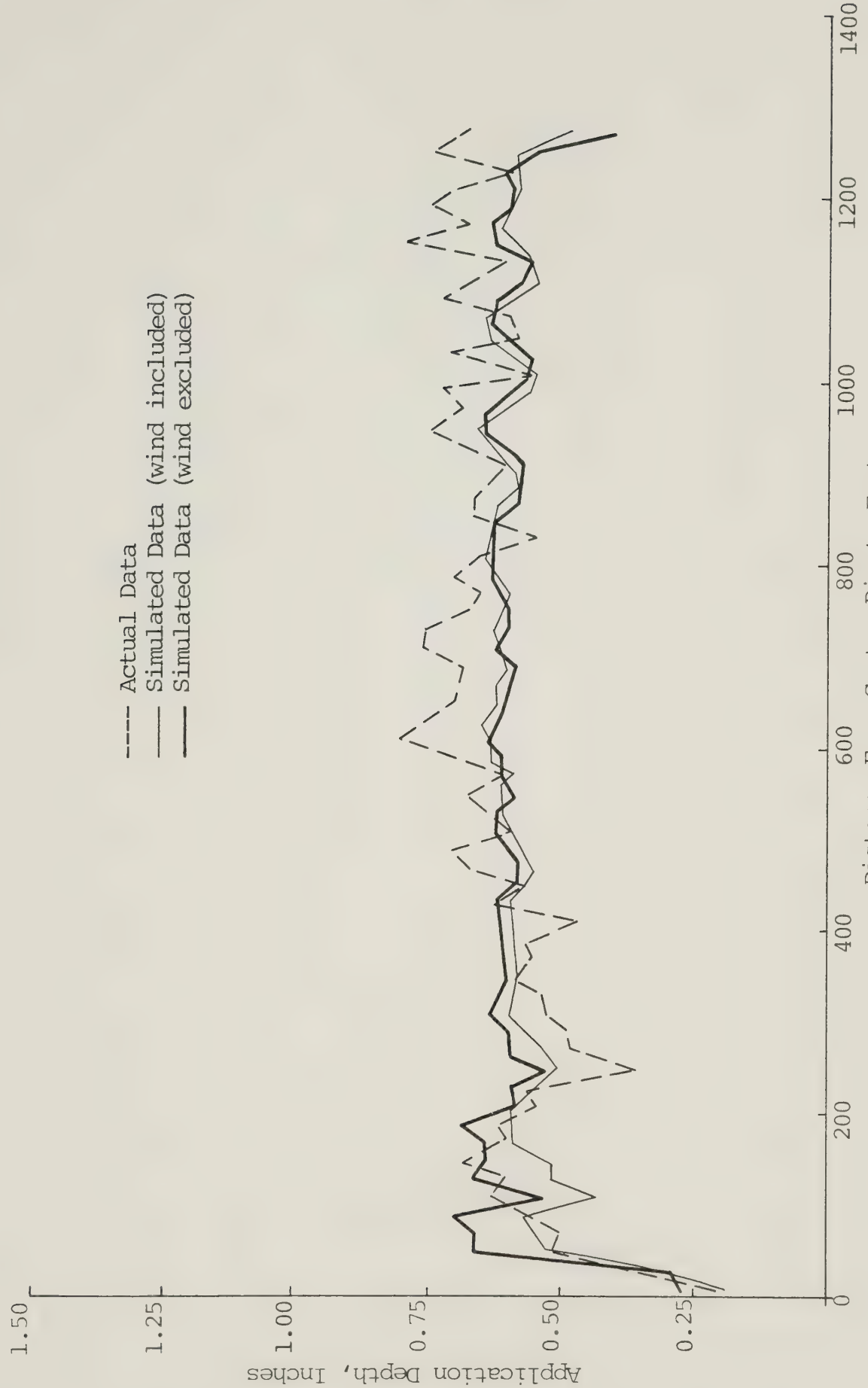

Figure 17. Comparison of field and simulated application depths. "Circle Master" C.P. System test 8 row 2.

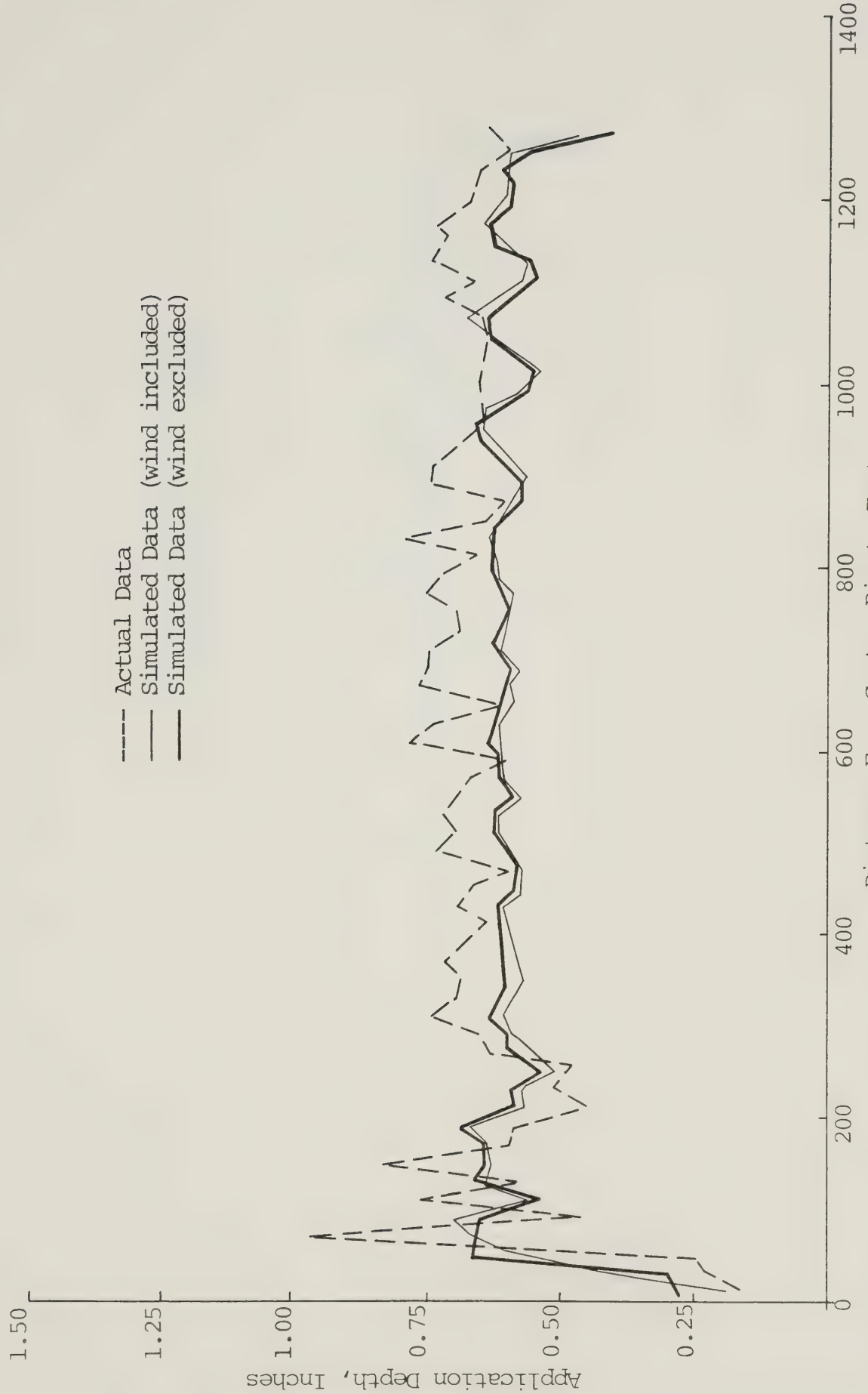

Figure 18. Comparison of field and simulated application depths. "Circle Master" C.P. System test 9 row 2.

Figure 19. Comparison of field and simulated application depths. "Circle Master" C.P. System test 10 row 2.

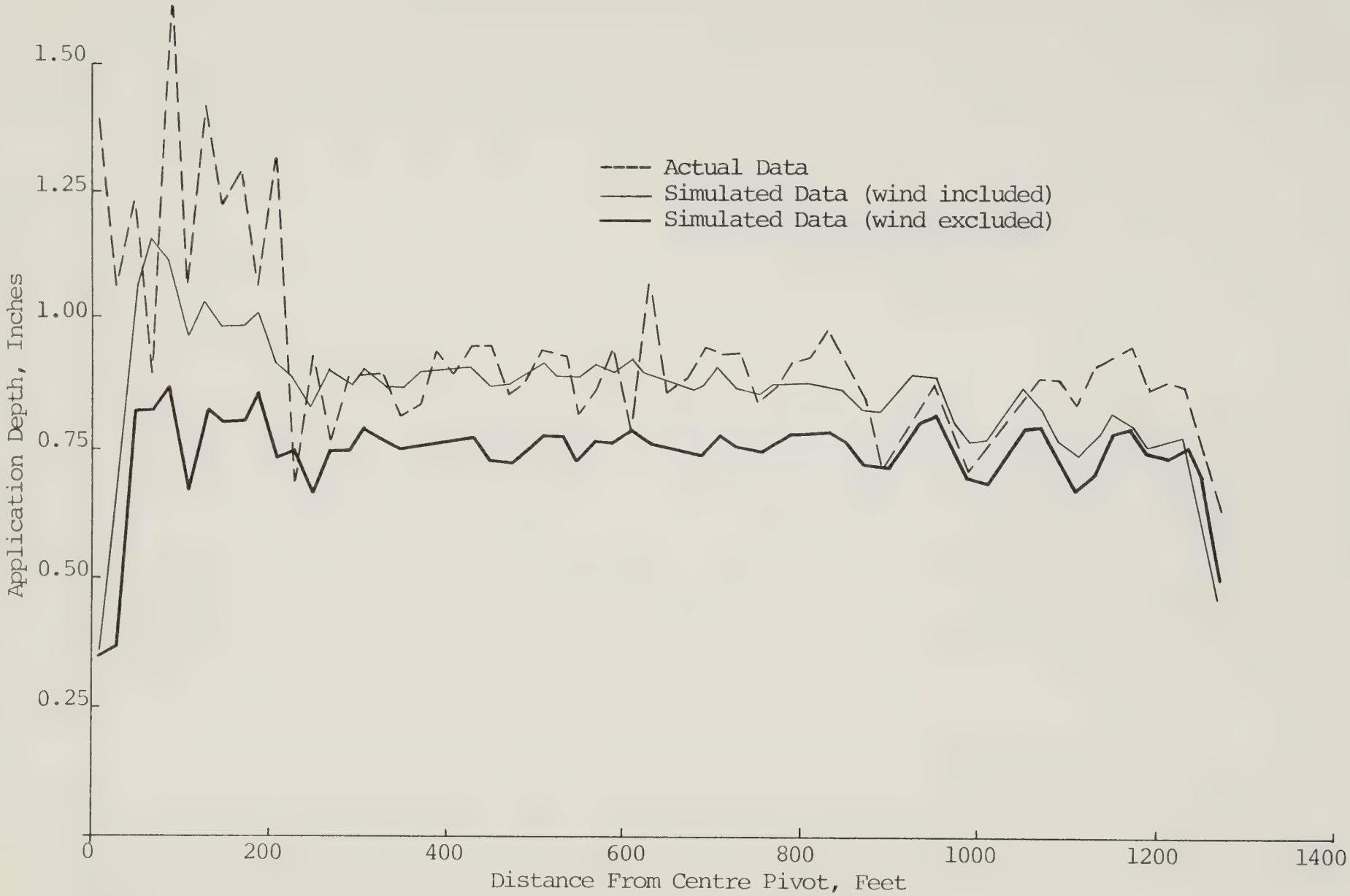

Figure 20. Comparison of field and simulated application depths. "Circle Master" C.P. System test 11 row 2.

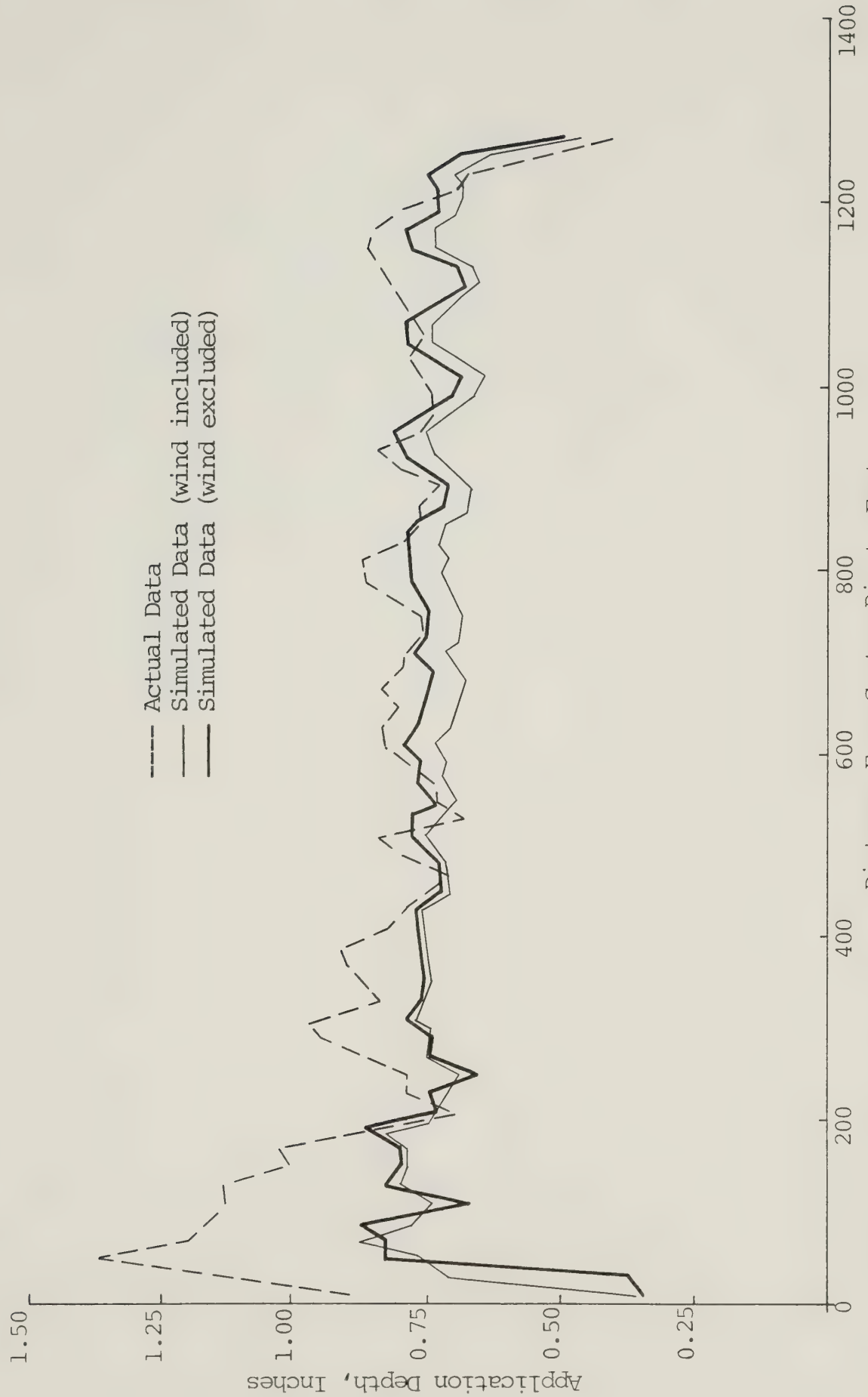

Figure 21. Comparison of field and simulated application depths. "Circle Master" C.P. System test 12 row 2.

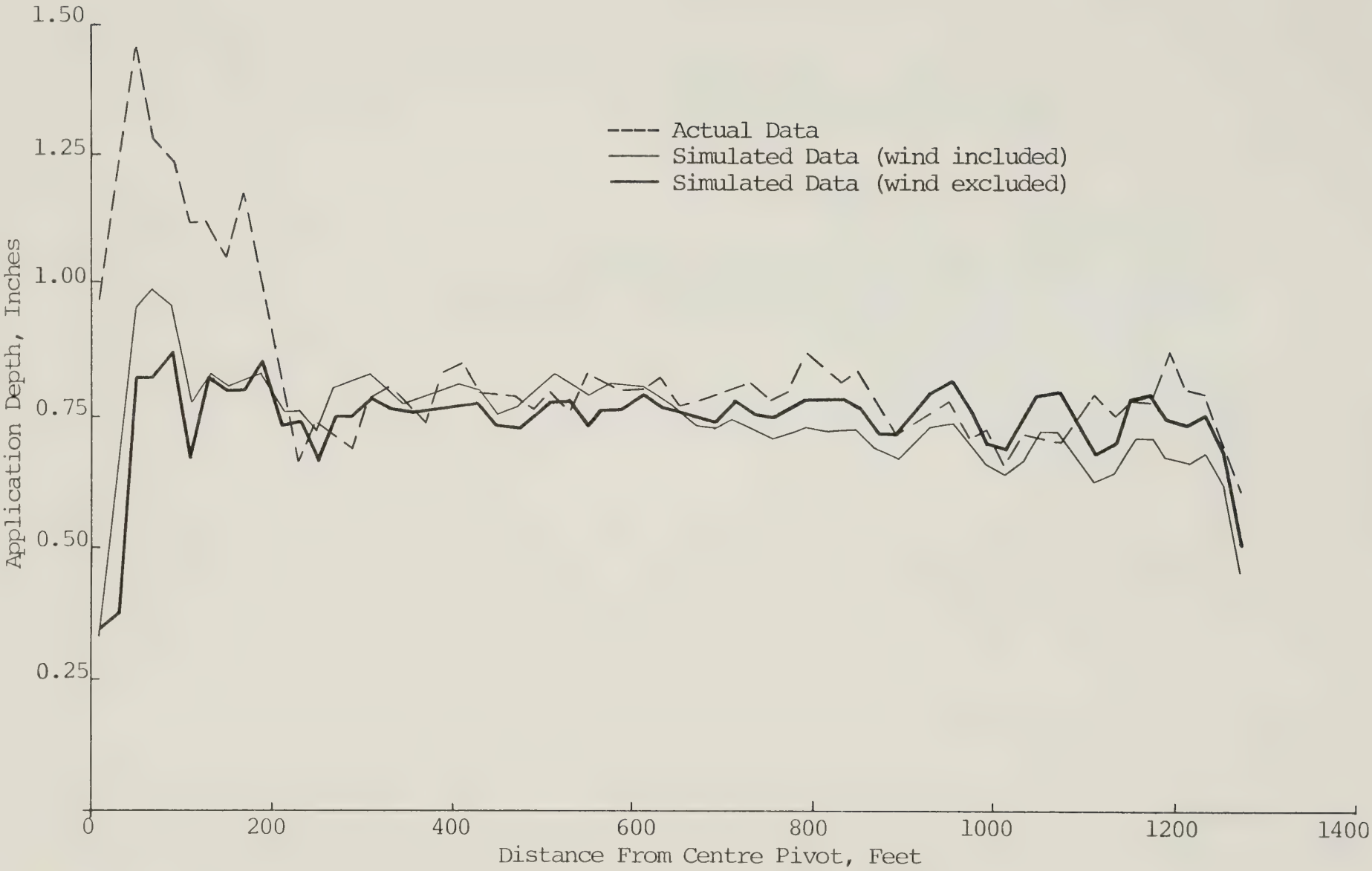

Figure 22. Comparison of field and simulated application depths. "Circle Master" C.P. System test 13 row 2.

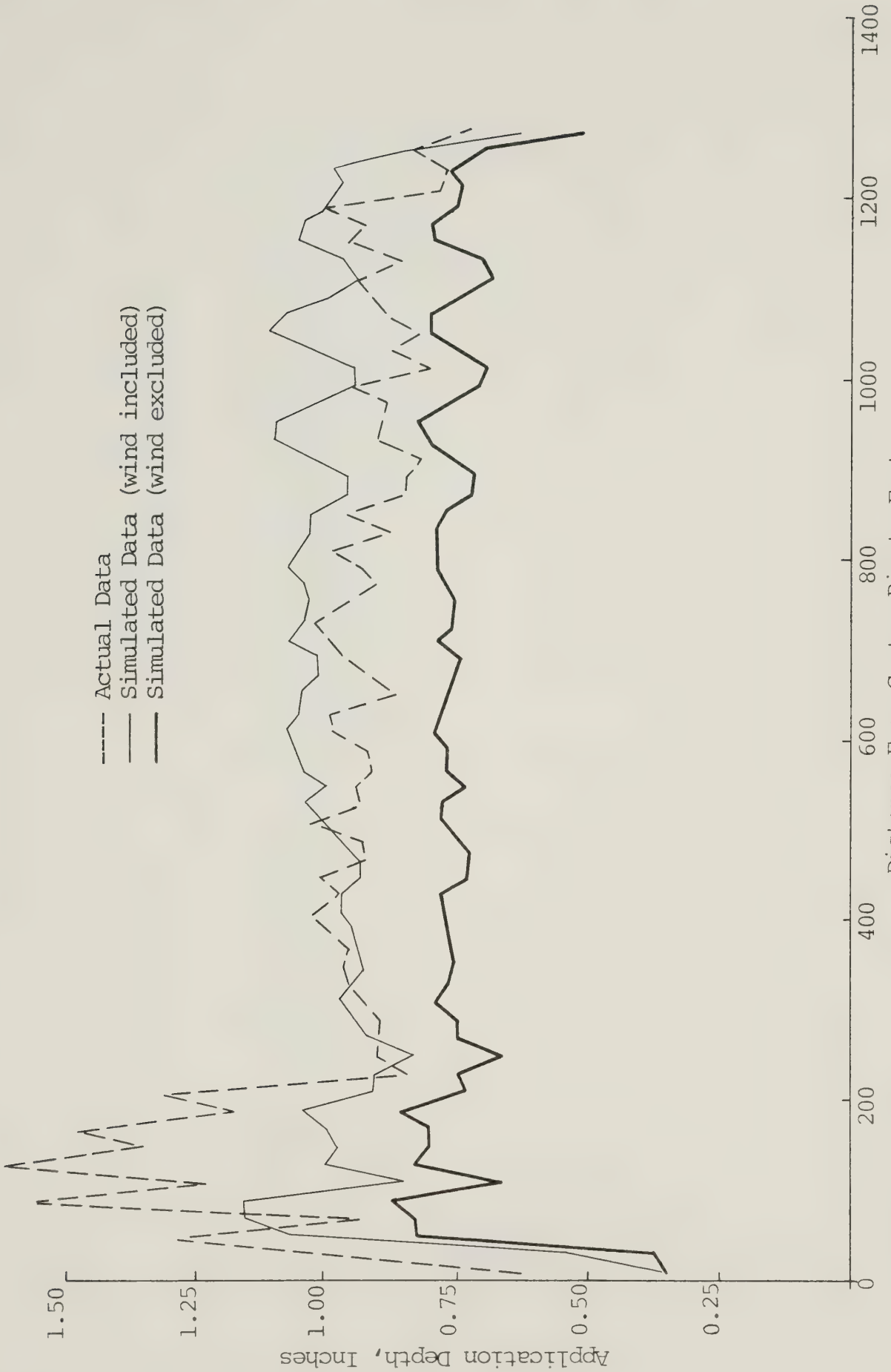

Figure 23. Comparison of field and simulated application depths. "Circle Master" C.P. System test 14 row 2.

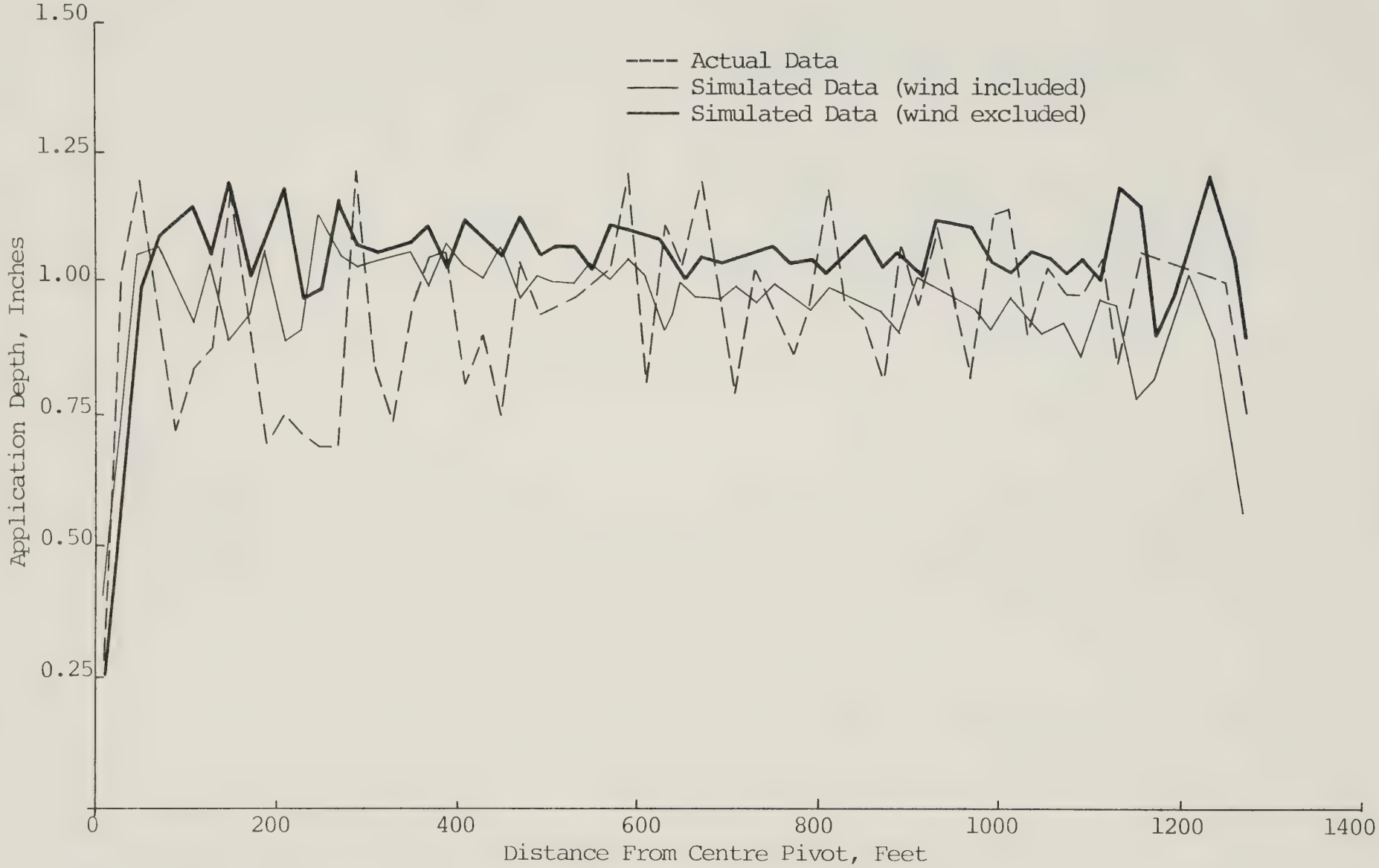

Figure 24. Comparison of field and simulated application depths. "Valley 1160" C.P. System test 2 row 2.

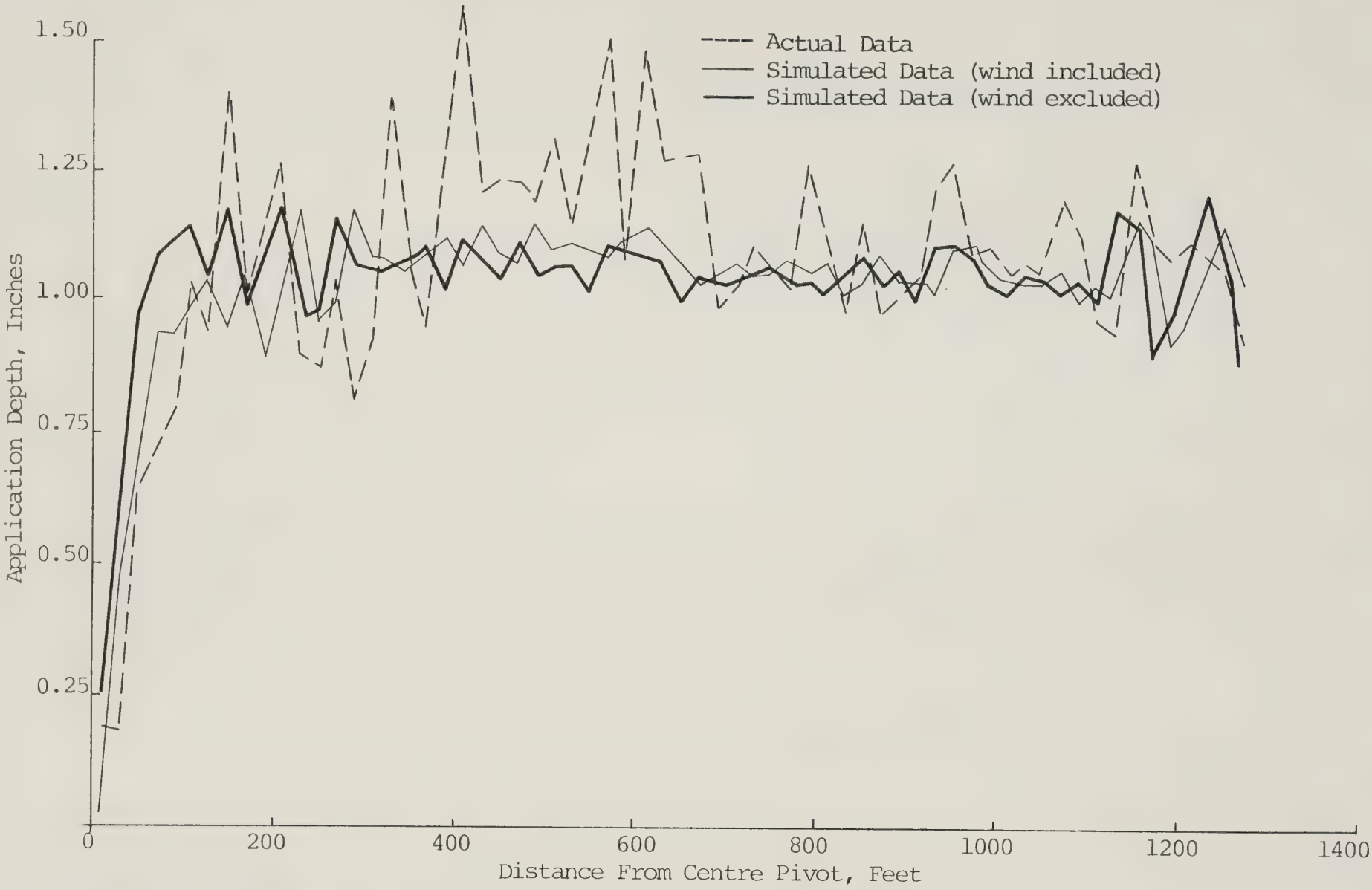

Figure 25. Comparison of field and simulated application depths. "Valley 1160" C.P. System test 3 row 2.

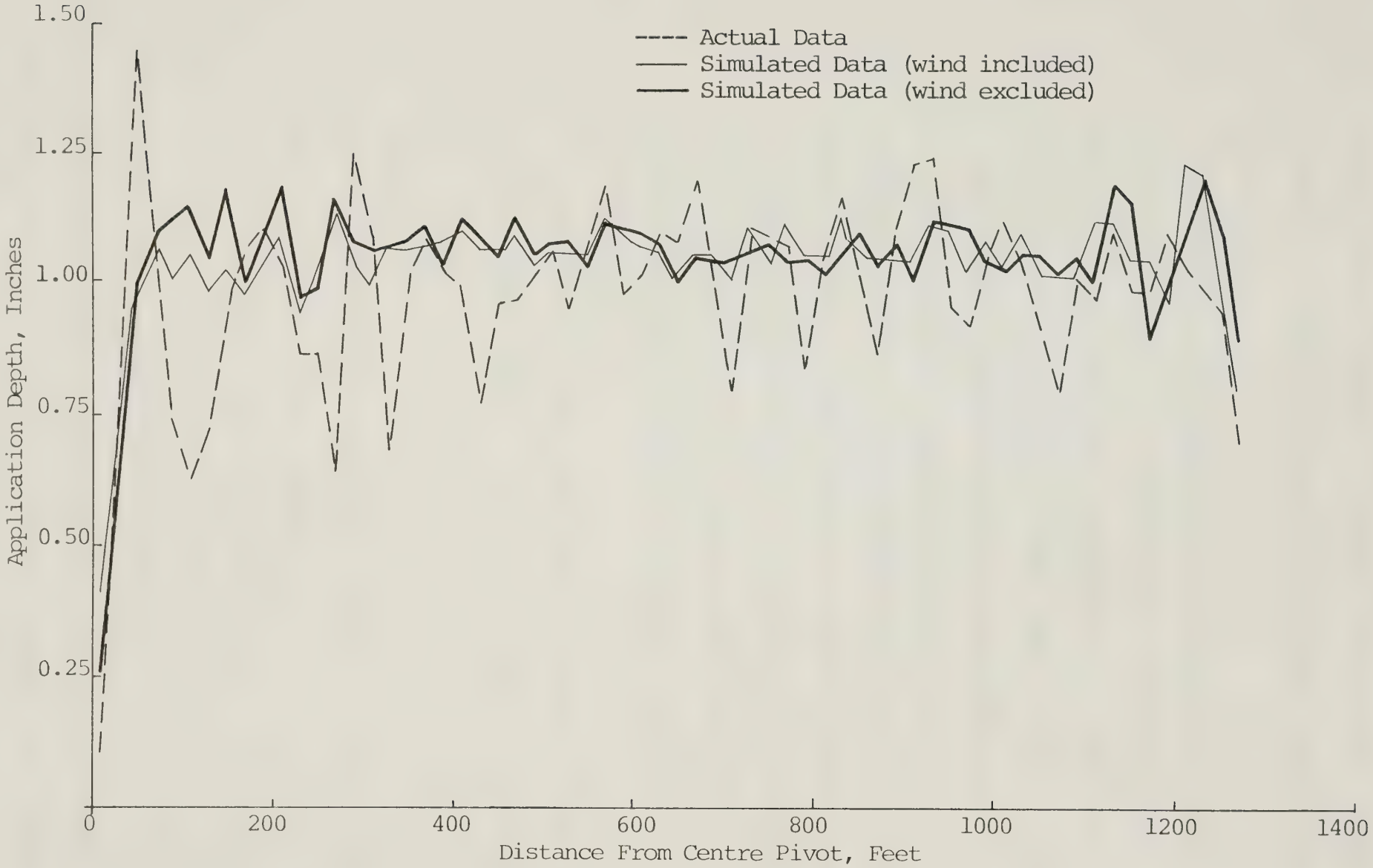

Figure 26. Comparison of field and simulated application depths. "Valley 1160" C.P. System test 6 row 2.

cases, however, the effect of the wind is minimal (see figure 18, 21,26). Either the effect of the wind is insignificant or an overall "averaging out" effect occurs in the above cases.

(iii) In most cases a large application depth is noted near the center of rotation. The application rate near the pivot point is low but the time of application is long. As a design attempt to achieve a uniform depth the time of application on a point decreases with a corresponding increase in in application rate outwardly from the centre pivot.

(iv) Fluctuations of the measured depths along most of the lateral is evident. These fluctuations may be attributed to the localized chaotic effect of the wind on the superimposed adjacent patterns. The overlapping sprinkler effect may be magnified or greatly reduced because of a rapid change in wind direction.

(v) A lag between the field and theoretical depths is noticeable near the centre pivot. Inaccurate time synchronization in the input of the simulation model is most likely to cause these shifts.

The simulation model is best evaluated in terms of the percentage absolute deviation (AAD2) which was computed earlier from equation 37, section 6.4.1. On the whole, theoretical depths deviated approximately 14 percent from the actual field measurements. The spread of average deviations for the "Circle Master" C.P. system varied from 11 to 18 percent as compared to the "Valley 1160" system of 14.3 to 30.8 percent (see table 5,6,7 and 8). In general a better agreement was obtained

for the former C.P. system as compared to the latter system. A mean deviation of 14.7 percent and a standard deviation of 1.96 percent in contrast to 19.4 percent and 4.7 percent, respectively, was observed. This disparity may be attributed to the individual system performance characteristics and statistical differences probably because eight fewer tets were carried out on the "Valley 1160" C.P. system. When the effect of the wind was not included in the model the mean absolute deviations were increased to 17.5 percent for the "Circle Master" C.P. system compared to 19.4 percent of the "Valley 1160" system. The influence of the wind is not prevalent in the latter C.P. system because of the wide fluctuations of the measured depths along the lateral, (see figures 25 and 26). In terms of mean absolute deviation, no valid assessment of the theoretical values were possible in this case.

6.4.2 Factors Affecting Model Performance

The differences in measured application depths and those theoretically derived by the simulation model could be attributed to inaccuracies in field measurements of significant parameters and variables, changes in system characteristics and in the assumptions used in the mathematical model.

Inaccuracies in field measurements of application depths may be the result of a number of factors that often occurred in the field. Detrimental factors such as the occurrence of tipped receptacles under wind conditions, the influence of surrounding vegetation, malfunction of sprinklers, splashing effect of water streams emitted from leaks, and the propelling mechanism (Valley 1160) often were not compensated in this study. The variation of system discharge due to change in pressure as well as the intermittent change in sectional angular velocity of the lateral, are

probable causes of the large fluctuation in the measured application depths. Difficulty in measuring the chaotic nature of wind magnitude and direction of the localized area is another probable reason for these fluctuations in field measured depths. The overlapping effect of the sprinklers is either enhanced or reduced depending on the wind conditions at a particular given time.

Errors in the theoretically determined depths are the rusult of inaccurate input variables and the assumptions made in the model. Proper synchronization of the starting and ending time of the field experiment is necessary to determine the appropriate range of monitored wind input data for the simulation model. The length of experimental time often was not easily estimated for rain gauge monitors. In the simulation models, the effect of the wind is considered in sequential times of 15 minutes and the chaotic nature of the actual wind conditions were considered as a one dimensional vector. The error incurred was necessary because of the long computer simulation time of the test run as well as the limitation of wind monitoring equipment. Therefore, the influence of the localized chaotic windy condition on the application depths was not accurately modelled in the program. The range of particle size estimated using the method discussed in Section 5.4, Chapter 5, is only an approximate estimate. If the distributions of the particle sizes for each nozzle were specified the desired wetted patterns would then be very accurately determined for the flight trajectories.

The distorting effect of the wind on the assumed triangular and elliptical distribution profiles were not considered in the simulation, since the particle size distribution pattern was not known. However,

an attempt was made to determine the point of maximum concentration when the patterns were distorted (see section 6.2). This point of maximum application depth was idealized as the origin of the distorted wetted pattern. Accurate determination of the point of maximum concentration made under the chaotic influence of wind was not possible. Error in assuming a triangular or elliptical distribution profile is relatively small (11), however, the distorting influence of the chaotic wind conditions could greatly emphasize or reduce the overlapping effect of the profiles of adjacent sprinklers.

The effect of a change of wind direction on the application depth could be theoretically studied by using a constant wind direction relative to the pivot throughout the analysis. For wind velocity of 0, 20, 40 mph and a change of direction of 0, 90, and 180 degrees, relative to the pivot, the application depths for both C.P. systems are shown in Appendix V, figures $V_{(1)}$ to $V_{(6)}$. The effect of constant wind direction was minimal throughout for most of the lateral. Disturbance at the beginning and at the end was most obvious when wind direction is at 0 degree relative to the pivot. The plots for windy conditions (20, 40 mph) as listed in figures $V_{(1)}$ and $V_{(4)}$, showed a shift of the curves towards the centre of the pivot. For a wind direction 180 degrees relative to the pivot the opposite effect was observed (see figures $V_{(3)}$ and $V_{(6)}$. An intermediate response of these two extremes was observed for a wind direction of 90 degrees in the figures $V_{(1)}$ and $V_{(5)}$. The effect of change in wind velocity was insignificant in the application depths for constant wind direction. It may be noted that the effect of chaotically changing wind direction has a greater overall effect on the distribution of the application depths along the lateral than

the magnitude of wind.

6.4.3 Coefficient of Uniformity

Christiansen's coefficient of uniformity was used to evaluate the performance of the C.P. systems. A similar weighted coefficient of uniformity suggested by Heerman and Hein (11) is also included in this analysis to give more weight to the application depths further from the pivot where the area of influence is increasingly larger.

Comparison of the field and model simulated coefficients for both weighted and non-weighted values are shown in tables 5,6,7 and 8. The uniformity coefficients in this table were calculated by excluding the area at the outer radius where the large nozzle (end gun) sprinklers are located. The deviation of the mean of the sprinkler system is affected by a large area at the end guns and reduces the coefficient accordingly. The coefficients of uniformity determined for both triangular and elliptical distribution did not differ greatly (see table 9). As discussed earlier (see section 6.4.1) the overlapping effect of closely spaced adjacent sprinklers for the two assumed distributions gave only small differences. In general, however, the theoretical simulated coefficients were higher than those measured. This is evident because of the wide fluctuations in field measured depths and the initial larger response close to the pivot. Closer agreements were obtained for the measured weighted coefficients and those simulated in the model as a standard deviation of 1.26 compared to 1.56 was noted in the above case. The accuracy of the simulation model cannot be definitley assessed irrespective of the reasonable agreements of the theoretical computed and measured coefficients. The coefficient of the uniformity is only a performance parameter of the application depths along the lat-

TABLE 9. MEAN COEFFICIENT OF UNIFORMITY.

C.P. System	Field Distribution		Theoretical Distribution (Simulated)			
			Triangular Pattern		Elliptical Pattern	
	(Wt.)	(N.Wt.)	(Wt.)	(N.Wt.)	(Wt.)	(N.Wt.)
	%	%	%	%	%	%
Circle Master	91.3	86.9	94.6	92.6	94.1	92.2
Valley 1160	90.2	86.1	95.1	92.9	94.6	93.0

eral. The variation of application depths at any given point beneath the lateral cannot be fully accounted for without imposing an averaging effect. The effect of wind conditions on the coefficient of uniformity is theoretically predicted in table 10 and 11. In this analysis the wind direction was held constant is in a direction relative to the centre pivot. At 0 degree direction where the line of measurement is directly opposite to the wind a noticeable reduction in uniformity coefficient occurs. The extreme distortion of the overlapping distribution patterns in this direction accounts for the lower coefficients. From tables 9 and 10 the coefficients obtained under the range of wind magnitude and direction are within the acceptable 80 to 90 percent design requirements.

6.4.4 C.P. Field Performance Analysis

A summary of the field measurements that were conducted (as discussed in Section 5.1 to 5.4, Chapter 5) are shown in table 12 and 13. The average application and coefficients of uniformity were computed for the various test runs in each C.P. system. In each C.P. system the average application depth and coefficient of uniformity showed only small variation (Std. Dev. of approximately 1.1) for each selected speed of lateral rotation. Although a wide range of wind velocities were measured , the average wind directions that were recorded did not indicate the actual fluctuations recorded during the experimental test period.

The possibility of determining the performance of the two C.P. systems in relation to the varying environmental parameters from the results shown in table 12 and 13 was restricted. The available measurements of average wind directions and velocities in tables 12 and 13 cannot be related to the determined application depths and coefficients of uniformity because of long experimental runs of approximately 14

TABLE 10. PREDICTED COEFFICIENTS OF UNIFORMITY FOR THE "CIRCLE MASTER" SYSTEM.

Wind Velocity	Wind Direction	Triangular Distribution Pattern		Elliptical Distribution Pattern	
		Cu. (Wt.)	Cu. (N.Wt.)	Cu. (Wt.)	Cu. (N.Wt.)
m.p.h.		%	%	%	%
0		95.82	95.00	94.86	93.33
20	0	87.30	92.05	86.91	91.76
	90	95.56	91.72	94.85	90.89
	180	96.02	89.88	95.72	89.49
40	0	74.5	85.93	74.14	85.90
	90	89.35	81.25	89.80	81.40
	180	93.46	82.07	93.37	81.28

TABLE 11. PREDICTED COEFFICIENTS OF UNIFORMITY FOR THE "VALLEY 1160" SYSTEM.

Wind Velocity	Wind Direction	Triangular Distribution Pattern		Elliptical Distribution Pattern	
		Cu. (Wt.)	Cu. (N.Wt.)	Cu. (Wt.)	Cu. (N.Wt.)
m.p.h.		%	%	%	%
0		95.96	93.73	95.31	93.59
20	0	91.40	93.81	90.81	93.30
	90	95.62	92.54	94.29	91.42
	180	96.54	89.18	94.50	89.03
40	0	78.93	88.58	79.56	88.60
	90	95.30	86.82	93.56	86.07
	180	95.76	83.25	94.00	83.32

TABLE 12. PERFORMANCE OF THE "CIRCLE MASTER" C.P. SYSTEM UNDER LOCAL CLIMATIC CONDITIONS.

Field Test No.	Ave. Applic. Depth	Cu. (Ave.-Wt.)	Cu. (Ave.-N.Wt.)	Range of Wind Velocities	Ave. Wind Velocity	Ave. Wind Direction	Ave. Temp	Ave. Relative Humidity
	ins.	%	%	m.p.h.	m.p.h.		C	%
1	0.67	90.84	89.42	N.A.	N.A.	N.A.	21	32
2	0.76	91.88	91.22	N.A.	N.A.	N.A.	13	55
4	0.69	93.64	90.82	N.A.	N.A.	N.A.	28	29
5	0.79	93.63	91.93	N.A.	N.A.	N.A.	14	69
6	0.70	92.14	91.26	N.A.	N.A.	N.A.	22	48
7	0.65	93.22	85.33	0.0-20	8.1	182	30	20
8	0.68	92.15	87.96	1.0-14.0	5.9	114	13	60
9	0.67	92.03	87.41	2.0-15.0	9.0	264	22	52
10	0.73	92.73	90.48	1.0-16.0	6.5	283	20	67
11	0.87	92.20	88.09	0.0-10.0	4.3	135	25	36
12	0.79	90.53	88.59	1.0-14.0	6.0	63	14	76
13	0.82	94.44	88.59	0.0-12.0	4.5	219	30	33
14	0.95	93.93	89.79	1.0- 9.0	4.9	168	12	72

TABLE 13. PERFORMANCE OF THE "VALLEY 1160" C.P. SYSTEM UNDER LOCAL CLIMATIC CONDITIONS.

Field Test No.	Ave. Applic. Depth	Cu. (Ave.-Wt.)	Cu. (Ave.-N.Wt.)	Range of Wind Velocities	Ave. Wind Velocity	Ave. Wind Direction	Ave. Temp.	Ave. Relative Humidity
	ins.	%	%	m.p.h.	m.p.h.		C	%
1	0.90	90.81	87.44	1-12	60	N.A.	15	60
2	0.98	92.89	88.62	0-16	6.3	173	20	35
3	1.12	92.61	86.90	1-14	5.8	182	17	51
4	0.90	90.16	84.66	N.A.	N.A.	N.A.	N.A.	N.A.
5	0.75	87.31	77.75	6-30	16	N.A.	22	33
6	0.90	91.19	87.71	0-14	6.0	139	22	33
7	0.92	89.76	86.85	0-12	5	N.A	N.A.	N.A.
8	0.94	85.19	79.96	N.A.	N.A.	N.A.	N.A.	N.A.
9	0.98	90.35	83.24	0-16	5	N.A.	N.A.	N.A.
10	1.21	90.00	85.29	0-6	2	N.A.	N.A.	N.A.
11	1.02	89.0	83.25	0-5	1	N.A.	N.A.	69
12	0.86	83.89	89.47	0-10	3	N.A.	20	55
13	1.05	90.73	87.47	0-14	5	N.A.	24	23
14	1.03	91.89	87.73	0-6	2	N.A.	27	20

hours involved in each test. The measured field data, however, provided a guide in the development of the C.P. simulation model.

CHAPTER VII

SUMMARY AND CONCLUSIONS

The main objective of this study was to evaluate the performance of two Centre Pivot irrigation systems operating under local climatic conditions. A mathematical model was developed to simulate the dynamic operation of a C.P. system. The simulation model could then be used as a tool to determine the system performance under actual windy conditions.

In the first part of the model the dynamics of water droplets in flight were formulated as second order differential equations to determine the basic wetted patterns. The required input information such as the range of droplet particle size and initial particle velocities were obtained from experimental analyses and the manufacturer's sprinkler specification, respectively. Basic information on wind direction and magnitude in discrete time intervals of 15 minutes were considered in the analysis to study the distortion of the wetted patterns and the overlapping effect of the adjacent sprinklers. The wetted pattern of sprinklers for no wind condition is described by an equation of a circle. Under windy conditions, however, the wetted pattern is approximated by curve fitting using two overlapping ellipses with common minor axis. The point of maximum concentration in this case is distorted a distance (c) from the origin (i.e., the sprinkler's location).

Triangular and elliptical cross-sectional distribution profiles were assumed to represent the extremes for individual sprinkler patterns. Interpolation techniques were used to determine the desired wetted patterns from those derived from closely related initial conditions. This was necessary because of the extremely long computer simulation time required to compute the actual wetted patterns from the droplet

trajectories.

The second part of the model involved the simulation of the operating C.P. system in relation to the rows of measuring receptacles used in field measurements. Actual simulation of the moving wetted patterns for the rotating sprinklers were developed for ½ degree incremental angular change of the lateral. Actual wind information monitored during the testing period were modelled in the program to assess the performance of the simulation model in terms of application depths and the coefficient of uniformity.

From the development of the performance from available experimental data the following conclusions were drawn:

1. Wetted patterns of a rotating sprinkler on a moving C.P. system can be defined from the equation of motion of sprinkler droplets emitted.
2. The distorted wetted patterns (under windy conditions) can be approximated using the equations of two ellipses having a common minor axis. The point of maximum concentration of particles in this case is a function of the magnitude and direction of the wind.
3. The range of particle sizes that was obtained experimentally for use in the simulation model was an approximation. For greater precision in the application of the simulation model more accurate techniques are suggested. The differences between the actual wetted patterns and those simulated are most likely greatly affected by the discrepancies in the selection of appropriate particle sizes. Range of particle size is the significant criteria in determining boundaries of the wetted patterns.

4. The interpolation techniques used such as bi-cubic spline were valid in determining the desired wetted patterns for the purpose of reducing the extremely long computing time. Correlation coefficients of 0.98 were obtained for interpolated and simulated parameters describing the wetted patterns.

5. Comparisons of experimental and simulated application depths for most test runs gave good agreement. A deviation of approximately 14 percent of the simulated , compared to that of measured, was observed. Wider fluctuations occurred in the field. This is attributed to the chaotic nature of the wind and discrepancies in field measurement techniques. However, a reasonably similar trend was obtained in the plot of application depths simulated by the computer.

6. Triangular and elliptical distribution profiles that were assumed in the simulation model did not differ under most conditions tested. In general, however, the triangular distribution profile gave slightly better agreement with the actual distribution profile.

7. Time synchronization of the experimental process and accuracy in recording measurements of influencing environmental parameters (such as wind velocity and direction) is required to improve the accuracy of the model so that the wide fluctuations in the field are accounted for. The simulation model can then be accurately validated.

8. The two Christiansen coefficients of uniformity used in this study gave only a satisfactory measure of uniformity. A better agreement is obtained when the uniformity is evaluated using the weighted coefficient. In general, although wide fluctuation

in application depths occurred under the experimental conditions, the coefficients of uniformity derived fell within the higher limits of acceptance. The overlapping effect of the closely spaced adjacent sprinklers is most probably resposible for such values of coefficient of uniformity.

9. As a result of a number of field experimental errors in the measurements of application depths, environmental parameters and long experimental test times, no valid relationships can be made between the coefficient of uniformity and the variation in the environmental factors that occurred during the experiment.

10. The simulation model provided a method for studying the effect of wind magnitude and direction which was a continuous phenomenon throughout the experimental period. With proper validation of the simulation model, further improvement in design criteria for C.P. sprinkler irrigation systems can be made. For example, the optimum spacing of sprinklers, sprinkler type, and size of the nozzles for a given set of known system characteristics, can be theoretically determined.

CHAPTER VIII

SUGGESTIONS FOR FURTHER STUDY

Further research oriented toward improving the accuracy and the efficiency of the simulated model should consider the following areas of work:

1. More accurate determination of the sprinkler droplet sizes.
2. Construction of the sprinkler distribution patterns entirely on the basis of droplet size distribution within the sprinkler wetted patterns.
3. Implementing losses due to evaporation and wind drift into the equations of motion.
4. Elimination of the interpolation procedures used in the model.
5. Validation of the simulated model based firstly on experimental research in the laboratory under controlled climatic conditions and secondly under actual field conditions.

CHAPTER IX

REFERENCES

1. American Scociety of Agricultural Engineers. ASAE R264.2 Minimum requirements for the design, installation, and performance of sprinkler irrigation equipment. 1978 Agricultural Engineers Yearbook, pp . 526-528.

2. Benami, A. and F.R. Hore. 1964. A new irrigation-sprinkler distribution coefficient. Trans. Amer. Soc. Agr. Eng. 7(1):157-158.

3. Bilanski, W.K. and E.H. Kidder. 1958. Factors that affect the distribution of water from a medium-pressure rotary irrigation sprinkler. Trans. Amer. Soc. Agr. Eng. 1(1):19-23, 28.

4. Bittinger, M.W. and R.A. Longenbaugh. 1962. Theoretical distribution of water from a moving irrigation sprinkler. Trans. Amer. Soc. Agr. Eng. 5(1):26-30.

5. Christiansen, J.E. 1941. The uniformity of application of water by sprinkler systems. Agr. Eng. 89-92.

6. Christiansen, J.E. 1942. Irrigation by sprinkling. California Agr. Expt. Sta. Bull. 670.

7. Criddle, W.D., et al. 1956. Methods for evaluating irrigation systems. US Dept. Agr.-Soil Conserv. Handbook 82. US Supt. Doc., Washington, D.C.

8. Daugherty, R.L. and J.B. Franzini. 1965. Fluid mechanics with engineering applications (6th. ed.). McGraw-Hill, New York.

9. Greville, T.N.E. 1967. Mathematical methods for digital computers. Vol. II. John Wiley, New York, N.Y.

10. Hall, M.J. 1970. Use of the stain method in determining the drop-size distributions of coarse liquid sprays. Trans. Amer. Soc. Agr. Eng. 13(1):33-37,41

11. Heerman, D.F and P.R. Hein. 1968. Performance characteristics of self-propelled center-pivot sprinkler irrigation system. Trans. Amer. Soc. Agr. Eng. 11(1):11-15.

12. .....International Mathematical and Statistical Libraries Ltd. 1973. IMSL Library 1, Vol. 1 and 2. Dept. of Computing Science, University of Alberta, Edmonton, Alberta.

13. Kohl, R.A. 1974. Drop size distribution from medium-sized agricultural sprinklers. Trans. Amer. Soc. Agr. Eng. 17(4):690-693.

14. Korven, H.C. 1952. The effect of wind on the uniformity of water distribution by some rotary sprinklers. Sci. Agr. 32(4): 226-239.

15. Merrington, A.C. and E.G. Richardson. 1947. The breakup of liquid jets. Proc. Phy. Soc. (London) 59(2):1-3.

16. Miesse, C.C. 1955. Correlation of experimental data on the disintegration of liquid jets. Indust. Eng. Chem. 47(9):1690-1701.

17. Okamura, Shunichi. 1968. Theoretical study of sprinkler sprays (part one)(under conditions of no wind). Transcription from Transactions of the Japanese Society of Irrigation, Drainage and Reclamation Engineering, No. 26.

18. Okamura, Shunichi. 1968. Theoretical study of sprinkler sprays (part two)(under conditions of wind drift). Transcription from Transactions of the Japanese Society of Irrigation, Drainage and Reclamation Engineering, No. 26.

19. Pair, C.H. (editor). 1969. Sprinkler Irrigation (3rd. ed.). Sprinkler Irrigation Association, Washington, D.C.

20. Rouse, Hunter et al. 1952. Experimental investigation of fire monitors and nozzles. Trans. Amer. Soc. Civil Eng. 117: 1147-1188.

21. Seginer, I. 1963. Water distribution from medium pressure sprinklers. J. Irr. Div., Proc. Amer. Soc. Civ. Engrs. 89: (IR2) 13-29.

22. Seginer, I. 1965. Tangential velocity of sprinkler drops. Trans. Amer. Soc. Agr. Eng. 8(1):90-93.

23. Tezer, E. 1971. Investigation into distribution uniformity of water from sprinkler heads. University of Ankara Yearbook of the Faculty of Agriculture-Adana.

24. Umback, C.R. and W.D. Lembke. 1966. Effects of wind on falling water drops. Trans. Amer. Soc. Agr. Eng. 9(6):805-808.

25. Wilcox, J.C. and J.M. McDougald. 1955. Water distribution patterns from rotary sprinklers. Can. Jour. of Agr. Sc. 35: 217-228.

26. Wilcox, J.C. and G.E. Swailes. 1947. Uniformity of water distribution of some undertree orchard sprinklers. Sci. Agr. 27(9):565-583.

APPENDICES

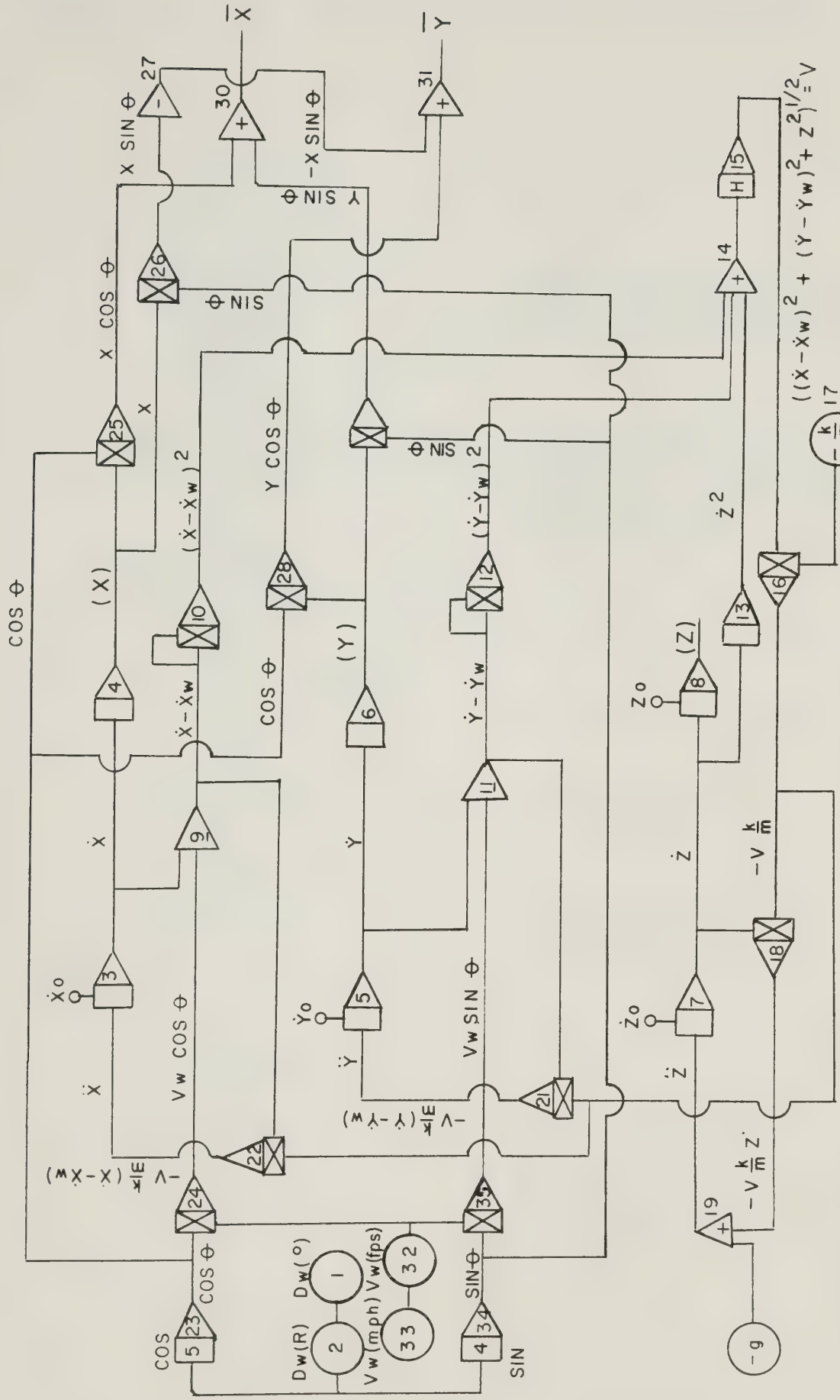

APPENDIX I. BLOCK DIAGRAM OF MODEL SIMULATING THE DYNAMICS OF FLYING WATER DROPLET EMITTED BY A SPRINKLER.

APPENDIX II. FLOW CHART OF THE OPERATING SIMULATION MODEL.

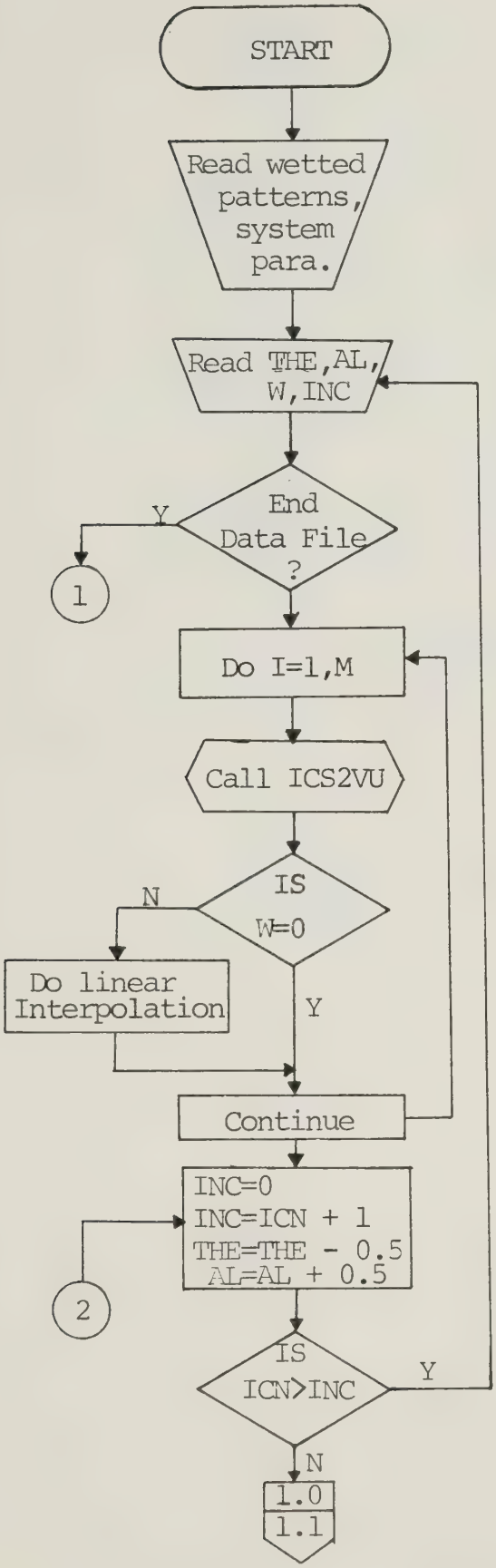

Input variables defining basic wetted patterns and system specifications.

Input position of the lateral, direction of wind, wind velocity, number of ½° increments of lateral rotation.

Do for each sprinkler.

Do two dimensional interpolation.

If wind velocity greater than zero, do linear interpolation.

Set counter to zero.
Count no. of ½° incr. of lat. rota.
Generate position of lateral.
Generate constant wind direction for given no. of ½° increments.

APPENDIX II. CONTINUED

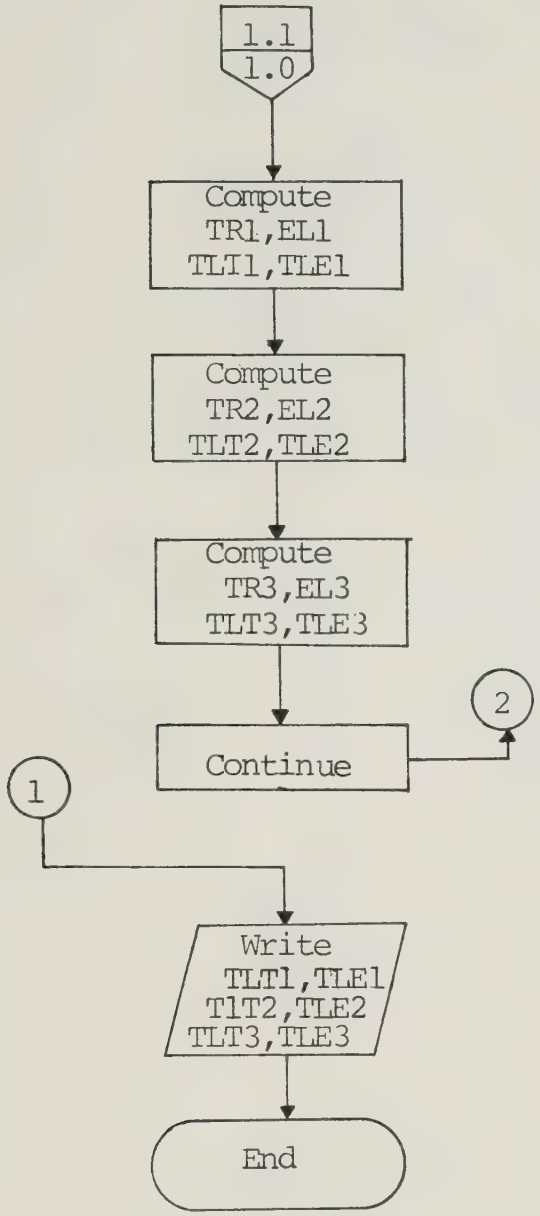

Compute application rates and application depth for each point of the first row.*

Compute application rates and application depths for each point of the second row.*

Compute application rates and application depths for each point of the third row.*

Write application depths for each of the three rows.

*See detail flow chart on the following page.

APPENDIX II. CONTINUED.

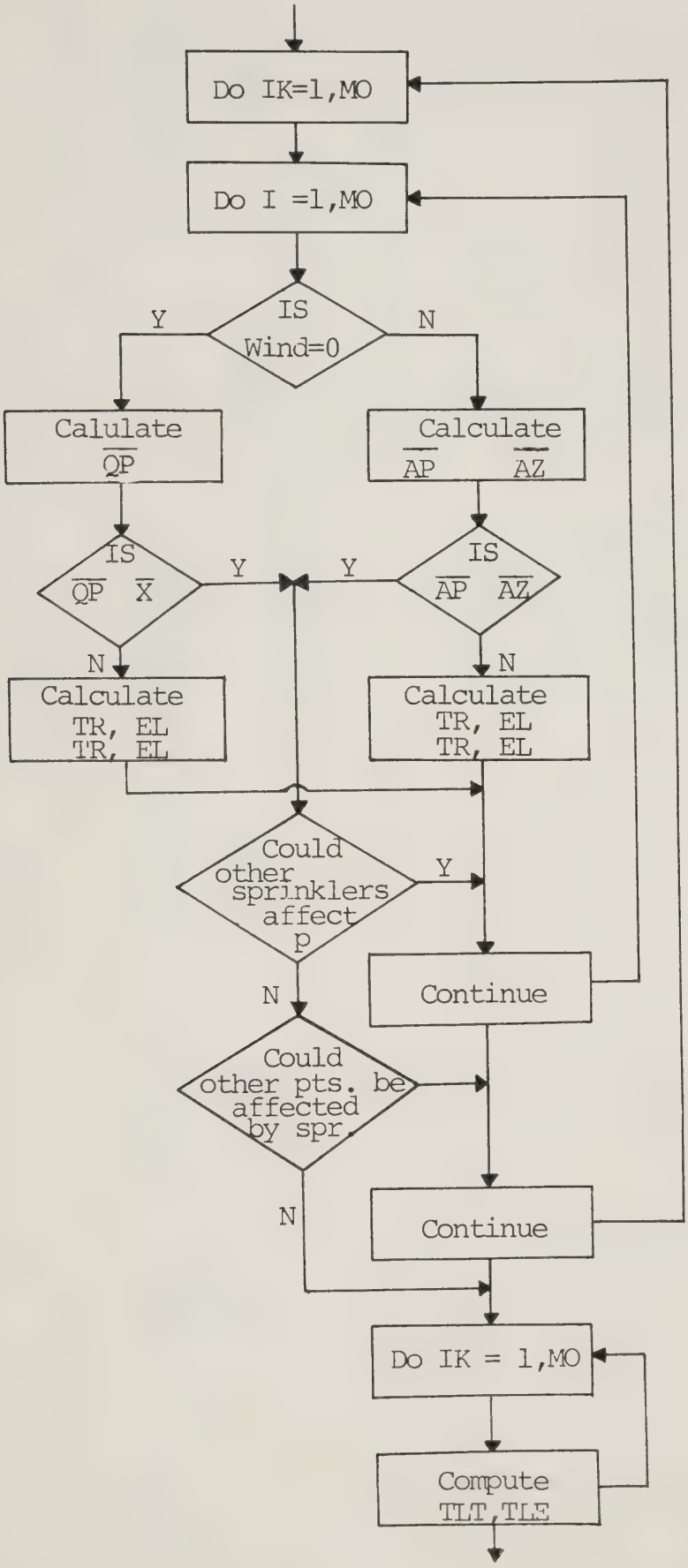

Do for each point (P).

Do for each sprinkler (Q).

Consider: Circular patterns (W=0) or Ellip. patterns (W=0).

Compute distance from point of max. appl. rate (Q or A) to point under consideration (P) and to point on bndry. (Z).

Search if pt. (P) is within the wetted pattern.

Compute appl. rate and partial appl. depth for triang. and ellipt. distr.

Search if any other wetted pattern encloses point (P).

Search if any other point (P) receives water application

Compute total appl. depth for each point (P).

APPENDIX IIIA. DETAILED CHARACTERISTICS DATA OF THE "CIRCLE MASTER"C.P. SYSTEM.

Sprinkler No.	Distance From Pivot (FT)	Available Pressure (P.S.I.)	Actual Pressure (P.S.I.)	Rain Bird Sprinkler	Nozzle (INS)	Sprinkler Discharge (G.P.M.)
	0	80.0				
1	29.2	79.0	61.0	14 V TNT	5/64	1.39
2	69.2	77.7	53.5	20 TNT	1/8	3.30
3	109.2	76.3	76.3	30 EW TNT	5/32	5.99
4	154.8	78.8	78.8	30 E TNT	11/64 +1/16	8.26
5	194.8	73.5	73.5	30 EW TNT	13/64	9.27
6	234.8	72.2	72.2	30 EW TNT	7/32	11.78
7	270.4	71.1	71.1	30 EN TNT	11/64	7.04
8	290.4	70.5	70.5	30 EW TNT	11/64	7.01
9	310.4	69.8	69.3	30 EW TNT	11/64	6.98
10	330.4	69.2	69.2	30 E TNT	11/64 + 1/16	7.94
11	350.4	68.6	68.6	30 EW TNT	3/16	8.27
12	370.4	68.0	68.0	30 E TNT	13/64 + 1/16	9.90
13	396.0	67.3	67.3	30 E TNT	13/64 + 3/32	11.0
14	416.0	66.7	66.7	30 E TNT	13/64 + 1/16	9.81
15	436.0	66.2	66.2	30 E TNT	13/64 + 5/64	10.25

APPENDIX IIIA. CONTINUED.

Sprinkler No.	Distance From Pivot (FT)	Available Pressure (P.S.I.)	Actual Pressure (P.S.I.)	Rain Bird Sprinkler	Nozzle (INS.)	Sprinkler Discharge (G.P.M.)
16	456.0	65.6	65.6	30 E TNT	13/64 + 3/32	10.86
17	476.0	65.1	65.1	30 EW TNT	7/32	11.18
18	496.0	64.6	64.6	30 E TNT	13/64 + 3/32	10.78
19	511.6	64.2	64.2	30 E TNT	11/64 + 1/16	7.64
20	521.6	63.9	63.9	30 E TNT	5/32 + 1/16	6.41
21	531.6	63.7	63.7	30 E TNT	5/32 + 1/16	6.40
22	541.6	63.4	63.4	30 E TNT	5/32 + 1/16	6.39
23	551.6	63.2	63.2	30 EW TNT	11/64	6.63
24	561.6	62.9	62.9	30 EW TNT	11/64	6.62
25	571.6	62.7	62.7	30 EW TNT	11/64	6.61
26	581.6	62.5	62.5	30 EW TNT	11/64	6.59
27	591.6	62.2	62.2	30 E TNT	11/64 + 1/16	7.52
28	601.6	62.0	62.0	30 E TNT	11/64 + 1/16	7.51
29	611.6	61.8	61.8	30 E TNT	11/64 + 1/16	7.41
30	621.6	61.6	61.6	30 E TNT	13/64 + 1/16	9.43
31	637.2	61.2	61.2	30 E TNT	13/64 + 5/64	9.86

APPENDIX IIIA. CONTINUED.

Sprinkler No.	Distance From Pivot (FT)	Available Pressure (P.S.I.)	Actual Pressure (P.S.I.)	Rain Bird Sprinkler	Nozzle (INS)	Sprinkler Discharge (G.P.M.)
32	647.2	61.0	61.0	30 EW TNT	1/16	7.79
33	657.2	60.8	60.8	30 EW TNT	1/16	7.78
34	667.2	60.6	60.6	30 EW TNT	1/16	7.76
35	677.2	60.4	60.4	30 EW TNT	3/16	7.75
36	687.2	60.2	60.2	30 EW TNT	13/64	8.40
37	697.2	60.0	60.0	30 EW TNT	13/64	8.39
38	707.2	59.8	59.8	30 EW TNT	13/64	8.38
39	717.2	59.7	59.7	30 EW TNT	13/64	8.36
40	727.2	59.5	59.5	30 EW TNT	13/64	8.35
41	737.2	59.3	59.3	30 EW TNT	13/64	8.34
42	747.2	59.1	59.1	30 E TNT	7/32 + 1/16	11.57
43	762.8	58.9	58.9	30 E TNT	7/32 + 1/16	11.55
44	772.8	58.7	58.7	30 E TNT	13/64 + 1/16	9.21
45	782.2	58.5	58.5	30 E TNT	13/64 + 1/16	9.20
46	792.9	58.4	58.4	30 E TNT	13/64 + 5/64	9.64
47	802.8	58.2	58.2	30 E TNT	13/64 + 5/64	9.62
48	812.8	58.1	58.1	30 E TNT	13/64 + 5/64	9.61

APPENDIX IIIA. CONTINUED.

Sprinkler No.	Distance From Pivot (FT)	Available Pressure (P.S.I.)	Actual Pressure (P.S.I.)	Rain Bird Sprinkler	Nozzle (INS)	Sprinkler Discharge (G.P.M.)
49	822.8	57.9	57.9	30 E TNT	13/64 + 5/64	9.60
50	832.8	57.8	57.8	30 E TNT	13/64 + 3/32	10.20
51	842.8	57.7	57.7	30 E TNT	13/64 + 3/32	10.19
52	852.8	57.5	57.5	30 E TNT	13/64 + 3/32	10.18
53	862.8	57.4	57.4	30 E TNT	13/64 + 3/32	10.17
54	872.8	57.3	57.3	14070 W TNT	1/4	12.98
55	888.4	57.1	57.1	14070 TNT	1/4 + 1/16	13.86
56	898.4	57.0	57.0	30 EW TNT	7/32	10.46
57	908.4	56.9	56.9	30 EW TNT	7/32	10.45
58	918	56.8	56.8	30 E TNT	7/32 + 1/16	11.34
59	928.4	56.7	56.7	30 E TNT	7/32 + 1/16	11.33
60	938.4	56.6	56.6	30 E TNT	7/32 + 1/16	11.32
61	948.2	56.5	56.5	30 E TNT	7/32 + 1/16	11.31
62	958.4	56.4	56.4	30 E TNT	7/32 + 1/16	11.30
63	968.4	56.3	56.3	30 E TNT	7/32 + 5/64	11.73
64	978.4	56.2	56.2	30 E TNT	7/32 + 5/64	11.72
65	988.4	56.1	56.1	30 E TNT	7/32 + 5/64	11.71

APPENDIX IIIA. CONTINUED.

Sprinkler No.	Distance From Pivot (FT)	Available Pressure (P.S.I.)	Actual Pressure (P.S.I.)	Rain Bird Sprinkler	Nozzle (INS)	Sprinkler Discharge (G.P.M.)
66	998.4	56.0	56.0	14070 TNT	17/64 + 1/16	15.32
67	1014.0	55.9	55.9	14070 TNT	17/64 + 1/16	15.30
68	1024.0	55.8	55.8	14070 W TNT	15/64	12.01
69	1034.0	55.8	55.8	14070 W TNT	15/64	12.00
70	1044.0	55.7	55.7	14070 W TNT	1/4	12.79
71	1054.0	55.7	55.7	14070 W TNT	1/4	12.79
72	1064.0	55.6	55.6	14070 W TNT	1/4	12.78
73	1074.0	55.5	55.5	14070 W TNT	1/4	12.77
74	1084.0	55.5	55.5	14070 W TNT	1/4	12.77
75	1094.0	55.4	55.4	14070 W TNT	1/4	12.76
76	1104.0	55.4	55.4	14070 W TNT	1/4	12.76
77	1114.0	55.4	55.4	14070 TNT	1/4 + 1/16	13.64
78	1124.0	55.3	55.3	14070 TNT	9/32 + 5/64	16.93
79	1139.7	55.3	55.3	14070 TNT	9/32 + 3/32	17.52
80	1149.7	55.2	55.2	14070 TNT	1/4 + 1/16	13.63
81	1159.7	55.2	55.2	14070 TNT	1/4 + 1/16	13.62

APPENDIX IIIA. CONTINUED.

Sprinkler No.	Distance From Pivot (FT)	Available Pressure (P.S.I.)	Actual Pressure (P.S.I.)	Rain Bird Sprinkler	Nozzle (INS)	Sprinkler Discharge (G.P.M.)
82	1169.7	55.2	55.2	14070 TNT	1/4 + 5/64	14.06
83	1179.7	55.2	55.2	14070 TNT	1/4 + 5/64	14.05
84	1189.7	55.1	55.1	14070 W TNT	17/64	14.31
85	1199.7	55.1	55.1	14070 W TNT	17/64	14.31
86	1209.7	55.1	55.1	14070 W TNT	17/64	14.31
87	1219.7	55.1	55.1	14070 W TNT	17/64	14.30
88	1229.7	55.1	55.1	14070 W TNT	17/64	14.30
89	1239.7	55.1	55.1	14070 TNT	17/64 + 1/16	15.19
90	1249.7	55.1	55.1	14070 TNT	17/64 + 1/16	15.19
91	1259.7	55.0	55.0	14070 TNT	17/64 + 1/16	15.19
92	1269.7	55.0	55.0	14070 TNT	17/64 + 1/16	15.18
93	1279.7	55.0	55.0	14070 W TNT	1/4	12.71
94	1286.7	55.0	55.0	30 EW TNT	3/16**	7.39
95	1289.2	55.0	55.0	(2)85 E TNT	1/2 + 7/64*	56.10 each

**Sprinkler not available

*Large volume "end gun"

APPENDIX IIIB. DETAILED SYSTEM CHARACTERISTICS OF THE "VALLEY 1160" C.P. SYSTEM.

Sprinkler No.	Distance From Pivot (FT)	Line Pressure (P.S.I.)	Nozzle Pressure (P.S.I.)	Sprinkler Series	Nozzle Size (INS)	Sprinkler Discharge (G.P.M.)
	18.23		80.00			
1	50.61	79.09	35.00	20	7/64	2.10
2	82.99	78.19	60.00	20	7/64	2.74
3	115.37	77.29	60.00	20	9/64	4.45
4	147.75	76.40	60.00	20	5/32	5.42
5	180.13	75.52	60.00	30	11/64	6.63
6	212.51	74.65	60.00	30	9/64 + 7/64	7.12
7	244.89	73.79	60.00	30	11/64 + 3/32	8.58
8	277.27	72.94	60.00	30	3/16 + 3/32	9/83
9	309.65	72.11		30	3/16 + 3/32	10.57
10	342.03	71.30		30	3/16 + 1/8	12.12
11	374.41	70.50		30	13/64 + 1/8	13.46
12	406.79	69.73		30	13/64 + 9/64	14.33
13	439.17	68.98		30	7/32 + 9/64	15.76
14	471.55	68.25		30	7/32 + 5/32	17.27
15	503.93	67.54		30	7/32 + 11/64	17.77

APPENDIX IIIB. CONTINUED.

Sprinkler No.	Distance From Pivot (FT)	Line Pressure (P.S.I.)	Nozzle Pressure (P.S.I.)	Sprinkler Series	Nozzle Size (INS)	Sprinkler Discharge (G.P.M.)
16	536.31	66.86		30	7/32 + 3/16	18.92
17	568.69	66.21		30	7/32 + 13/64	20.17
18	601.07	65.59		70	7/32 + 32	22.07
19	633.45	65.00		70	7/32 + 7/32	21.97
20	655.83	64.44		70	7/32 + 7/32	21.88
21	698.21	63.90		70	1/4 + 7/32	24.91
22	730.59	63.40		70	1/4 + 7/32	24.81
23	762.97	62.93		70	9/32 + 7/32	28.05
24	795.35	62.50		70	9/32 + 7/32	27.95
25	827.73	62.09		70	5/16 + 3/16	28.99
26	860.11	61.72		70	5/16 + 3/16	28.96
27	892.49	61.38		70	5/16 + 7/32	32.62
28	924.87	61.08		70	11/32 + 3/16	32.62
29	957.25	60.81		70	11/32 + 7/32	34.86
30	989.63	60.56		70	11/32 + 7/32	34.79
31	1022.01	60.35		70	3/8 + 3/16	36.45

APPENDIX IIIB. CONTINUED.

Sprinkler No.	Distance From Pivot (FT)	Line Pressure (P.S.I.)	Nozzle Pressure (P.S.I.)	Sprinkler Series	Nozzle Size (INS)	Sprinkler Discharge (G.P.M.)
32	1054.39	60.17		70	3/8 + 3/16	36.39
33	1086.77	60.02		70	3/8 + 7/32	38.53
34	1119.15	59.89		70	3/8 + 7/32	38.49
35	1151.53	59.79		70	3/8 + 7/32	38.46
36	1183.91	59.71		80	3/8 + 1/4	43.06
37	1216.29	59.65		80	3/8 + 1/4	43.04
38	1248.67	59.61		70	3/8 + 7/32	38.46
39	1272.87	59.59		70	1/4 + 7/32	24.06
40	1284.97	59.59		70	9/32 + 7/32	27.29
42	1289.97	59.54	53.69	85	5/8 + 7/32 *	85.55

* Large volume "end gun"

APPENDIX IV

This appendix contains figures $IV_{(1)}$ to figures $IV_{(11)}$, showing the comparison of field and simulated application depths for the "Circle Master" and "Valley 1160" C.P. systems.

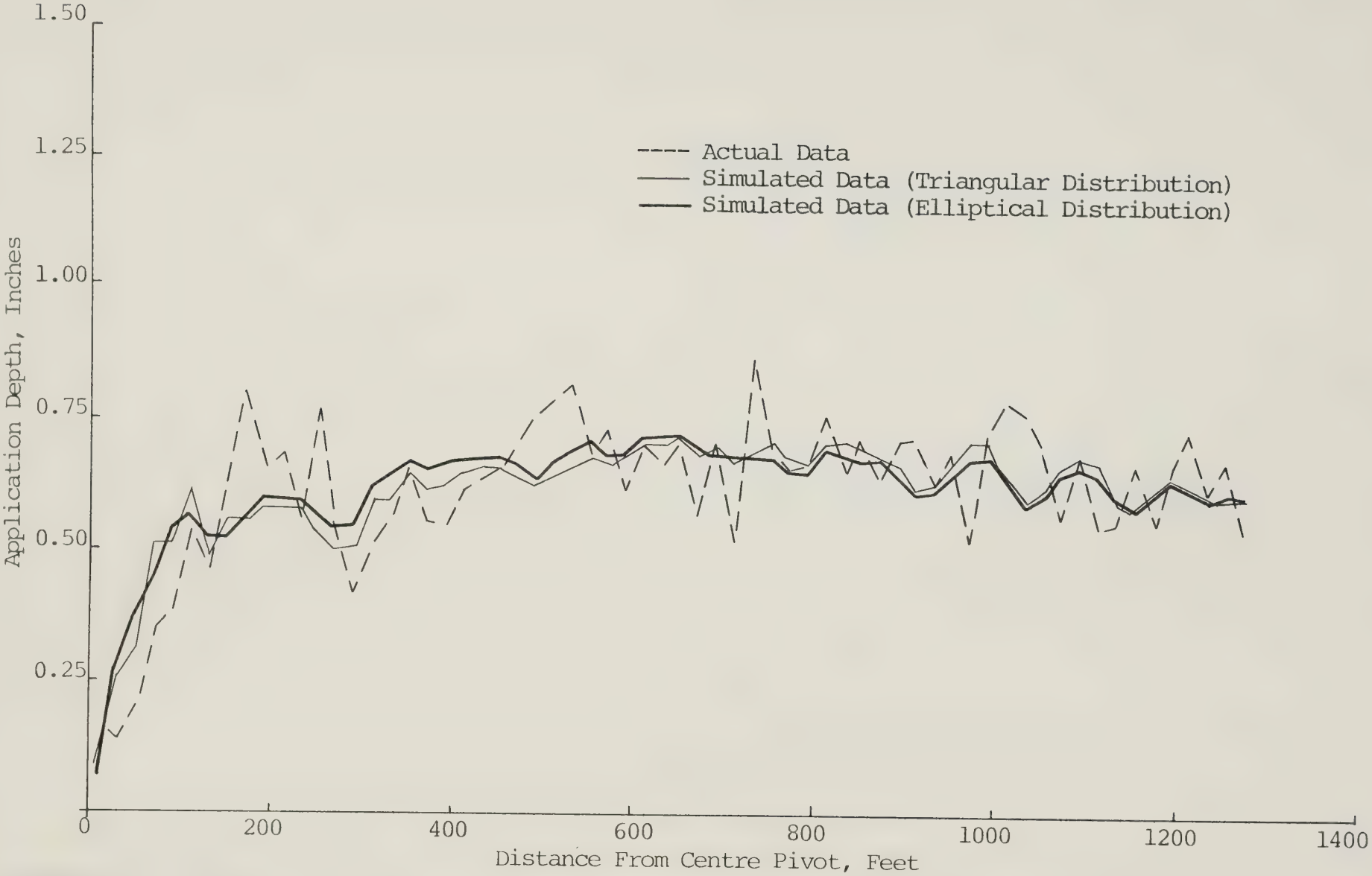

APPENDIX IV. Figure IV$_{(1)}$. Comparison of field and simulated application depths. "Circle Master" C.P. System test 7 row 2.

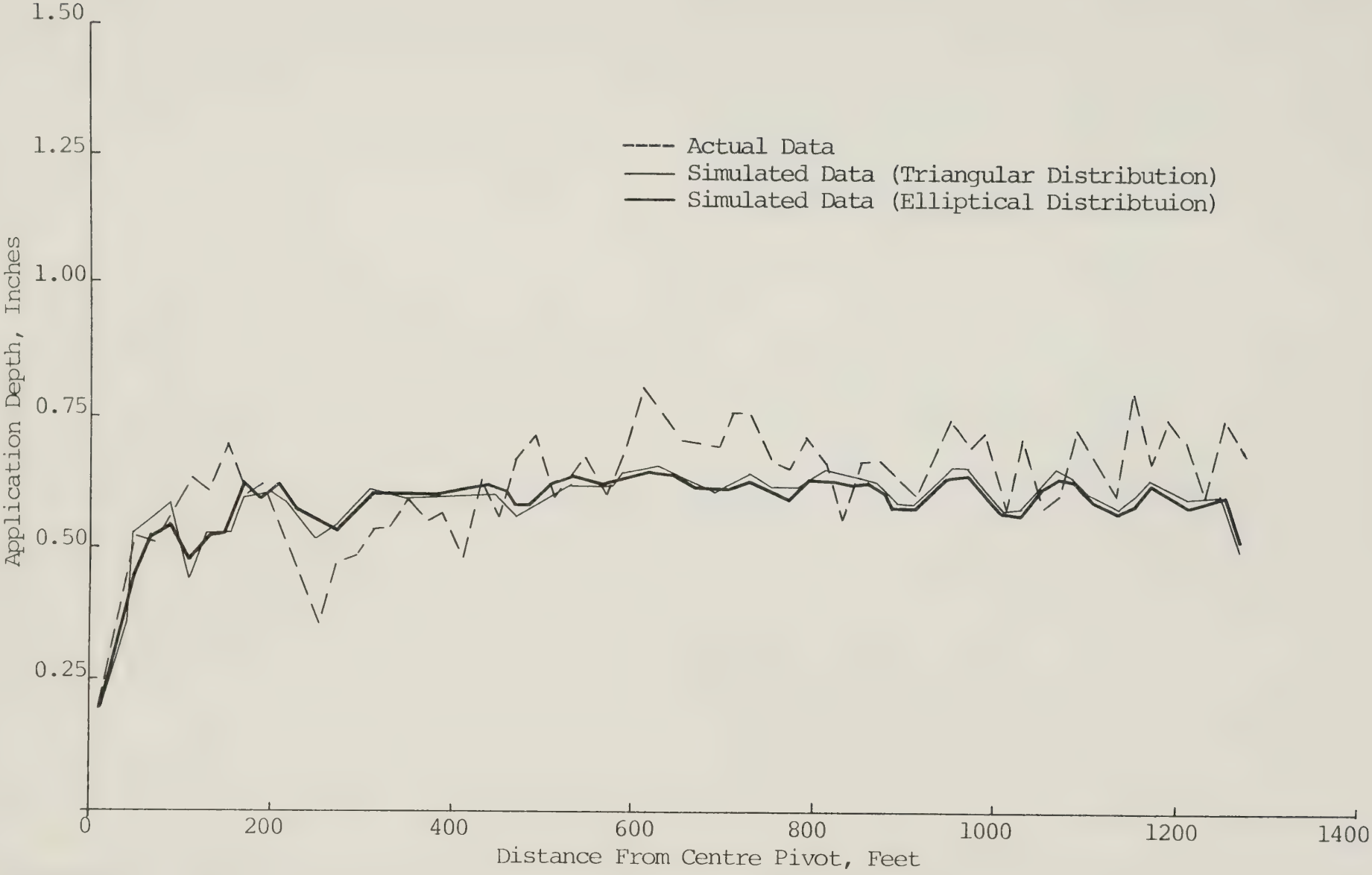

APPENDIX IV. Figure $IV_{(2)}$. Comparison of field and simulated application depths. "Circle Master" C.P. System test 8 row 2.

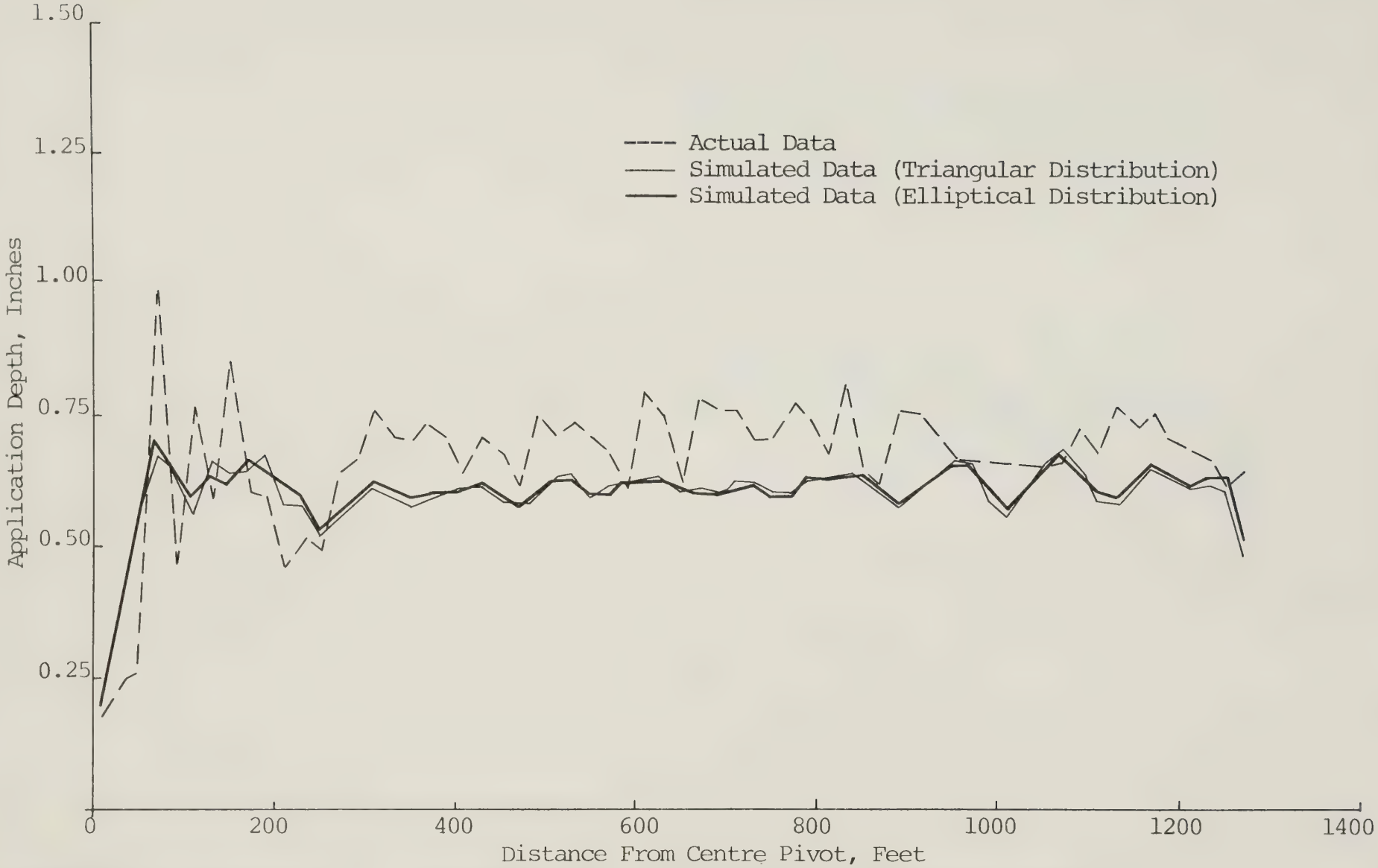

APPENDIX IV. Figure $IV_{(3)}$. Comparison of field and simulated application depths. "Circle Master" C.P. System test 9 row 2.

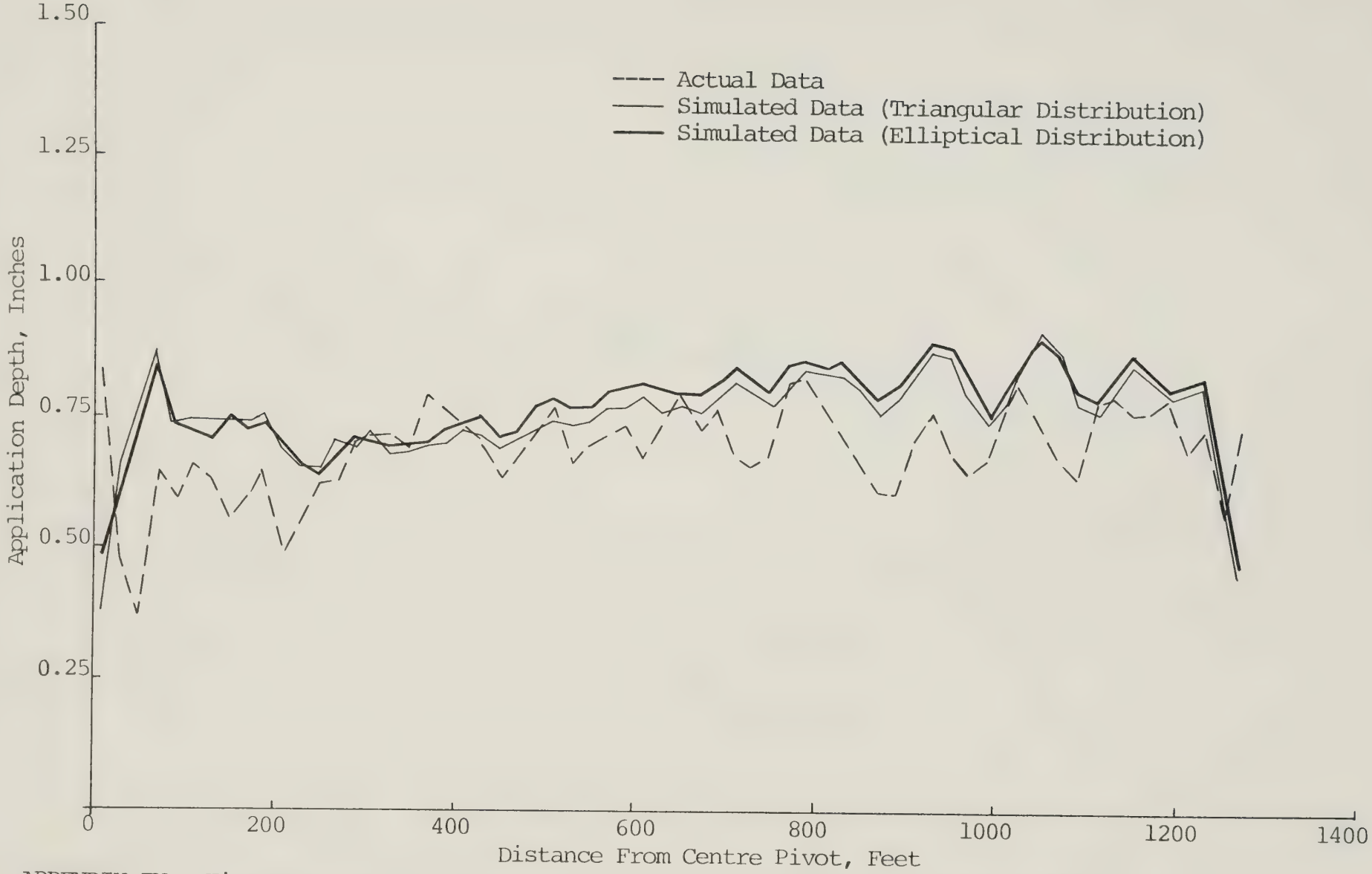

APPENDIX IV. Figure IV.(4). Comparison of field and simulated application depths. "Circle Master" C.P. System test 10 row 2.

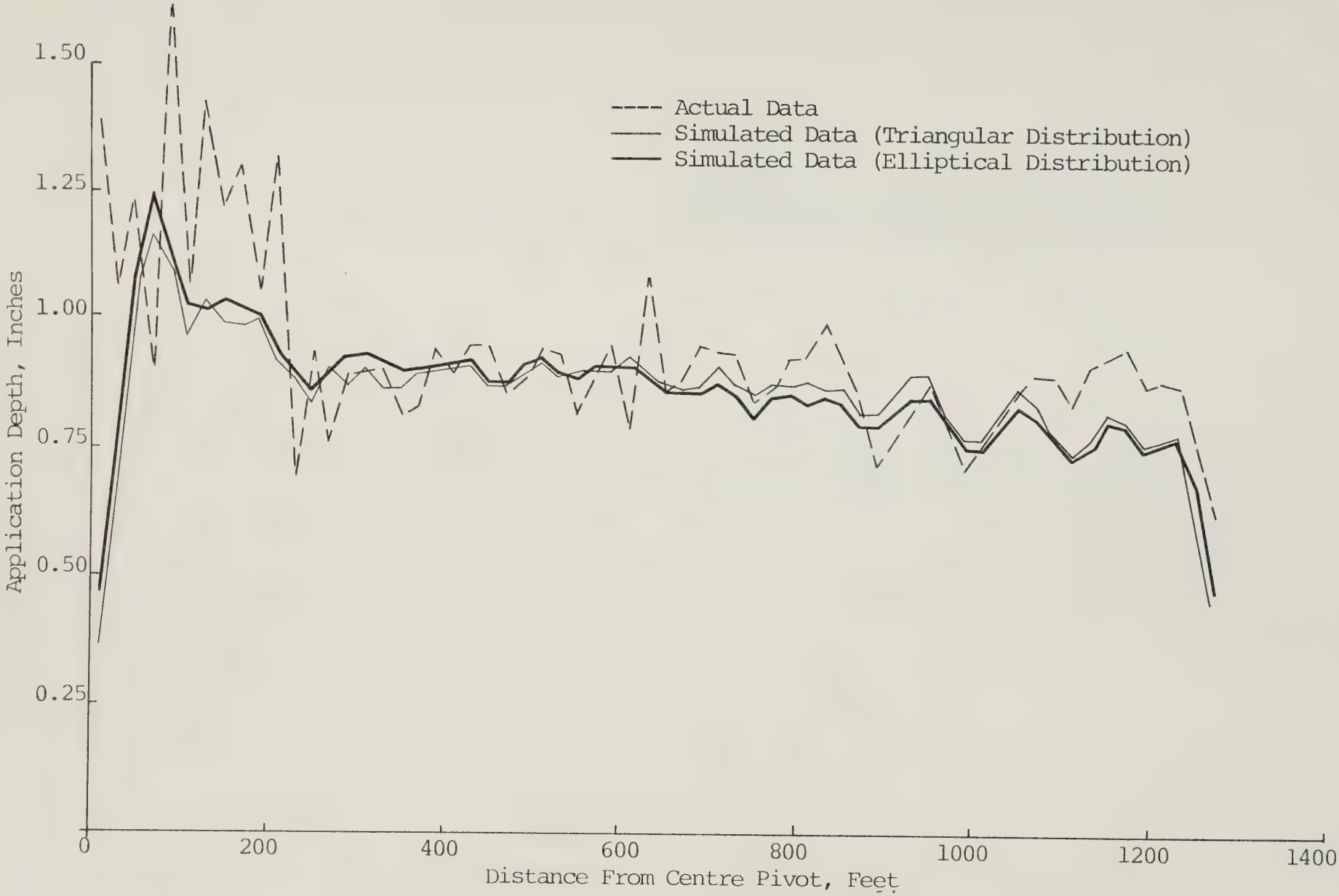

APPENDIX IV. Figure IV$_{(5)}$. Comparison of field and simulated application depths. "Circle Master" C.P. System test 11 row 2.

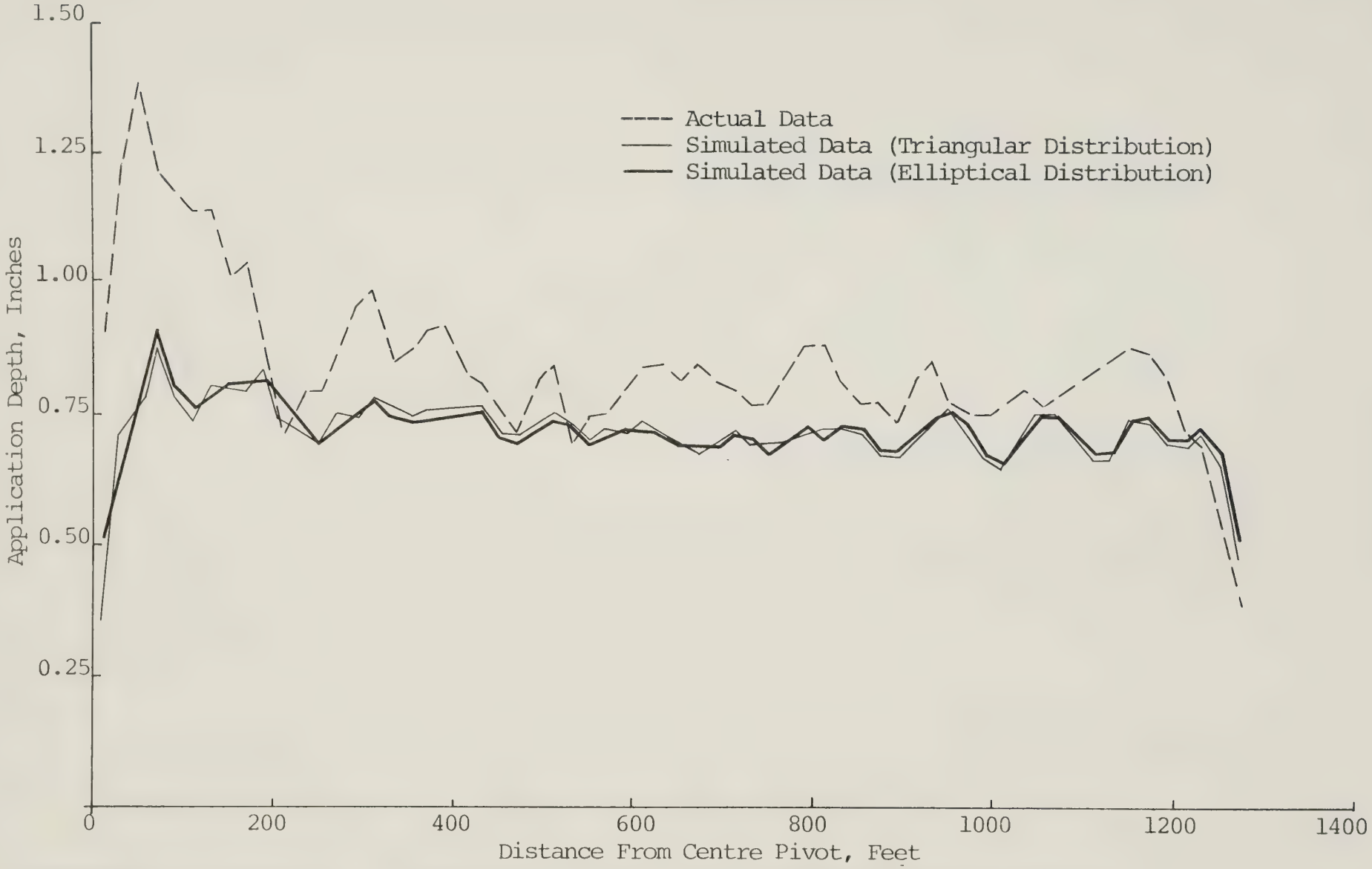

APPENDIX IV. Figure $IV_{(6)}$. Comparison of field and simulated application depths. "Circle Master" C.P. System test 12 row 2.

APPENDIX IV. Figure IV$_{(7)}$. Comparison of field and simulated application depths. "Circle Master" C.P. System test 13 row 2.

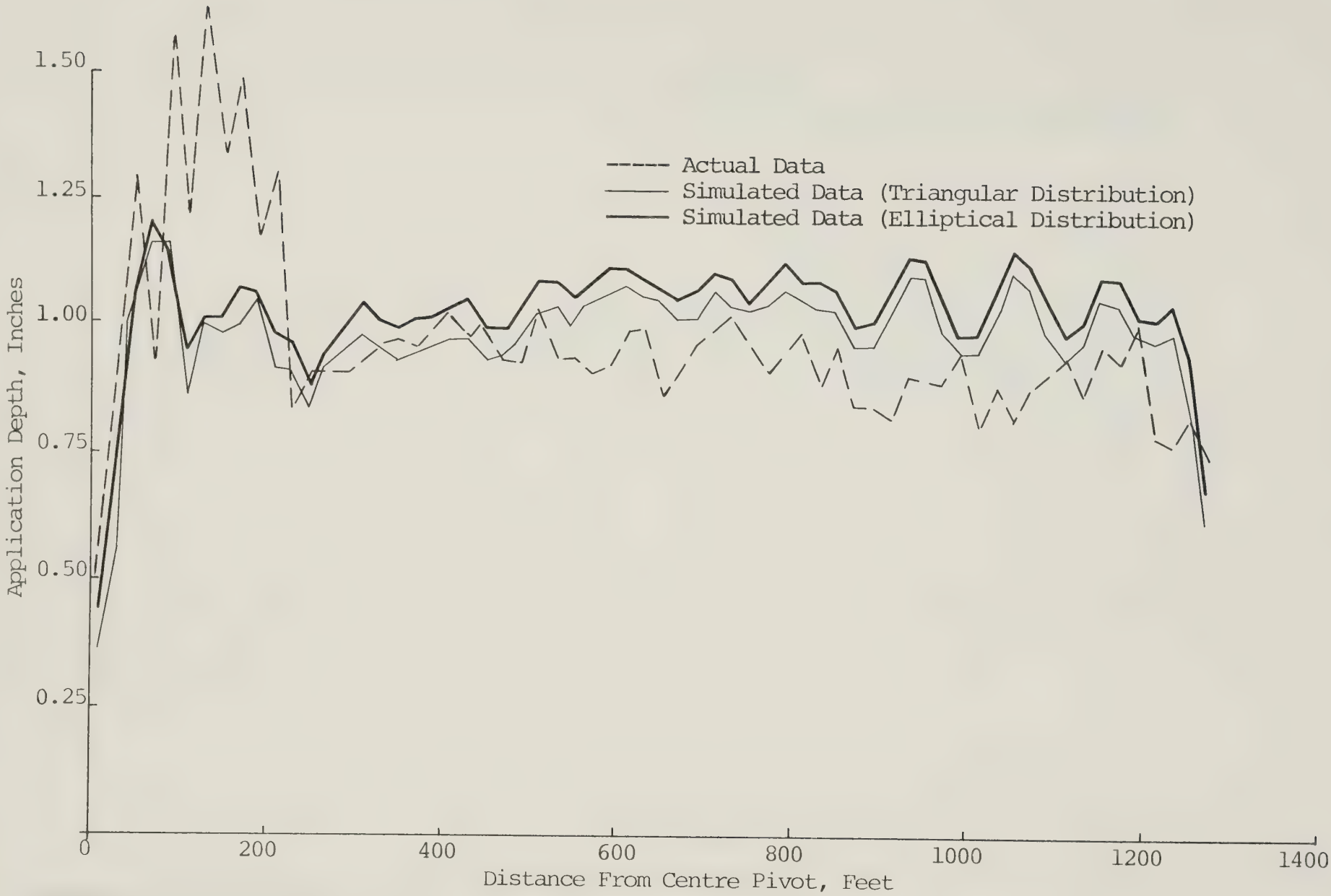

APPENDIX IV. Figure IV$_{(8)}$. Comparison of field and simulated application depths. "Circle Master" C.P. System test 14 row 2.

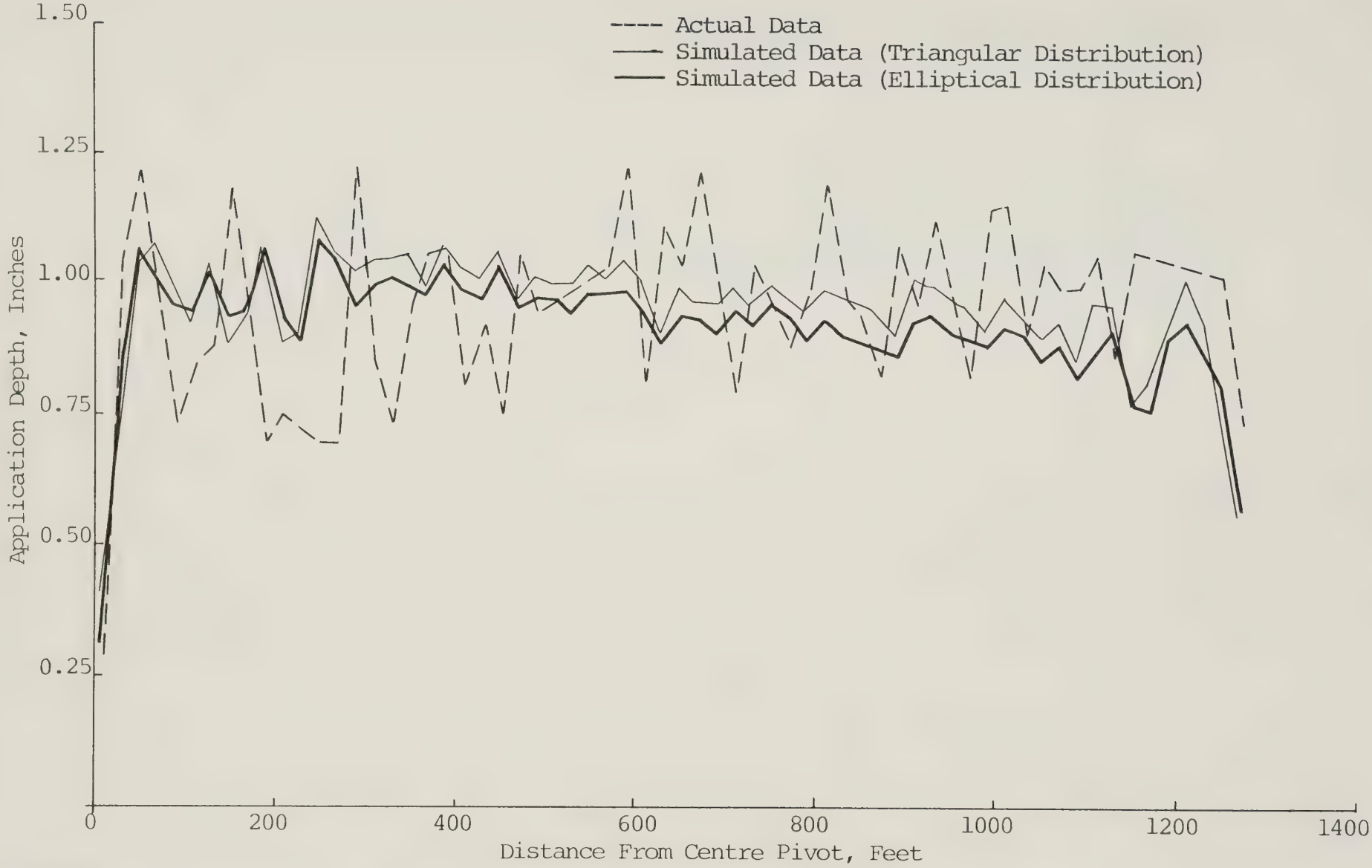

APPENDIX IV. Figure $IV_{(9)}$. Comparison of field and simulated application depths. "Valley 1160" C.P. System test 2 row 2.

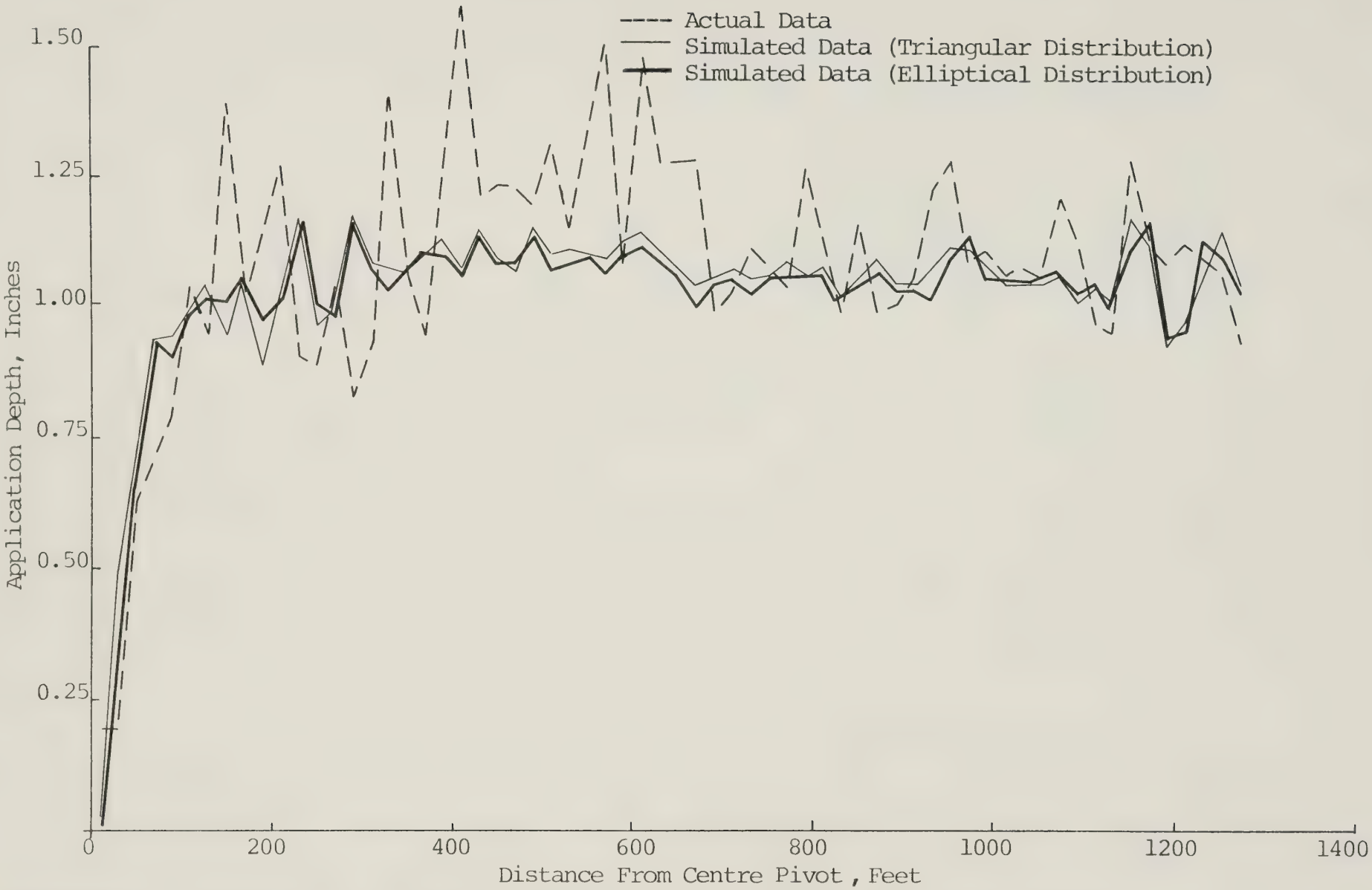

APPENDIX IV. Figure IV$_{(10)}$. Comparison for field and simulated application depths. "Valley 1160" C.P. System test 3 row 2.

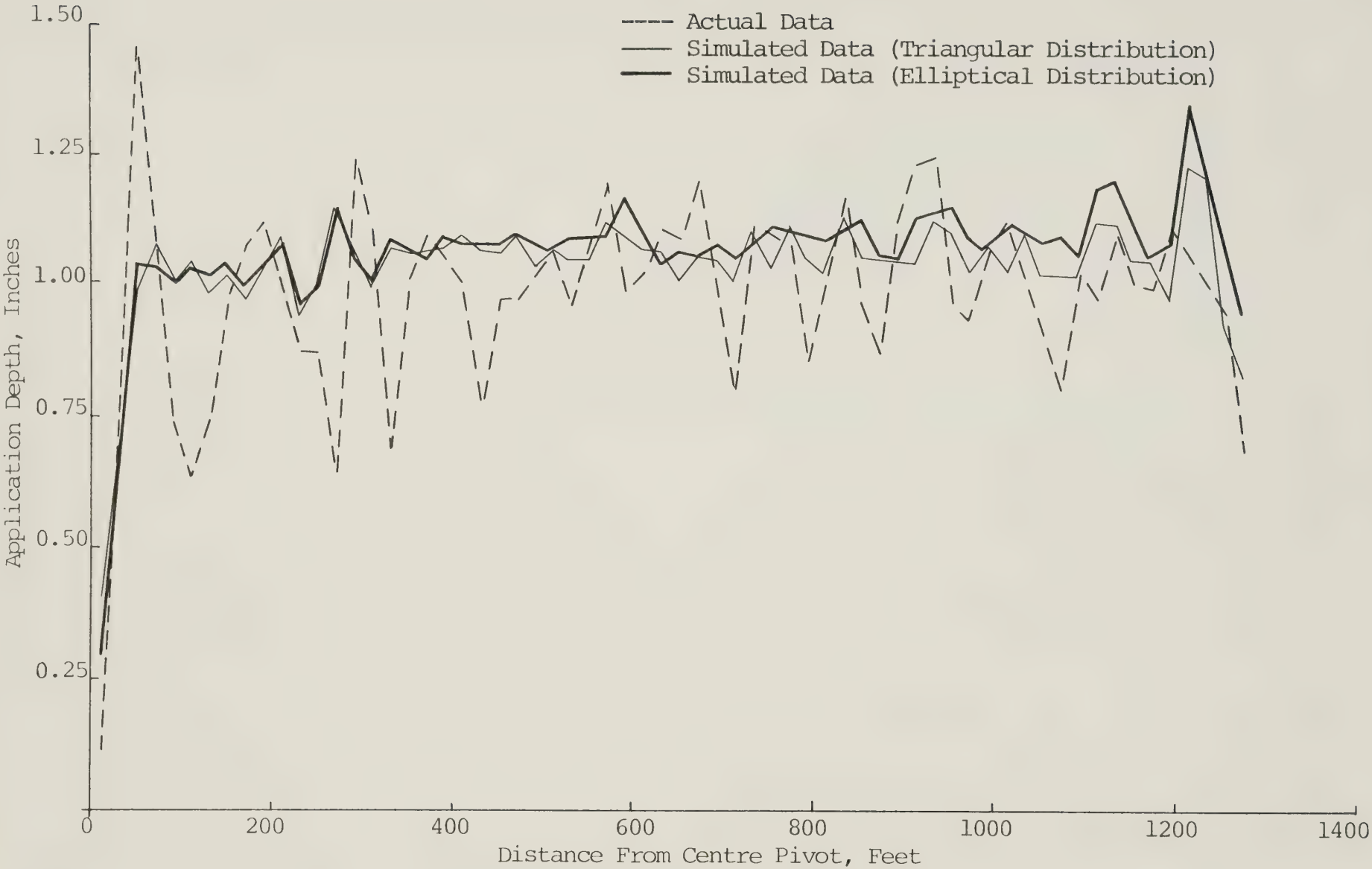

APPENDIX IV. Figure $IV_{(11)}$. Comparison of field and simulated application depths. "Valley 1160" C.P. System test 6 row 6.

APPENDIX V

This appendix contains figures $V_{(1)}$ to $V_{(6)}$, showing the distribution of application depths for the "Circle Master" and "Valley 1160" C.P. systems.

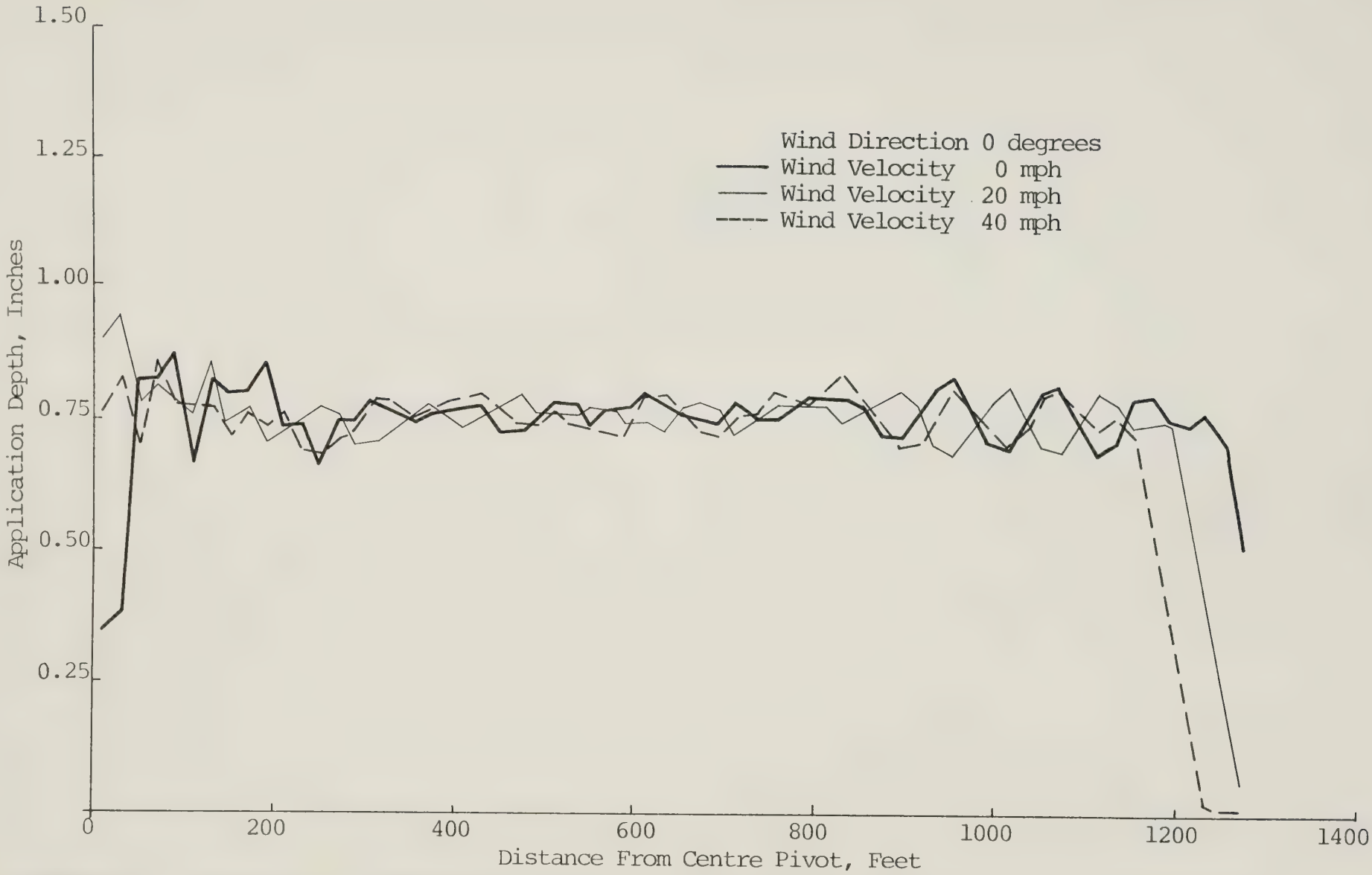

APPENDIX V. Figure $V_{(1)}$. Predicted distribution of application depths for the "Circle Master" C.P. Systems.

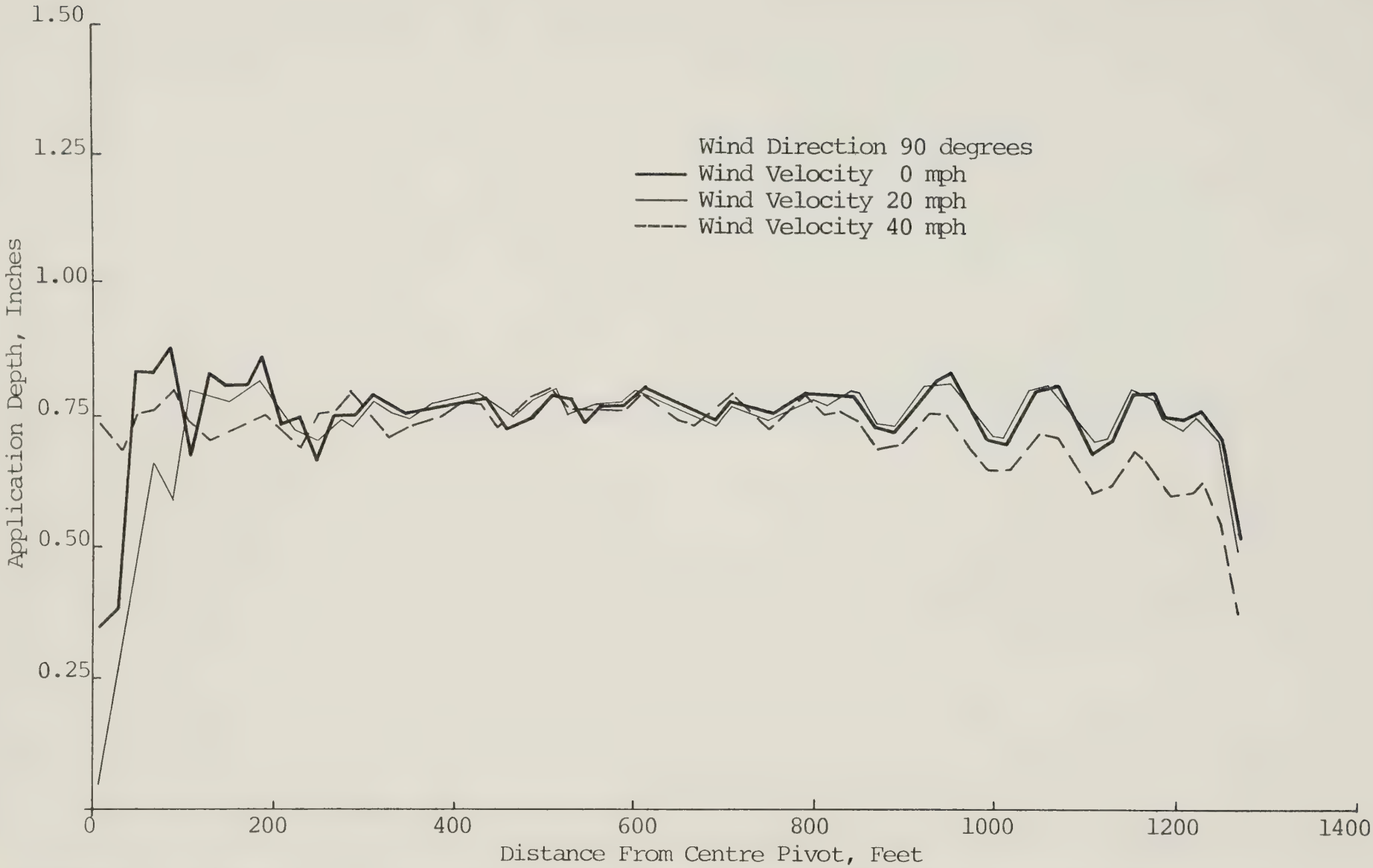

APPENDIX V. Figure $V_{(2)}$. Predicted distribution of application depths for the "Circle Master" C.P. Systems.

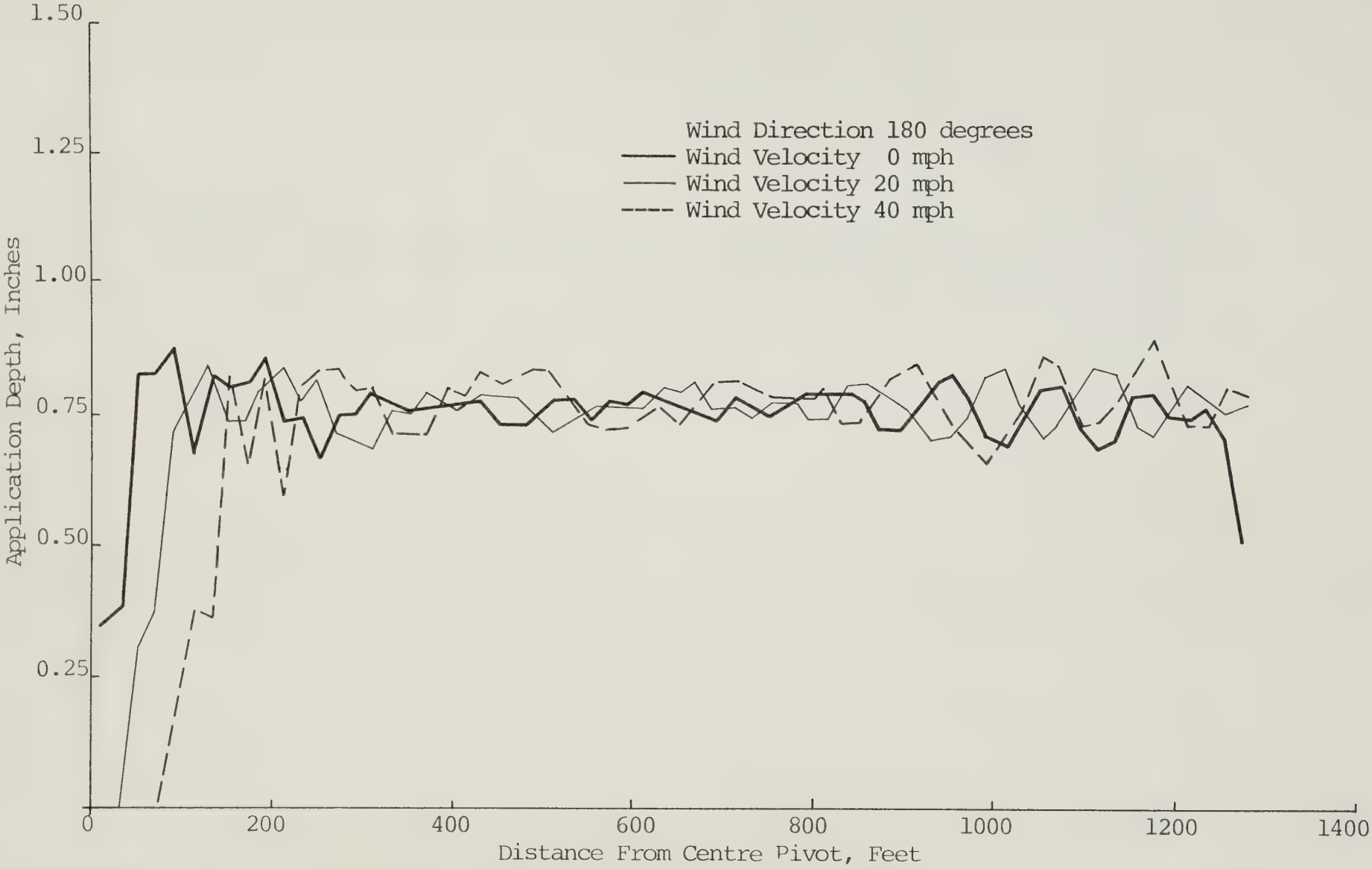

APPENDIX V. Figure $V_{(3)}$. Predicted distribution of application depths for the "Circle Master" C.P. Systems.

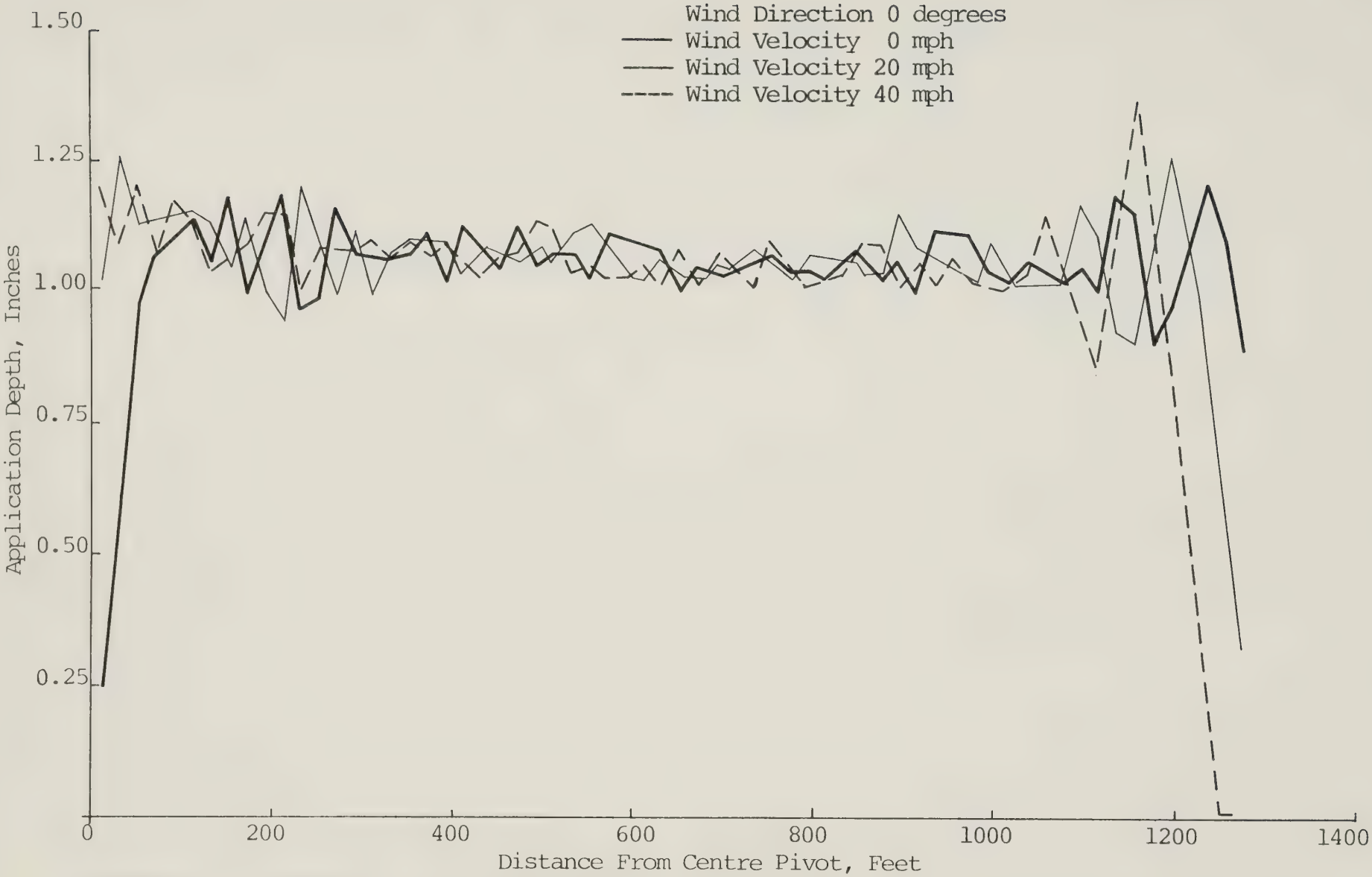

APPENDIX V. Figure $V_{(4)}$. Predicted distribution of application depths for the "Valley 1160" C.P. Systems.

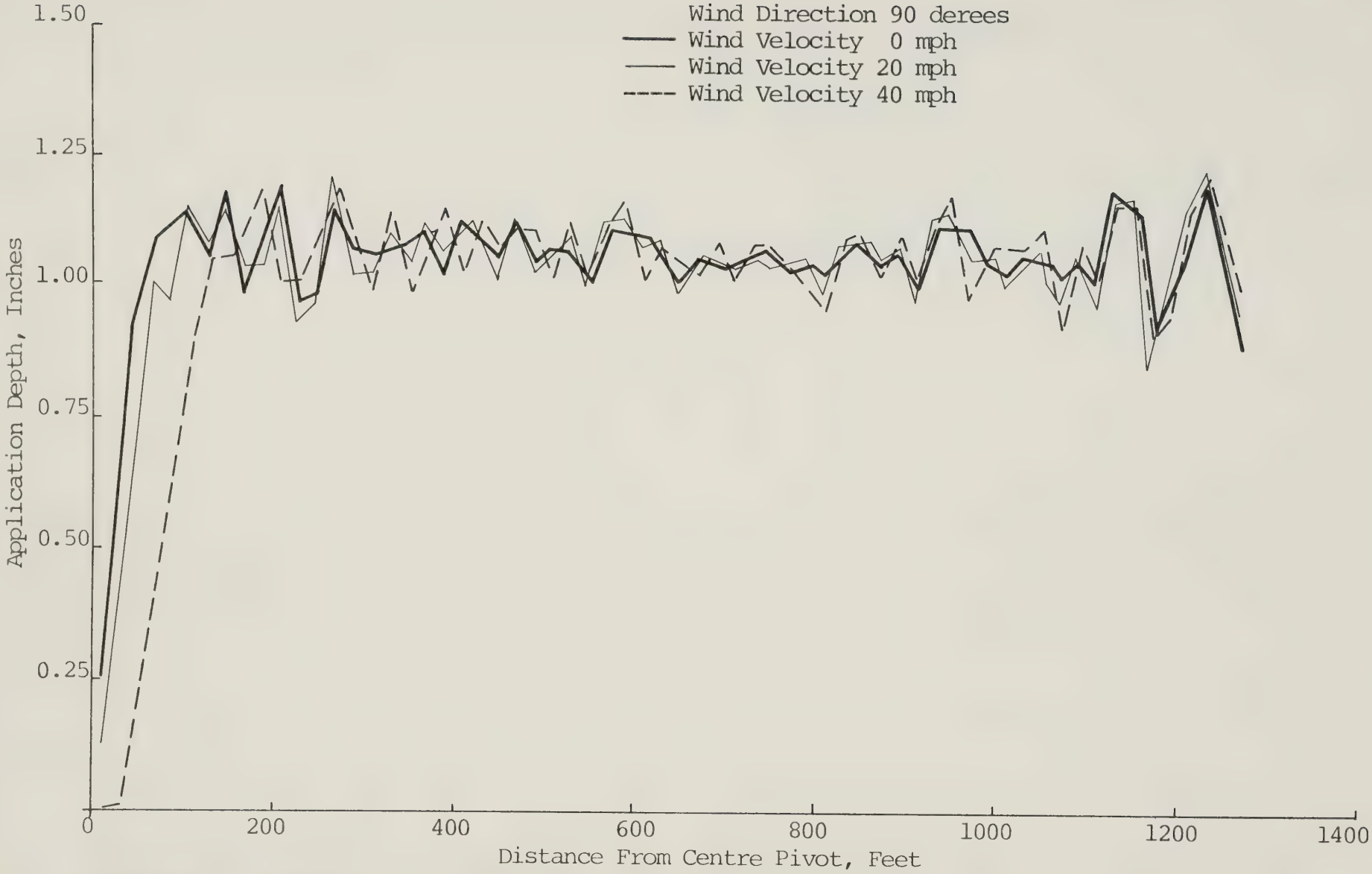

APPENDIX V. Figure $V_{(5)}$. Predicted distribution of application depths for the "Valley 1160" C.P. Systems.

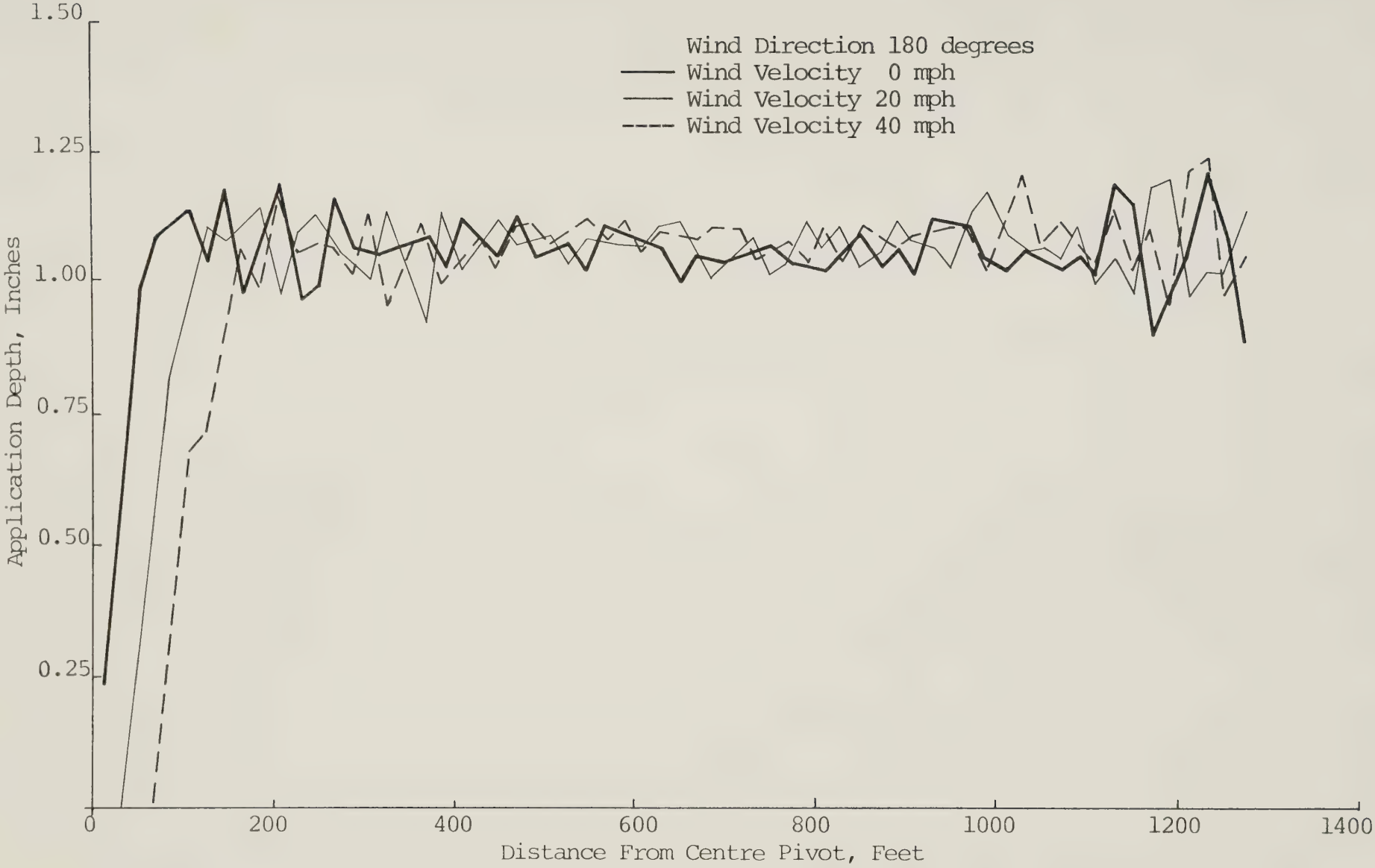

APPENDIX V. Figure $V_{(6)}$. Predicted distribution of application depths for the "Valley 1160" C.P. Systems.